TAMPERE UNIVERSITY OF TECHNOLOGY

SERGIO LUNA

DESIGN AND IMPLEMENTATION OF RECTIFYING CIRCUITS WITH ENERGY STORAGE FOR WIRELESS POWER TRANSFER

Master of Science Thesis

Examiners:
Adj. Professor Olli-Pekka Lunden
D.Sc. Jouko Heikkinen
Examiner and topic approved in the
Computer and Electrical
Engineering Faculty Meeting
May 9th, 2012

ABSTRACT

TAMPERE UNIVERSITY OF TECHNOLOGY
Faculty of Computing and Electrical Engineering
Department of Electronics
LUNA, SERGIO: Design and implementation of rectifying circuits with energy storage for wireless power transfer
Master of Science Thesis, 68 pages, 4 Appendix pages
September 2012
Examiners: Adj. Professor Olli-Pekka Lunden, D.Sc. Jouko Heikkinen
Keywords: rectification, energy storage, wireless power transfer

The main goal of this thesis was to study the possibility of storing the energy obtained from the rectification of a low-level alternating current (AC) signal used as the input. This divided the research in two main parts: the rectifying circuit, which obtained a direct current (DC) signal from the AC signal available at the input, and the energy storage circuitry, which manipulated the output of the rectifying circuit to obtain a signal that was suitable to deliver charge to an energy storage component, and at the same time provided a way to retrieve the energy stored in said component.

Much of the research done so far has dealt with high input powers, over 10dBm, and a load resistance below 1kΩ, achieving very high conversion efficiencies, up to 80-90%. In this work, however, the research was done with lower input power levels, below 0dBm, and load impedance in the order of tenths of kΩ. The efficiencies obtained under these conditions were much lower, under 10%, but the goal of the research was achieved.

The work was focused in two frequency bands, 868MHz and 2.4GHz. Thus, different rectifying circuits were designed and manufactured for both bands in order to obtain the optimal performance for the given conditions. The energy storage circuitry, on the other hand, remained the same for both bands, since its behaviour did not depend on the frequency. Two patch antennas, designed by the supervisor of this thesis and manufactured by the author, were used for the final measurements carried out in an anechoic chamber, and the possibility of storing energy from an electromagnetic wave radiated by a transmitting antenna was demonstrated.

This research may be further extended to obtain self-sustainable devices that would harvest energy radiated by nearby equipment operating at those frequencies, eliminating the need of an external power source. Moreover, studies might be carried out to harvest energy from the whole frequency spectrum.

PREFACE

The work for this thesis was carried out at the Department of Electronics, Tampere University of Technology (TUT), from September 2011 until May 2012. The topic was suggested by the Radio Frequency (RF) Electronics group.

I would like to thank in the first place my supervisor and examiner Dr.Sc. Jouko Heikkinen for all the help provided during the development of this thesis, and the sharing of his vast knowledge and expertise in the subject, without which this work would have certainly taken much longer. I would also like to thank Adj. Prof. Olli-Pekka Lunden for examining this work.

Thanks to the rest of workers at the RF Electronics group, especially Adj. Prof. Riku Mäkinen and M.Sc. Hannu Sillanpää, for their valuable help with some practical matters.

I wish also to express my gratitude to M.Sc. Sanna Lahokallio for her assistance, patience and availability when the same circuits needed to be manufactured over and over until they worked.

Thanks to all my friends this year, the old ones and the new, for making these months full of good times and memories. To those who came back to their home country, I wish you all the best.

I thank my family, especially my parents, for their loving and unconditional support. Without their understanding none of this would have come to happen, and even if it was difficult for them to see me go so far away once again, they always let me know that they were there for me. For that I am deeply grateful.

Finally, thanks to Kaisla-Maria for everything we have lived together so far.

Tampere, Finland.
10.08.2012

Sergio Luna

CONTENTS

LIST OF SYMBOLS AND ABBREVIATIONS

B_V	parallel capacitance
C	capacitance
C_{j0}	zero-bias junction capacitance
C_P	parallel capacitance
C_D	diode capacitance
D	directivity of an antenna
d	maximum linear dimension of an antenna, or distance of a stub from a load, or distance between stubs
E_G	energy gap
e_c	conduction efficiency
e_{cd}	radiation efficiency
e_d	dielectric efficiency
e_r	reflection (or mismatch) efficiency
e_0	total antenna efficiency
$F(\theta, \phi)$	radiation pattern
f	frequency
G	gain of an antenna
h	substrate thickness
I	current
I_{BV}	current at breakdown voltage
I_D	diode current
I_L	current at the load
I_Q	quiescent current
I_S	saturation current
L	length of the patch in a patch antenna, or matching network with lumped elements
L_S	self-inductance
l	length of a stub
m	grading coefficient
N	bottom ideality factor
n	emission coefficient
P_B	bulk potential
$P_{DC\ OUT}$	available DC power at the output of a rectifier
P_{in}	input power
P_{out}	output power
P_T	saturation current temperature exponent
R	resistance
R_L	load resistance

R_S	series resistance
S_{11}	port 1 voltage reflection coefficient
t	conductor thickness
V	voltage
V_D	diode voltage
V_F	forward voltage
V_L	voltage at the load
V_{IN}	input voltage
W	width of the patch in a patch antenna
Y	admittance
Y_0	admittance corresponding to the characteristic impedance of a line
Z_L	load impedance
Z_0	characteristic impedance of a transmission line
Z_1	characteristic impedance of a quarter-wave transformer
z_L	normalized load impedance
ε_r	relative permittivity
η	rectification efficiency
θ	elevation angle
λ	wavelength
λ_0	free-space wavelength
λ_d	wavelength in a dielectric media
τ	time constant
τ_T	transition time
ϕ	azimuth angle
ϕ_T	thermal voltage
ϕ_0	junction potential
AC	Alternating current
CCTV	Closed Circuit TeleVision
DC	Direct Current
DFN	Dual Flat No lead
DSSS	Direct-Sequence Spread Spectrum
EDLC	Electric Double-Layer Capacitor
ERP	Effective Radiated Power
ESR	Equivalent Series Resistance
FHSS	Frequency-Hopping Spread Spectrum
IC	Integrated Circuit
ISM	Industrial, Scientific and Medical
ITU	International Telecommunication Union
KERS	Kinetic Energy Recovery System
LAN	Local Area Network

LDO	Low-DropOut
LHCP	Left Hand Circular Polarization
LIB	Lithium-Ion Battery
LIP	LIthium-Polymer
MSOP	Micro Small Outline Package
PCB	Printed Circuit Board
RF	Radio Frequency
RFID	Radio Frequency IDentification
RHCP	Right Hand Circular Polarization
SMA	SubMiniature version A
SMD	Surface Mount Device
SOC	State-Of-Charge
SOT	Small Outline Transistor
SPICE	Simulation Program with Integrated Circuit Emphasis
SRD	Short Range Device
SSOP	Shrink Small Outline Package
TUT	Tampere University of Technology
UTDFN	Ultra Thin Dual Flat No lead
UWB	Ultra Wide Band
VNA	Vector Network Analyser
WPT	Wireless Power Transfer

1. INTRODUCTION

The process of rectification consists on the manipulation of an AC signal in order to obtain a DC signal. As it will be studied through this thesis, different configurations are possible in order to carry out this conversion. Rectification finds a major application in Wireless Power Transfer (WPT), where power is transmitted between two points that do not share a physical connection. Antennas are the elements in charge of transmitting and receiving this power. The receiver antenna intercepts a portion of the electromagnetic energy stored in the incident field, providing an AC signal at its output, and thus some amount of the originally transmitted power can be converted into DC power by using of a rectifying circuit attached to the antenna. The device formed by the receiving antenna and the rectifying circuit is called rectenna.

Two frequency bands are considered for the designs of the rectifying circuits. Both bands are Industrial, Scientific and Medical (ISM) bands, defined by the International Telecommunication Union (ITU). These bands can be used without the need of a license, as long as certain power limits are not reached. Many devices from different nature operate at this bands, including, for example, microwave ovens or wireless sensors. However, in the last years the tendency has been to use them for short-range, low power communication systems, such us Bluetooth or ZigBee.

Research on rectification and rectennas has been carried out extensively for many years. Very efficient designs have been achieved at high power levels. This thesis focuses, however, on rectification at low power levels, meaning that the input levels will not exceed 0dBm.

1.1. Objectives of the thesis

Although higher efficiencies are usually preferred, the main goal of this work was to design a combination of a rectifying circuit and energy storing circuitry that would make it possible to deliver charge to an energy storage component from the DC signal obtained after rectification. A study of previously done research on different rectifying configurations and achieved results was carried out, and the most promising candidates were further analysed by simulations. The size of the components was an important factor that needed to be taken into account when the designs were being developed, as it was preferred to obtain a prototype as small as possible for its possible use in future applications.

1.2. Thesis outline

This work is divided into five chapters. After the introduction presented in the first chapter, some theoretical basic principles involved in the designs carried out are presented in Chapter 2. A review of currently available energy storage components and their main characteristics is presented in Chapter 3, along with a brief discussion that allows the decision of the best candidate among these components. From this decision yields the need of some extra circuitry that makes it possible to deliver charge to the energy storage component, and several candidates are studied and discussed.

Chapter 4 presents the whole process of design, implementation and obtained results of the rectifying circuit and the energy storage circuitry. In spite of being similar, the steps followed for both frequency bands and the results obtained after the implementations are presented separately for an easier comprehension of the work. Finally, some conclusions and final remarks are presented in Chapter 5.

2. THEORETICAL BACKGROUND

This chapter is divided into four sections, each of them discussing some theoretical aspects needed for the development of this thesis. In the first section, basic concepts of an antenna are explained, including its main parameters and classification. Although the design of the antenna was not a part of the work carried out by the author of the thesis, it is wise to review these concepts in order to understand the results obtained when implementing it. In the second section, concepts about the matching network that will be placed between the antenna and the rectifying circuitry are discussed. The third section deals with the theory necessary to understand the behaviour of the diode. Finally, the different parts of said rectifying circuitry are studied, and different configuration options are explained in the fourth section.

2.1. Antenna

An antenna is an electrical device that converts a wave propagating on a transmission line to a plane wave propagating in free-space, when used for transmission, or vice versa in reception. There is a wide variety of antenna types and shapes, but all of them can be described with the following set of parameters and terms [1], [2], [3].

- The radiation pattern $F(\theta, \phi)$, where θ represents the elevation angle and ϕ the azimuth angle, describes the power radiated (or received) by an antenna as a function of angular position and radial distance from the antenna. The variation of power density with angular position is determined by the type and design of the antenna.
- Far-field is the region away from the antenna where the radiated wave behaves essentially as a plane wave. The distance at which this region starts can be expressed by the expression

  $$\frac{2d}{\lambda^2} \tag{2.1}$$

  where d is the maximum linear dimension of the antenna and λ the operating wavelength. The radiation pattern is usually assumed to be in the far-field region of the antenna.
- Directivity D of an antenna is the ratio of power density in the direction of maximum radiation to the average power density at the same distance from the antenna.
- The total antenna efficiency e_0 accounts for losses at the input terminals and within the structure of the antenna. These losses may be due to reflections

because of the mismatch between the transmission lines and the antenna and to conduction and dielectric losses. This overall efficiency can be expressed as

$$e_0 = e_r e_c e_d \tag{2.2}$$

where e_r is the reflection (mismatch) efficiency, e_c the conduction efficiency and e_d the dielectric efficiency.

The terms e_c and e_d are very difficult to compute, and in most cases they are measured. Even if this is the case, it is not easy to measure them separately, and they are usually lumped together in a single term defined as $e_{cd} = e_c e_d$, known as radiation efficiency.

- Gain G of an antenna is the product of efficiency and directivity, and accounts for the fact that loss reduces the power density radiated in a given direction.
- Impedance. Any antenna presents a driving-point impedance to the source or load it is connected to, and so impedance mismatch with a feed line can occur. This degrades the antenna performance, and should be balanced using a matching network.
- Bandwidth is the usable frequency range of an antenna, which may be limited by impedance mismatch or pattern deterioration.
- Polarization of an antenna is the polarization of the electric field vector of the radiated wave. Typical polarizations include linear (vertical or horizontal) and circular (right hand circular polarization, RHCP, or left hand circular polarization, LHCP).

A brief classification of antennas can be done as follows [1], [2], [4].

- Electrically small antennas present a structure in which the extent is much less than the operation wavelength, λ. These antennas are characterized by very low directivity, low input resistance, high input reactance and low efficiency. Examples of this type of antenna are the short dipole and the small loop.
- Resonant antennas have a structure which extent is in the same order as half the operating wavelength. An antenna built this way operates well at a single or selected narrow frequency bands. They possess low to moderate gain, real input impedance and narrow bandwidth. The half-wave dipole, microstrip patch and Yagi antennas belong to this group.
- Broadband antennas present a wider frequency range than other antennas at which the pattern, gain and impedance present an acceptable performance. They are characterized by a constant and low to moderate gain, real input impedance and a wide bandwidth. The spiral antenna and the log periodic dipole array belong to this kind of structure.
- Aperture antennas have a physical aperture (opening) through which waves flow. They are often just flared sections of waveguide, as is the case of horn antennas, or even open-ended waveguides. Slots in a waveguide or a ground plane are additional examples. They present a high gain that increases with

frequency and a moderate bandwidth. They are most commonly used at microwave frequencies.

The antennas used in this project work are microstrip patch antennas, thus constructed using printed circuit fabrication techniques so that a portion of the metallization layer is responsible for radiation. These antennas were conceived in the 1950s, but it was not until the 1970s that extensive investigation of them started [5], [6]. They are popular among antenna engineers due to their low profile and the ease with which they can be configured to specialized geometries. A rectangular patch antenna with probe feed can be observed in Figure 2.1.

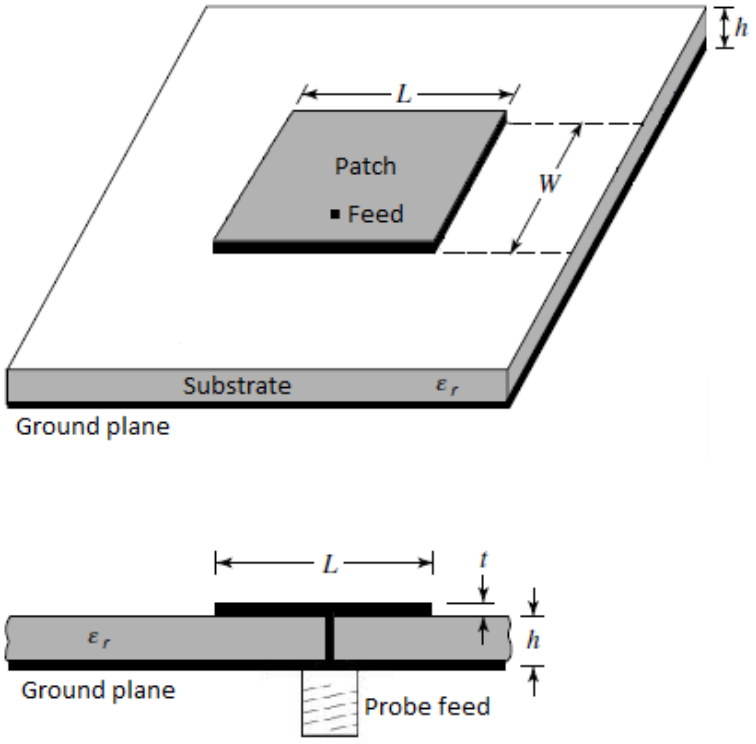

Figure 2.1. *Geometry of a microstrip patch antenna with probe feed.*

As any microstip device, patch antennas are basically a structure formed by two parallel conductors separated by a thin layer of dielectric substrate. The lower conductor acts as a ground plane, whereas the upper conductor is a patch that is an appreciable fraction of a wavelength in extent. As a resonant antenna, it presents a narrow bandwidth, which can be widened by increasing the thickness of the substrate.

The most commonly used microstrip patch antenna is the rectangular patch antenna, in which the patch has a rectangular shape and the substrate thickness is much less than a wavelength. The patch is usually operated near resonance in order to obtain a real input impedance. An approximate value for the length of a resonant half-wavelength patch is given by the equation

$$L \approx 0.49\lambda_d = 0.49\frac{\lambda_0}{\sqrt{\varepsilon_r}} \tag{2.3}$$

where λ_0 is the free-space wavelength, λ_d the wavelength in the dielectric and ε_r the relative permittivity of the substrate dielectric.

Techniques for feeding patches can be classified into three groups. Direct coupling, which is the oldest but most popular, only provides one degree of freedom to adjust the impedance and bandwidth of the antenna. Examples of this feeding are edge feed, edge feed with quarter-wave transformer, edge feed with inset or coaxial probe feed. The other two groups are electromagnetic coupling, also called proximity or gap feeding, such as the edge feed with gap or buried layer feed, and the aperture coupling, like the aperture coupled feed.

2.2. Impedance matching

The goal of a matching network in a general system like the one shown in Figure 2.2, where a transmission line is connected to a load through said network, is to match the characteristic impedance of the transmission line to the load impedance. If this is not achieved, part of the power is reflected back to the transmission line, resulting in power loss.

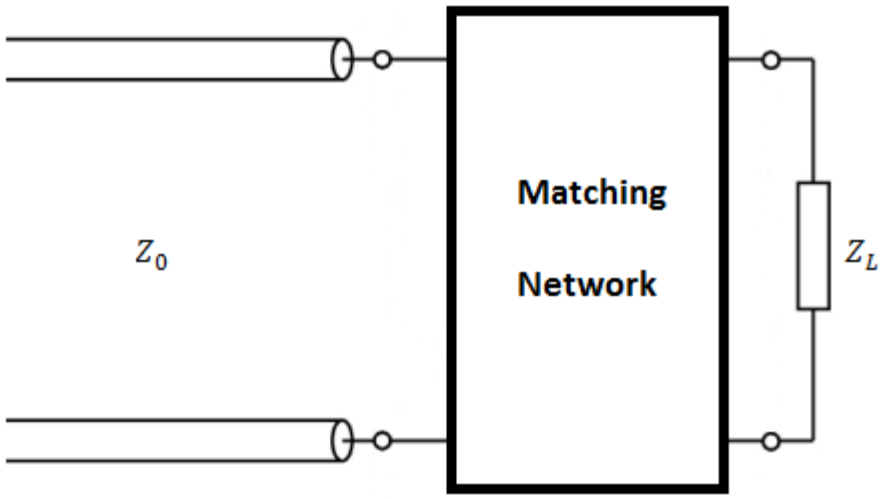

Figure 2.2. *Placement of the matching network between the transmission line and the load impedance.*

The matching network is ideally lossless, so that no additional power is lost due to the connection of the network, and is designed so that the impedance seen when looking from the transmission line into the matching network equals the load impedance. This avoids reflections back into the transmission line, although reflections will occur between the network and the load. When the perfect matching is achieved, the maximum power is delivered to the load [7].

A matching network can always be found as long as the load impedance Z_L has a real part different from zero. Many options for designing the network are available, and it depends on the specific situation which one would be more suitable. Some factors that

should be taken into account when designing the matching network are complexity (the simpler, the better), bandwidth, implementation and adjustability.

The most common methods for designing the matching network are described hereafter.

2.2.1. Matching with lumped elements (L networks)

This is probably the simplest method to match a transmission line to the load connected it. Using two reactive elements, any arbitrary load impedance can be matched to a transmission line. There are two possible configurations for these networks, depending on the normalized load impedance, defined as $z_L = Z_L/Z_0$, where Z_0 represents the characteristic impedance of the transmission line. If this load impedance falls inside the $1 + jx$ circle in the Smith chart, then the configuration in Figure 2.3a is to be used. Otherwise, the configuration shown in Figure 2.3b should be applied.

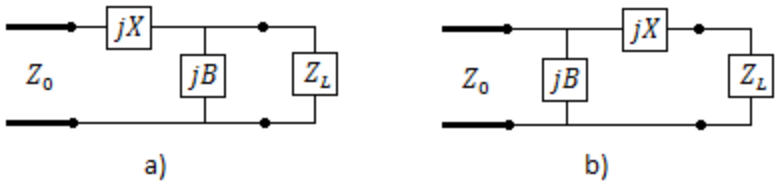

Figure 2.3. *Configurations for matching with lumped elements: a) normalized load impedance inside the* $1 + jx$ *circle, b) normalized load impedance outside the* $1 + jx$ *circle.*

Regardless of which configuration is used, the reactive elements can be either inductors or capacitors, depending on the value of the load impedance. There are thus four different configurations for each of the two networks, resulting in eight distinct possibilities for the matching network. The one to be used will be determined by the load impedance.

This type of matching may be feasible for frequencies up to around 1 GHz. However, there is a wide range of frequencies and circuit sizes where this matching network is not the best option, due to the fact that at higher frequencies lumped elements stop behaving as desired. Connection elements and package parasitic components are as well very complicated to model at these frequencies, and other configurations must be taken into account.

2.2.2. Single-stub matching

A stub is a certain length of transmission line ended either in short-circuit or open-circuit. With a stub connected in series or in parallel (shunt stub) with the transmission line at a certain distance from the load, the matching is always possible, as long as the load impedance has a nonzero real part. The parallel stub is especially easy to fabricate

in microstrip or stripline form. These two configurations are shown in Figure 2.4. The stub must be as short as possible in order to minimize the power loss.

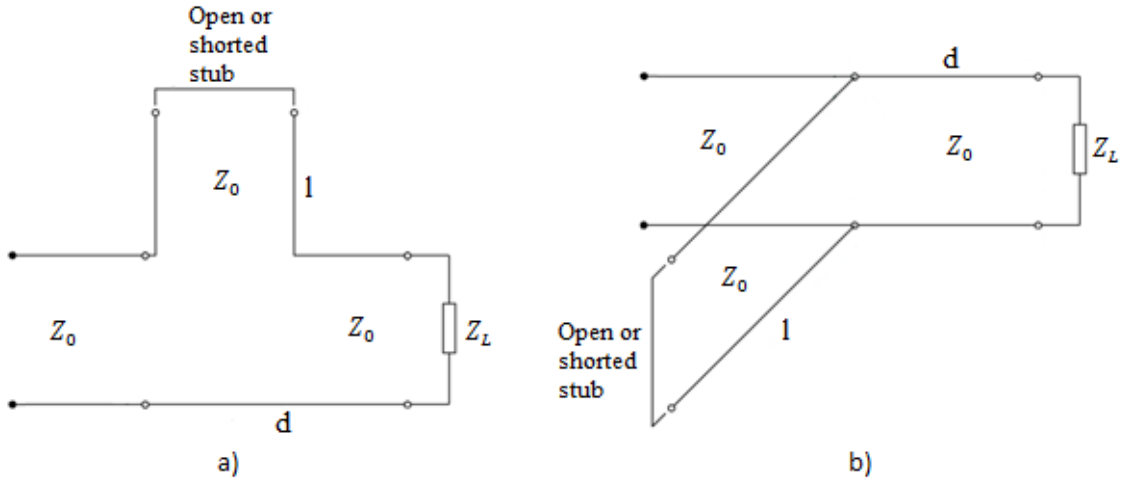

Figure 2.4. *Matching with single stub: a) series, b) parallel (shunt).*

There are only two parameters that must be determined: the distance d from the load to the stub, and the length l of the stub, which will determine its susceptance or reactance.

For the shunt-stub case, the idea is to select d in a way that the admittance Y when looking into a line at such distance from the load is of the form $Y = Y_0 + \mathrm{j}B$, where $Y_0 = 1/Z_0$. Then the length of the stub, l, is chosen so that its susceptance becomes $-\mathrm{j}B$. It is easy to see that the admittance seen before the stub loses its reactive part, becoming real and with a value of Y_0. The result is a matching condition between the transmission line and the load.

There are two ways to find the optimal values for d and l. The first one, which implies the usage of the Smith chart, is fast and intuitive, and usually the results are accurate enough. The analytical expressions bring a more accurate result, although the process is more complicated.

2.2.3. Double-stub matching

The single-stub matching has the disadvantage of requiring a variable length of transmission line between the stub and the load. This is not a problem when the load impedance (or circuit) is fixed, but may present difficulty if an adjustable tuner is desired. This matching cannot, however, match all load impedances.

The double-stub tuner uses two stubs in fixed positions, often fabricated in coaxial line, with adjustable stubs connected in parallel to the main coaxial line. There are four adjustable parameters: the distance between stubs, d, the distance between the second stub and the load, d', and the lengths of the stubs, l and l'. A general scheme, where the stubs are placed in parallel, is shown in Figure 2.5.

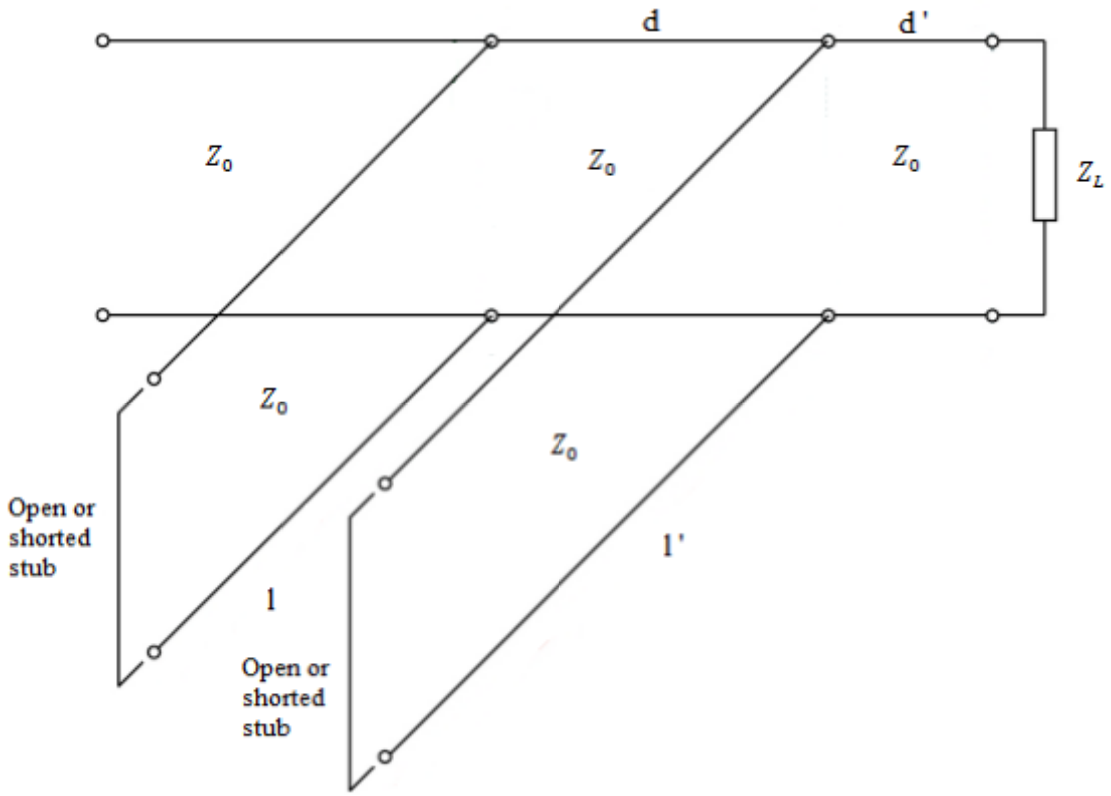

Figure 2.5. *Double-stub matching configuration.*

2.2.4. Quarter-wave transformer

The quarter-wave transformer is a simple and useful circuit for matching a real load impedance to a transmission line. However, any complex load impedance can always be transformed to a real impedance by using an appropriate length of transmission line between the transformer and the load, or a correctly designed series or shunt stub. The single-section quarter-wave matching transformer circuit is shown in Figure 2.6.

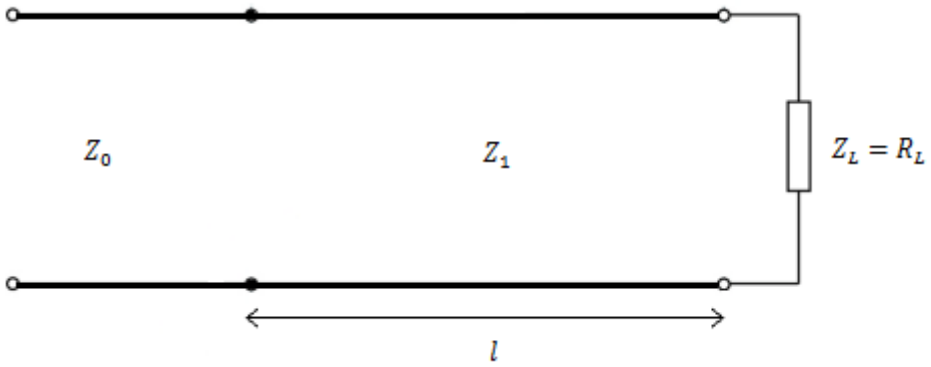

Figure 2.6. *Quarter-wave transformer configuration.*

The two parameters to be determined are the length and the characteristic impedance of the matching section. The first one is automatically determined at the design frequency f by the corresponding wavelength, λ, by the equation

$$l = \lambda/4 \tag{2.4}$$

On the other hand, the characteristic impedance can be obtained as:

$$Z_1 = \sqrt{Z_0 Z_L} \tag{2.5}$$

If a microstrip structure is used, Z_1 will determine the width of the transmission line.

2.3. The diode

The ideal diode is a nonlinear device with a current versus voltage (I-V) characteristic as shown in Figure 2.7a. In this case, if a positive voltage is attempted to be applied between the terminals of the diode, the device behaves as a short circuit, limiting the voltage to zero. On the other hand, if a negative voltage is applied, current does not flow through it and the diode behaves as an open circuit.

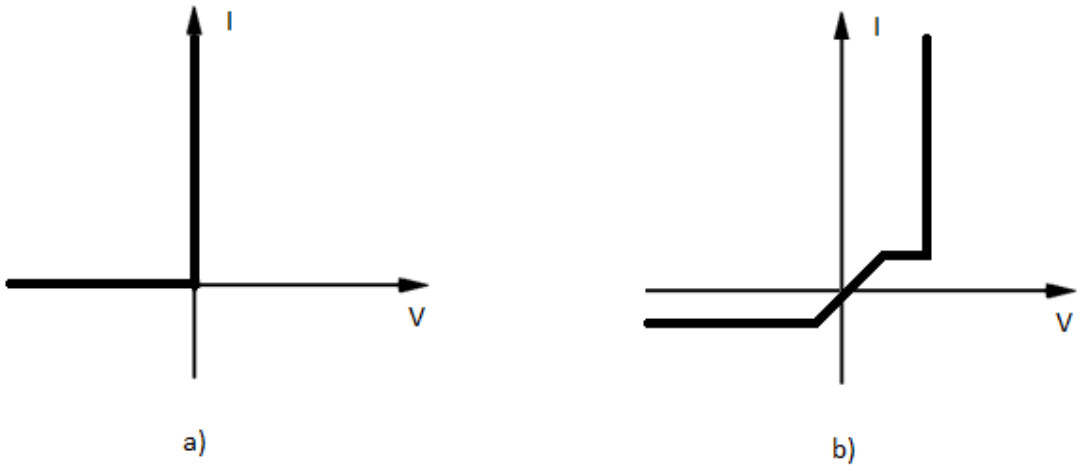

Figure 2.7. *I-V characteristic of a diode: a) ideal diode, b) real diode.*

A real diode, however, behaves quite differently. A more realistic I-V characteristic can be observed in Figure 2.7b.

A small current flows through the diode when the voltage available at its terminals is negative, and some voltage appears as well when the current is positive. The minimum positive voltage required to obtain a noticeable current, known as forward voltage (V_F) is approximately 0.7V for silicon semiconductors, and it is a very important parameter that needs to be kept in mind when designing rectifying circuits.

The SPICE (Simulation Program with Integrated Circuit Emphasis) diode model, which can be used to describe the diodes utilized in this work by using other SPICE parameters along with the ones explained in this section, is shown in Figure 2.8. This circuit models only the diode chip, and thus the effect of parasitic components introduced by the package must be modelled also. In this model, R_S represents the series resistance, C_D the diode capacitance, I_D the diode current and V_D the diode voltage [8].

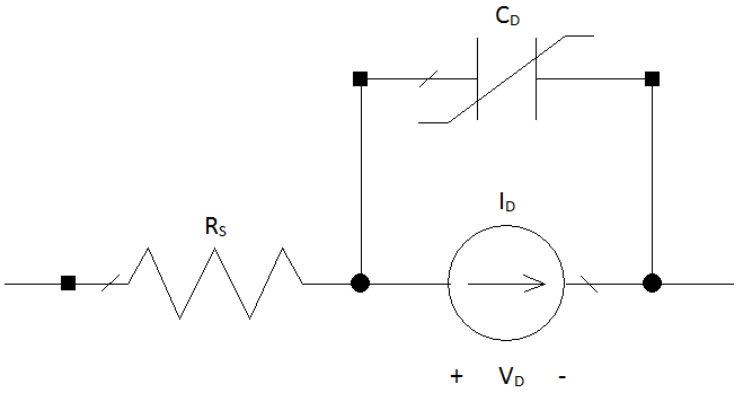

Figure 2.8. *SPICE model of a diode.*

The diode current and capacitance are related to the SPICE parameters as given in equations 2.6 and 2.7 respectively.

$$I_D = I_S\left(e^{V_D/n\phi_T} - 1\right) \tag{2.6}$$

$$C_D = \frac{\tau_T I_S}{\phi_T} e^{V_D/n\phi_T} + \frac{C_{j0}}{\left(1-V_D/\phi_0\right)^m} \tag{2.7}$$

In the two previous equations, ϕ_T represents the thermal voltage, whereas the rest are SPICE parameters. The definitions of these parameters can be seen in Table 2.1.

Table 2.1. *SPICE parameters of the diode model.*

Parameter name	Symbol	Units
Saturation current	I_S	A
Emission coefficient	n	-
Series resistance	R_S	Ω
Transit time	τ_T	s
Zero-bias junction capacitance	C_{j0}	F
Grading coefficient	m	-
Junction potential	ϕ_0	V

One of the major applications of diodes is rectification, which is the process of turning an AC signal into a DC signal. In order to be efficient, the forward voltage of the diode must be as low as possible, so that the power lost in the rectification is minimized. The diodes known as Schottky diodes are the best candidates for this application. With a range that goes from 0.15 to 0.45V versus the 0.6 to 1.7V of a normal silicon diode, they present the lowest forward voltage drop among the different types of diodes. A metal-semiconductor junction is formed, creating what is known as

Schottky barrier, instead of the conventional semiconductor-semiconductor junction present in conventional diodes.

Several configurations are possible when designing a rectifying circuit, which can include just one or several diodes.

2.4. Rectification

As mentioned previously, the process of converting an input alternating signal into one that is restricted to only one direction is called rectification. Several diode configurations are possible, three of them are shown in Figure 2.9.

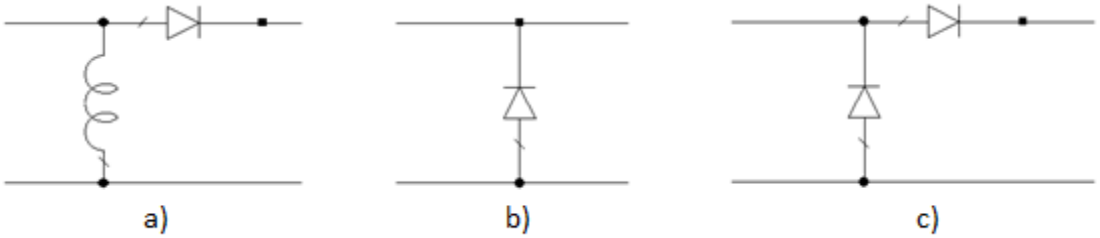

Figure 2.9. *Diode configurations for rectification: a) single series, b) shunt, c) voltage doubler.*

Rectification is generally classified as either half-wave or full-wave. The first one is achieved with only one diode, thus using one of the two first configurations shown above, whereas full-wave rectification requires the use of at least two of them. The single series diode configuration requires a shunt inductor to provide a current return path.

The efficiency of rectification, η, is defined as the ratio of available DC power at the output to the input power.

$$\eta = \frac{P_{DC\,OUT}}{P_{IN}} \tag{2.8}$$

2.4.1. Half-wave rectification

The basic scheme of a simple half-wave rectifier circuit is shown in Figure 2.10.

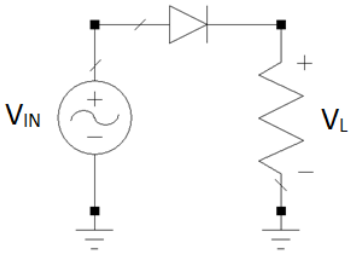

Figure 2.10. *Schematic of a half-wave rectifier.*

When the input voltage is positive, the diode can be replaced by a short circuit, and the output voltage takes the same value as the input voltage. However, when the input voltage becomes negative, the diode can be replaced by an open circuit, and thus the output voltage is zero. The voltage generated in the source versus the output voltage at the load is shown in Figure 2.11.

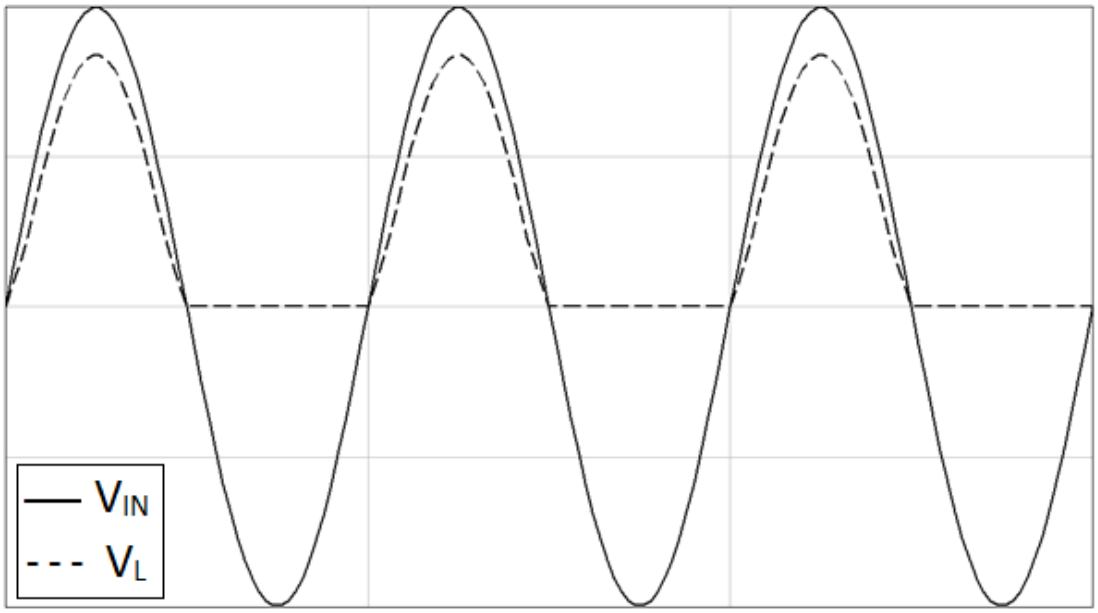

Figure 2.11. *Input voltage versus output voltage through time in a half-wave rectifier*

The voltage drop in the rectified output signal is due to the forward voltage parameter of the diode.

The half-wave rectifier can be used to create an almost constant DC output if a filter is applied, for example with a capacitor placed in parallel with the resistor. This capacitor increases its voltage when the input voltage is positive, and it maintains it approximately constant while the input voltage is negative. The voltage is however slightly decreased due to the capacitor discharge, which occurs at a rate established by the time constant $\tau = RC$. An example of this can be seen in Figure 2.12.

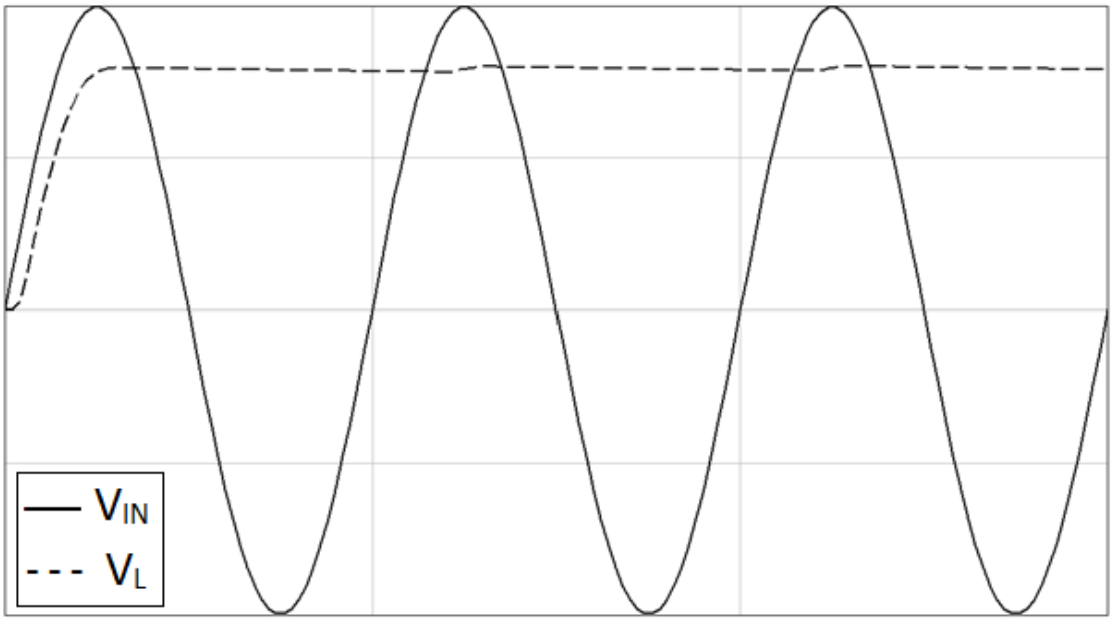

Figure 2.12. *Input voltage versus output voltage through time in a half-wave rectifier, when a capacitor is placed parallel to the load resistance.*

A single diode in shunt configuration was used in [9], for a 5.8GHz rectenna (antenna plus rectifier) design, achieving an efficiency of 82% at an input power level of 50mW and 327 ohms load. The same configuration is used in [10] for a dual-frequency rectenna at 2.45 and 5.8GHz, obtaining efficiencies of 65% and 46% respectively at when the power density is 10mW/cm^2. In [11] a microstrip circuit a single series configuration is studied, resulting in 80% efficiency at 1.25 GHz with an input power of 10mW. Series configuration is used also in [12] and [13] for the design of 2.45GHz rectennas at different input power levels. Series and shunt configurations are studied in [14], with the first one presenting a better performance.

2.4.2. Full-wave rectification

At least two diodes are necessary for the full-wave rectifier circuit. An option using a transformer is shown in Figure 2.13.

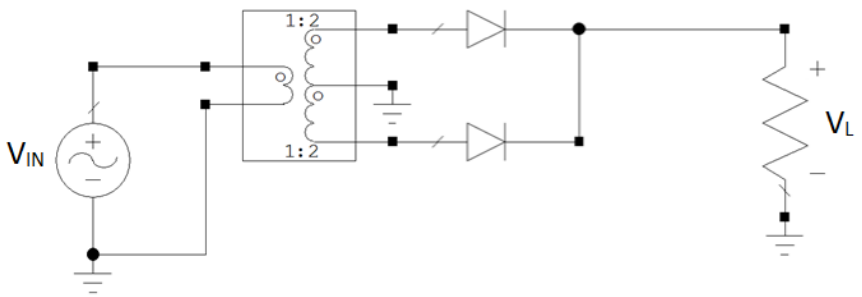

Figure 2.13. *Schematic of a full-wave rectifier using a 1:2 transformer.*

The corresponding voltage at the output load can be seen in Figure 2.14.

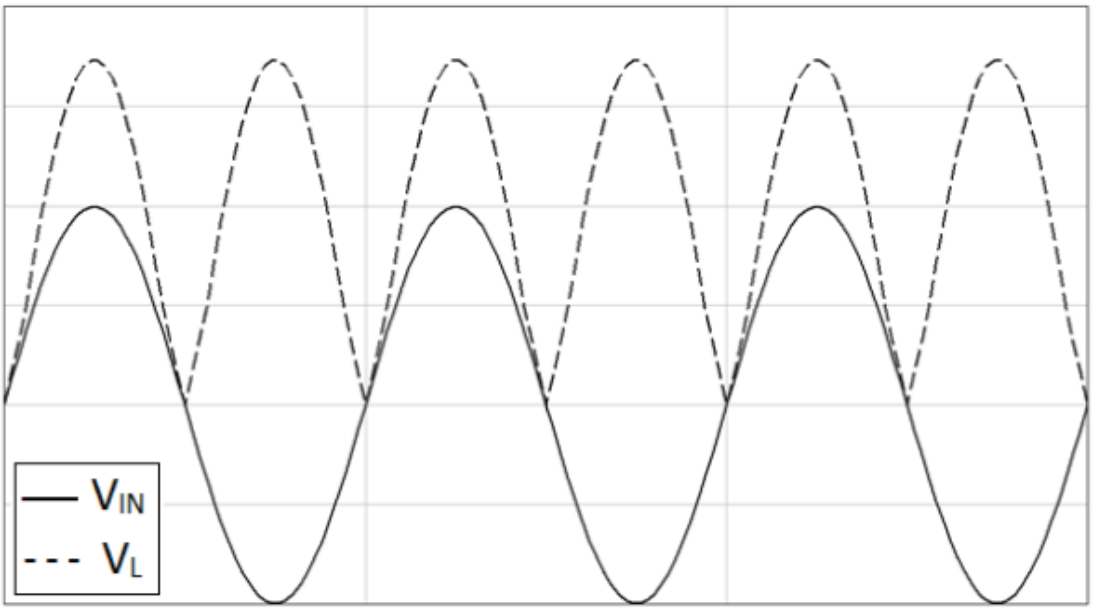

Figure 2.14. *Input voltage versus output voltage in a full-wave rectifier with a 1:2 transformer.*

The increase in voltage is due to the use of the transformer. The full-wave rectifier, as expected, transfers energy to the output in every half cycle, as opposed to the half-wave rectifier case. In a similar way than before, a capacitor can be placed in parallel with the resistor to act as a filter, thus obtaining an approximately constant DC output signal, shown in Figure 2.15.

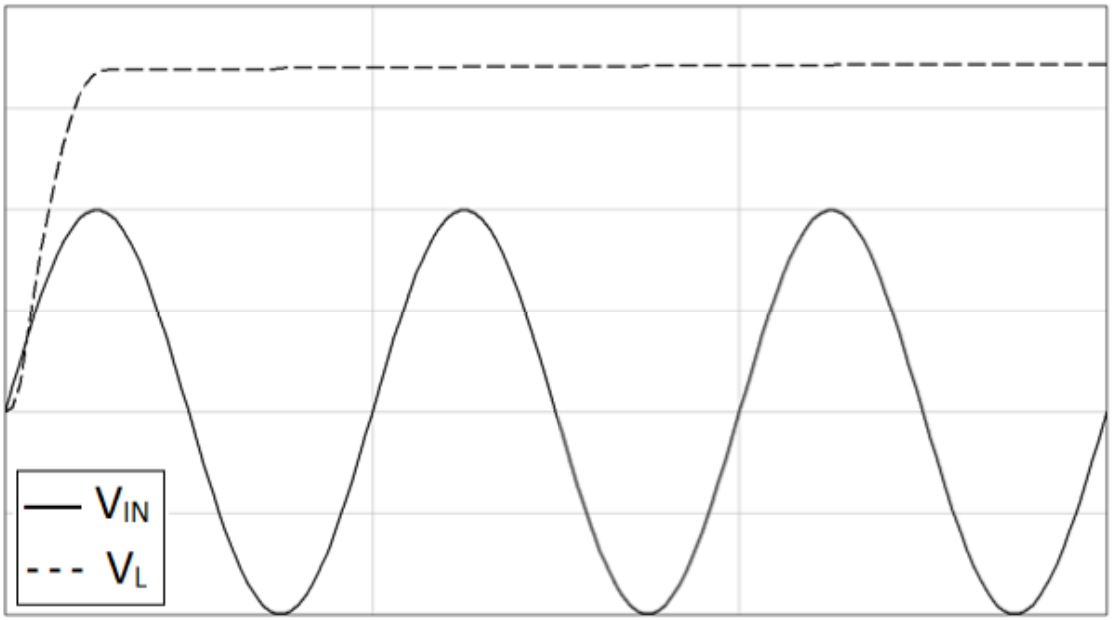

Figure 2.15. *Input voltage versus output voltage through time in a full-wave rectifier with a 1:2 transformer, when a capacitor is placed parallel to the load resistance.*

This configuration was used in [15] for the design of a 2.45GHz rectifier with a differential topology, which eliminates the need of capacitors. A 60% efficiency at 10mW input power was achieved.

A different version of full-wave rectification can be achieved by using four diodes in the so called bridge rectifier. The basic configuration can be seen in Figure 2.16.

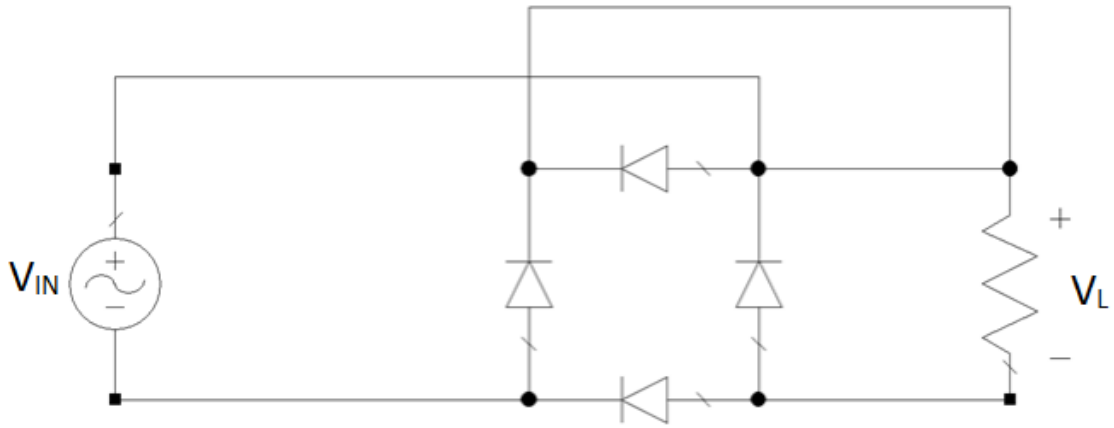

Figure 2.16. *Schematic of a bridge rectifier*

The voltage drop in this version is doubled, due to the fact that two diodes in series are conducting every half-cycle.

The bridge rectifier was used in [12] obtaining an efficiency of over 70%. A modified version is analysed in [16], where an efficiency of 61% at 10mW input power is achieved on a 2.45GHz rectenna.

2.4.3. The voltage doubler

This configuration optimizes the output voltage by using two diodes in the configuration shown in Figure 2.9c. If two capacitors are added at the input and output of the basic scheme, the configuration is shown in Figure 2.17.

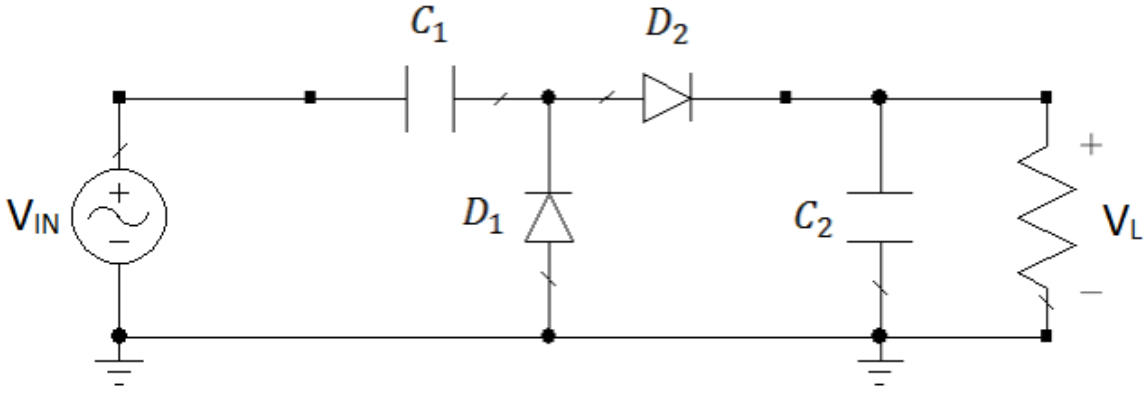

Figure 2.17. *Schematic of a voltage doubler, where a capacitor has been added at the input and the output of the basic configuration.*

When the source reaches its negative peak potential, diode D_1 allows current to flow from the ground into capacitor C_1, filling it up. When the input reverses polarity, D_1 switches off and D_2 switches on. At this point, current flows out of both the source and the capacitor C_1, charging the capacitor C_2 to twice the charge held in C_1. Every time the polarity of the source changes, the capacitors add to the upstream charge and boost the voltage level towards the output. If ideal components would be used, the output voltage would be twice the input voltage. The output voltage versus the input voltage using real components can be observed in Figure 2.18. The decrease in output voltage from the ideal situation is basically caused by the forward voltage drop of the diodes. This can be optimized by choosing Schottky diodes.

This configuration was studied in [14], [17], [18] and [19]. A 2.45GHz dual polarized rectenna using a voltage doubling circuit is used in [18], obtaining efficiencies of 15.7% and 42.1% at -20dBm and -10dBm respectively. The voltage doubler configuration was used in [19] for the design of a dual-frequency rectenna at 2.45 and 5.8GHz, where output DC voltages of over 2V and over 1V respectively were achieved. Efficiencies of 49% and 55% for the low-band rectifier were obtained at input power levels of -5dBm and 0dBm respectively, whereas 14% and 19% efficiencies where achieved for the high-band rectifier at the same input power levels.

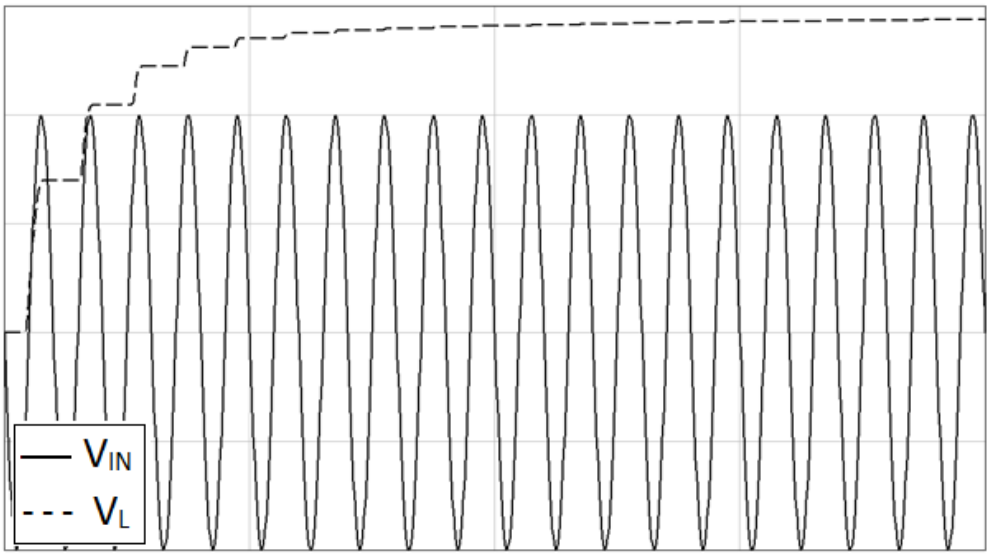

Figure 2.18. *Input voltage versus output voltage through time in a voltage doubler rectifier.*

As discussed in [14] and [17], if the output voltage is too low, several stages of the voltage doubler can be connected in series, with the output voltage increasing exponentially with the number of stages. Although the efficiency in terms of output voltage increases with the number of stages, the power loss and physical size increases as well with each new stage. A circuit with three voltage doubling stages would ideally multiply by eight the input voltage. An example using real components can be seen in Figure 2.19.

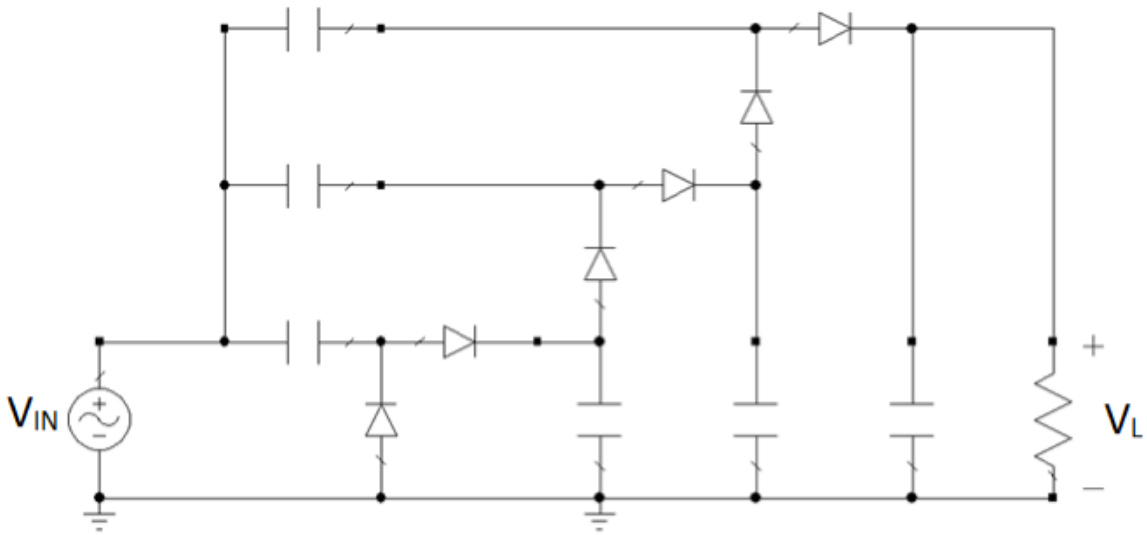

Figure 2.19. *Schematic of a voltage doubler rectifier with three stages.*

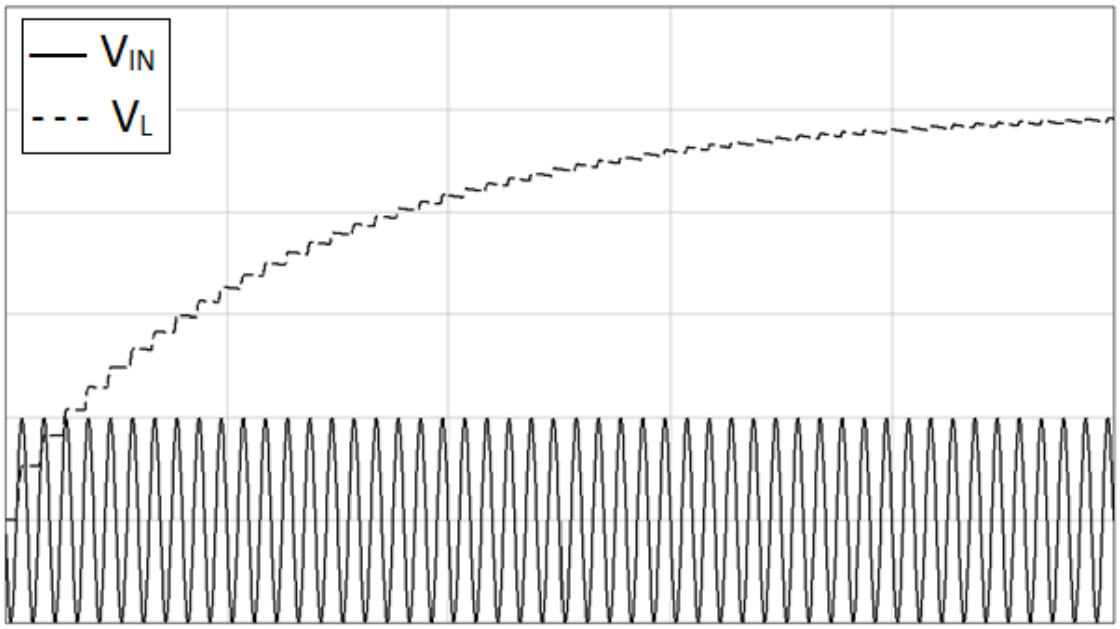

Figure 2.20. *Input voltage versus output voltage through time in a voltage doubler rectifier with three stages.*

The evolution of the output voltage for this circuit can be observed in Figure 2.20. Ideally, each stage doubles the voltage obtained in the previous stage. However, real diode components introduce a higher voltage drop with every new stage used in the configuration.

3. ENERGY STORAGE COMPONENTS REVIEW

In this chapter, different energy storage components are studied, their main characteristics are shown and a decision is made on which one of them should be used for this work, based on said characteristics and the advantages and disadvantages of each of them. Additionally, extra components needed to adequate the signal obtained from the rectification in order to successfully charge the energy storage component are discussed. Comparison tables can be found in Appendix A, where the main characteristics of the components studied in this chapter offered by several manufacturers are shown.

3.1 Supercapacitors

Supercapacitors, also known as electric double-layer capacitors (EDLC), supercondensers, electrochemical double layer capacitors or ultracapacitors, are electrochemical capacitors with relatively high energy density, which is typically hundreds of times greater than that of a conventional electrolytic capacitor [20]. It can be so high that they may sometimes be used in applications usually reserved for batteries.

The EDLC effect was first observed in 1957 by General Electric engineers experimenting with devices using porous carbon electrodes [21]. They noticed that the device exhibited exceptionally high capacitance, although the exact mechanism was unknown at that time. The modern version of the device was developed in 1966 by researchers at Standard Oil of Ohio [22]. Their cell design used two layers of activated charcoal separated by a thin porous insulator, and this basic mechanical design has still remained the basis of most electric double-layer capacitors. The market and research on these devices went slow for some time, but in the mid-1990s several advances in material science and refining of the existing systems led to rapidly improving performance and reduction in cost.

In a conventional capacitor, energy is stored by the removal of charge carriers, typically electrons, from one metal plate and depositing them on another. This charge separation creates a potential between the two plates. The total energy stored this way increases with both the amount of charge stored and the potential between the plates. The amount of charge stored per unit voltage is essentially a function of the size, the distance, and the material properties of the plates and the material in between the plates (the dielectric), while the potential between the plates is limited by the breakdown field strength of the dielectric. The dielectric controls the capacitor's voltage.

EDLCs do not have a conventional dielectric. They use instead virtual plates that are actually two layers of the same substrate. Their electrochemical properties, the so-called "electrical double layer", result in the effective separation of charge despite the extremely thin physical separation of the layers, which is on the order of nanometres. The lack of need for a bulky layer of dielectric, and the porosity of the material used, permits the packing of plates with much larger surface area into a given volume, resulting in high capacitances in practical-sized packages.

EDLCs have much higher power density than batteries. Power density combines the energy density with the speed at which the energy can be delivered to the load. Batteries have relatively slow charge and discharge times. Capacitors, however, can be charged or discharged at a rate that is typically limited by current heating of the electrodes.

EDLCs are used for energy storage rather than as general-purpose circuit components, although rather than a stand-alone energy storage device, supercapacitors work well as memory backup to bridge short power interruptions. They have applications as energy-storage and KERS (Kinetic Energy Recovery System) devices used in vehicles, and for smaller applications like home solar energy systems where extremely fast charging is a valuable feature. Other uses for supercapacitors have been found in computer systems, power conditioners, inverters, power supplies, cameras and power generators.

When compared to batteries, EDLCs present several advantages and disadvantages that can be summarized as follows.

Advantages:

- Long life, with little degradation over thousands of charge cycles. It will usually last for the entire lifetime of most devices, making it environmentally friendly.
- Low cost per cycle.
- Good reversibility.
- Very high rates of charge and discharge.
- Extremely low equivalent series resistance (ESR), resulting in a high cycle efficiency (95% or more) and extremely low heating levels.
- High output power.
- Easy to charge. The charge current is usually limited by the charger. No full-charge detection is needed, and there is no danger of overcharging; the current simply stops flowing when the capacitor is full. The charge time of a supercapacitor is about 10 seconds.

Disadvantages:

- The amount of energy stored per unit weight is usually lower than that of an electrochemical battery.
- The highest dielectric absorption of any type of capacitor.
- The self-discharge of a supercapacitor is substantially higher than that of an electrostatic capacitor and slightly higher than the electrochemical battery. The

stored energy of a supercapacitor decreases from 100 to 50 per cent in 30 to 40 days. Li-ion discharges only five per cent per month.

- The maximum voltage of a supercapacitor is low, usually §confined to 2.5-2.7V, needing series connection in order to obtain higher voltages, which reduces the total capacitance and may require voltage balancing to prevent any cell from going into over-voltage.
- The voltage across any capacitor, unlike practical batteries, drops significantly as it discharges, thus reducing the usable power spectrum and leaving behind much of the stored energy.
- Their very low ESR allows extremely rapid discharge when shorted, resulting in a spark hazard similar to any other capacitor.
- Supercapacitors are expensive in terms of cost per watt. However it must be noted that supercapacitors and chemical batteries are not in competition; rather they are different products serving different applications.

Supercapacitors can be modelled similarly to conventional capacitors. Figure 3.1 shows the lumped-element model of a capacitor for microwave circuits.

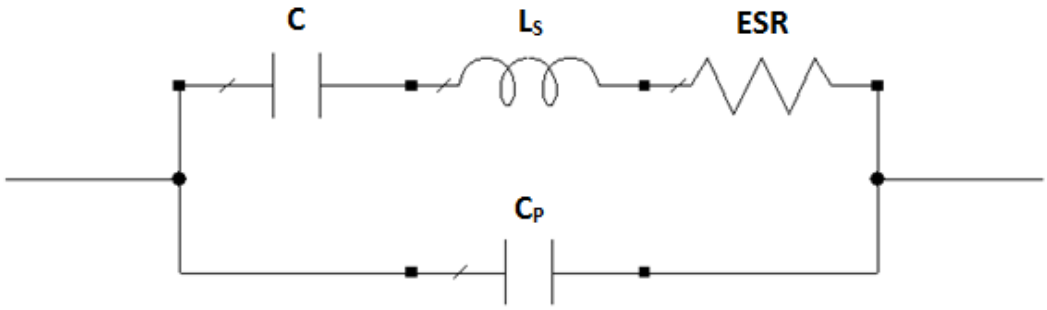

Figure 3.1. *Equivalent circuit model of a capacitor for microwave circuits*

C is the nominal capacitance value, whereas the rest of the elements are considered parasitic components. L_S is known as the self-inductance of the structure. ESR, the Equivalent Series Resistance, is the real part of the series impedance of a capacitor, and is what causes loss due to heat. C_P is known as the parallel capacitance.

As of today, many companies manufacture these components, available in different sizes and packages. For our purposes, one of the most critical factors is the size; the energy storing device should be as small as possible for being integrated in future applications.

3.2 Lithium ion batteries

A lithium-ion battery, also called Li-ion battery or LIB, is a rechargeable battery in which lithium ions move from the negative electrode to the positive electrode during discharge, and back when charging. Chemistry, performance, cost, and safety characteristics vary across LIB types. Unlike lithium primary batteries, which are

disposable, lithium-ion electrochemical cells use an intercalated lithium compound as the electrode material instead of metallic lithium. This is the lightest of all metals, has the greatest electrochemical potential and provides the largest energy density for weight.

The three primary functional components of a lithium-ion battery are the negative electrode, positive electrode, and the electrolyte. The negative electrode of a conventional lithium-ion cell is made from carbon. The positive electrode is a metal oxide, and the electrolyte is a lithium salt in an organic solvent. The electrochemical roles of the electrodes change between anode and cathode, depending on the direction of the current flowing through the cell.

Lithium batteries were first proposed by M.S. Whittingham while working for Exxon in the 1970s [23]. Whittingham used titanium (II) sulfide and lithium metal as the electrodes. However, the use of metallic lithium for the positive electrode presents safety issues, and so lithium-ion batteries were developed in which both electrodes are made of a material containing lithium ions. In 1979, John Goodenough demonstrated a rechargeable cell with high cell voltage in the 4V range using lithium cobalt oxide ($LiCoO_2$) as the positive electrode and lithium metal as the negative electrode [24]. $LiCoO_2$ acts as a donor of lithium ions, and opened a whole new range of possibilities for novel rechargeable battery systems.

The most commercially popular negative electrode material is graphite. This kind of electrode was discovered by Rachid Yazami in 1980 [25]. The positive electrode is generally one of three materials: a layered oxide (such as lithium cobalt oxide, first used by Akira Yoshino in 1985 [26]), a polyanion (such as lithium iron phosphate, first introduced in 1989 [27]), or a spinel (such as lithium manganese oxide, identified as a cathode material in 1983 [28]). The electrolyte is typically a mixture of organic carbonates such as ethylene carbonate or diethyl carbonate containing complexes of lithium ions [29].

Lithium-ion batteries are common in consumer electronics. They are one of the most popular types of rechargeable batteries for portable electronics, with one of the best energy densities, no memory effect, and only a slow loss of charge when not in use. Beyond consumer electronics, LIBs are also growing in popularity for military, electric vehicle, and aerospace applications.

Depending on materials choices, the voltage, capacity, life, and safety of a lithium-ion battery can change dramatically. Recently, novel architectures using nanotechnology have been employed to improve performance.

Li-ion cells are available in various formats, which can generally be divided into four groups: small cylindrical (solid body without terminals, such as those used in laptop batteries), large cylindrical (solid body with large threaded terminals), pouch (soft, flat body, such as those used in cell phones) and prismatic (semi-hard plastic case with large threaded terminals, often used in vehicles' traction packs).

The lack of case gives pouch cells the highest energy density; however, pouch cells as well as prismatic cells require an external means of containment to prevent expansion when their state-of-charge (SOC) level is high.

Both the advantages and disadvantages of these memory storage devices depend strongly on the materials and design used for their fabrication. The general advantages can be summarized as:

- High energy density.
- Wide variety of shapes and sizes
- Lighter than other energy-equivalent batteries.
- High open circuit voltage, which means that a bigger power can be transmitted at a lower current.
- No memory effect, i.e., there is no need to wait for it to discharge completely before charging it again. Relatively low self-discharge, approximately 5-10% per month.
- Environmentally safe, as there is no free lithium metal.

The main disadvantages that these components present are:

- The cell's capacity, and thus its life, diminishes over time. This loss can be hastened by high charge levels and elevated temperatures.
- The internal resistance of standard lithium-ion batteries is high compared to other rechargeable chemistries or lithium-polymer cells. It increases with both cycling and age, and it causes the voltage at the terminals to drop under load, which reduces the maximum current draw.
- If they are overheated or overcharged, lithium-ion batteries may suffer thermal runaway and cell rupture [30], which in extreme cases can lead to combustion. Thus, they require protection circuits to maintain voltage and current within safe limits.

Researchers are currently working to improve the power density, safety, recharge cycle and cost of lithium-ion batteries. Solid-state designs can deliver three times the energy density of a modern lithium-ion battery at less than half the cost per kilowatt-hour [31].

3.3 Lithium-polymer batteries

Also called lithium-ion polymer batteries and polymer lithium ion (abbreviated LIP), these batteries have technologically evolved from lithium-ion batteries. The primary difference between them is that, in LIP batteries, the electrolyte is not held in an organic solvent but in a solid polymer composite. This design offers simplifications with respect to fabrication, ruggedness, safety and thin-profile geometry. Thus, shape and size are more flexible than in lithium-ion batteries. They started appearing in consumer electronics around 1995, and are nowadays sold as pouch cells, which have a flexible, foil-type case. A new design announced in December 2007 by Toshiba and released onto the market in March 2008, which would offer a much faster rate of charge, is expected to have a major effect in consumer electronics [32].

LIP batteries suffer however from poor conductivity. Their internal resistance is too high and cannot deliver the current bursts needed to power modern communication devices. Heating the cell over 60 degrees may increase its conductivity, thus making it unsuitable for portable applications. No improvements in capacity gains are achieved, being in fact slightly inferior to the capacity in Li-ion batteries.

These batteries find their applications in radio controlled equipment, personal electronics and electric vehicles, where they have been by different companies .

The advantages of these batteries can be resumed as follows:

- Very thin geometries are possible, batteries resembling the profile of a credit card are feasible.
- Flexible form, allowing any reasonable size to be produced economically.
- Improved safety. More resistant to overcharge, less chance for electrolyte leakage.

They present the following limitations:

- Lower energy density, decreased cycle count and higher cost-to-energy ratio compared to lithium-ion.
- They must be charged carefully. Trickle charging is not recommended [33].
- There are no standard sizes.

3.4 Solid state batteries

A solid-state battery is a battery that has both solid electrodes and solid electrolytes. As a group, these materials are very good conductors of ions but are essentially insulating toward electrons, properties that are prerequisites for any electrolyte. They are still based in lithium-ion technology, but they replace the liquid electrolyte with a thin layer of non-flammable material. The high ionic conductivity minimizes the internal resistance of the battery, while the high electronic resistance minimizes its self-discharge rate, thus enhancing its shelf life.

Solid-state batteries generally fall into the low-power density and high-energy density category. The former limitation arises because of the difficulty of getting high currents across solid–solid interfaces. However, these batteries do have certain advantages that outweigh this disadvantage: they are easy to miniaturize (for example, they can be constructed in thin film form, which results in several advantages [34]), and there is no problem with electrolyte leakage. They tend to have very long shelf lives, and usually do not have any abrupt changes in performance with temperature, such as might be associated with electrolyte freezing or boiling.

As the batteries can exhibit a high power-to-weight ratio it could make them ideal for use in electric vehicles as they are estimated to have twice to three times the energy density of existing automotive batteries.

This is a very new technology that is currently being developed and improved constantly, and thus the information regarding it is scarce.

3.5 Decision on energy storage components

One of the most important factors to be taken into account when deciding the type of energy storage device that would be used for the project was the size. This size must go in accordance to the size of the rest of the circuit. Lithium-ion and lithium polymer batteries are the ones presenting the bigger sizes among the devices studied, and thus the less appropriate for the purposes of this work. Solid-state batteries, in spite of offering bigger physical sizes than some supercapacitors, have the advantage of being ultra-thin and somehow flexible, which make them a good candidate.

Other important characteristic that the chosen component must possess is a low self-discharge rate. In future applications, the energy source cannot be assumed to be present continuously, so the energy storage element should not easily lose part of the charge that has been stored after a long time harvesting energy, since it would make the system highly inefficient. In this way, supercapacitors present the worst self-discharging rate of all the elements studied, whereas solid-state batteries, thanks to their high electronic resistance, appear again as a good option.

Finally, something that must be kept in mind is the future development of these components. Lithium-ion batteries have been developed and improved for several decades now, and are not expected to gain significant improvements in the future. Solid-state batteries, on the other hand, have just started to be developed, and thus it is highly probable that in the following years their main characteristics, such as capacitance, size or voltage will be improved.

Taking all this into consideration, a decision was made that the solid-state batteries were to be used as the energy storage device to store the DC power obtained from the rectification of an AC signal. This implies the usage of extra circuitry that will make it possible to deal with the special characteristics of this kind of component, being three the most important ones:

- Unlike supercapacitors, solid-state batteries require a constant voltage level between their terminals in order to be charged properly. The optimal level is 4.1V. The rectified signal can in no way be expected to present a constant voltage level, since it will depend on the power received at the antenna, and thus on the power transmitted and distance from the transmitter, among others. The extra circuitry will need to adequate this highly variable output to a constant level of 4.1V.
- These batteries can be destroyed if an excessively high voltage is applied. Thus, the extra circuitry needs to have a mechanism to prevent this from happening, cutting off the charge when needed.
- They can be destroyed as well if they are overdischarged. To avoid this, the circuitry has to stop draining power from the battery if the minimum voltage limit is reached.

3.6 Chargers and protectors

Solid state batteries require a constant voltage between their terminals in order to be charged. In most cases this voltage must be 4.1V. However, the voltage obtained after the rectification of the electromagnetic signal is completely dependent on the input power level, which in reality cannot be constant, and can be assumed to be quite low at low input power. Thus, extra circuitry is needed to obtain the required voltage level regardless of the power received at the antenna. Three different candidates from two manufacturers are discussed.

3.6.1 LTC3105 – Linear Technology

The LTC3105 is a high efficiency step-up DC/DC converter that can operate from input voltages as low as 225mV and up to 5V [35]. The output voltage can be adjusted between 1.5V and 5.25V. It has an auxiliary 6mA low-dropout (LDO) regulator that can provide a regulated rail while the main output is charging. In operation, the quiescent current (I_Q) is set to 24 µA, whereas in shutdown it is reduced to 10 µA, and integrated thermal shutdown provides protection from overtemperature faults. This integrated circuit (IC) can be used for applications such as supercapacitor charger, energy harvesting and low power wireless transmitters. It is offered in 10-lead 3x3x0.75 mm DFN (Dual Flat No lead) and 12-lead MSOP (Micro Small Outline Package) packages. The pin configuration of the different packages is shown in Figure 3.2.

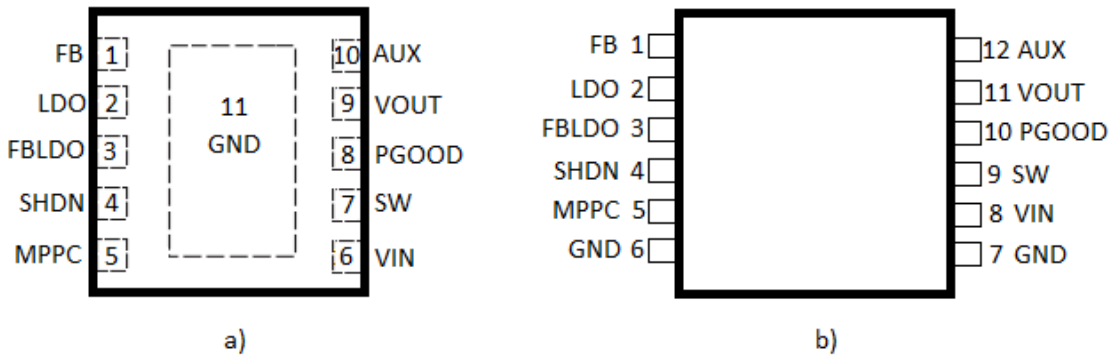

Figure 3.2. *Pin configuration of the LTC3105 component: a) DFN package, b) MSOP package.*

A typical application can be seen in Figure 3.3.

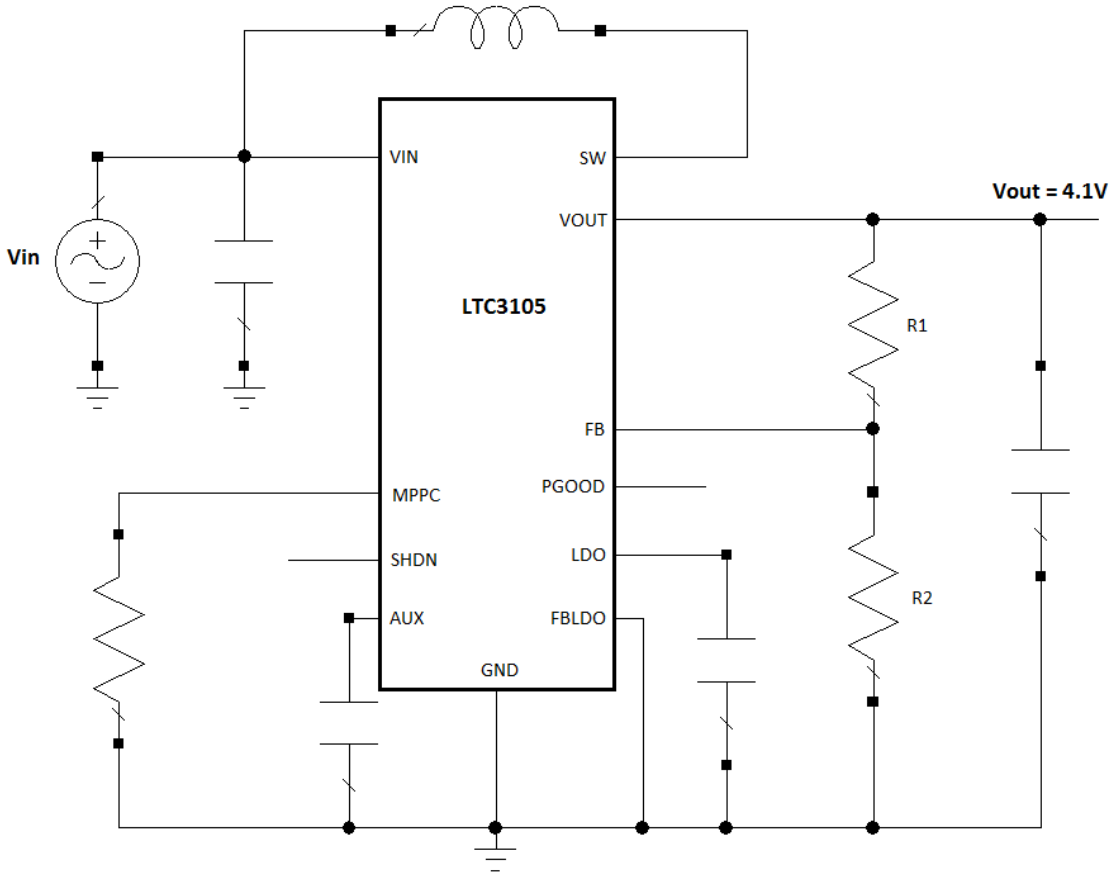

Figure 3.3. *Typical application configuration of the component LTC3105.*

In the previous figure, the photovoltaic cell would be replaced by the output of the rectifying circuit. It can be noticed that this device needs only passive components (resistors, inductors and capacitors) connected to its pins.

During start-up, the LDO is disabled and the AUX output is charged until it reaches approximately 1.4V; at this moment, the converter enters normal operation. The AUX output keeps charging until the LDO output enters regulation, time at which the converter begins charging the VOUT pin. Once this voltage rises above VAUX, an internal switch is enabled to connect the two outputs together.

The output voltage is controlled by a resistor divider. Being R1 the resistor connected between VOUT and FB, and R2 the resistor connected between FB and ground, the output voltage is given by:

$$V_{LDO} = 1.004 * \left(\frac{R1}{R2} + 1\right) \tag{3.1}$$

Thus, if R1 and R2 have a value of 1020kΩ and 332kΩ respectively, then the output voltage will be approximately 4.1V.

3.6.2 LTC3108 – Linear Technology

The LTC3108 is a highly integrated DC/DC converter ideal for energy harvesting and managing from extremely low input voltage sources [36]. It operates from inputs as low as 20mV. The output voltage can be programmed to one of the four fixed values: 2.35V, 3.3V, 4.1V and 5V. A second output can be enabled by the host. It has applications in remote sensors, energy harvesting, industrial wireless sensing and automatic metering. This IC is available in 12-lead 3x4 mm DFN or 16-lead SSOP (Shrink Small Outline Package) packages, as seen in the following Figure 3.5.

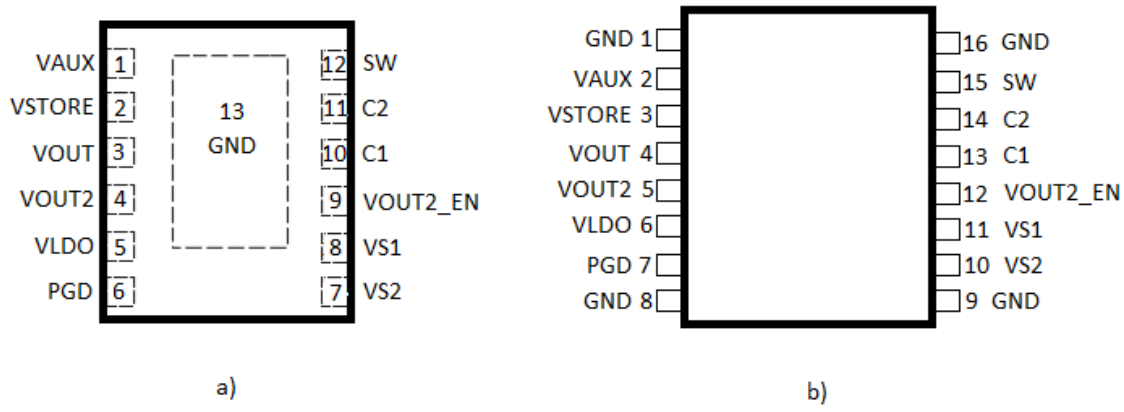

Figure 3.5. *Pin configuration of the LTC3108 component: a) DFN package, b) SSOP package.*

An example of a typical application is shown in Figure 3.6. It can be noticed that in order to work properly with very low input voltage levels, down to 20mV, it is necessary to use a step-up transformer before the IC. Because of this, the input voltage must not exceed 500mV when using a 1:100 transformer. The capacitor before the transformer provides power when the input voltage source is unavailable. The output voltage can be chosen by connecting the VS2 and VS1 pins to ground or to VAUX. The four different combinations provide the four output voltages available.

The AC voltage produced on the transformer is boosted and rectified using an external charge pump capacitor at pin C1 and the rectifiers inside the chip. Said rectifiers feed current into the VAUX pin, providing charge to the capacitor connected to it. Once VAUX exceeds 2.5V, the main VOUT is allowed to start charging.

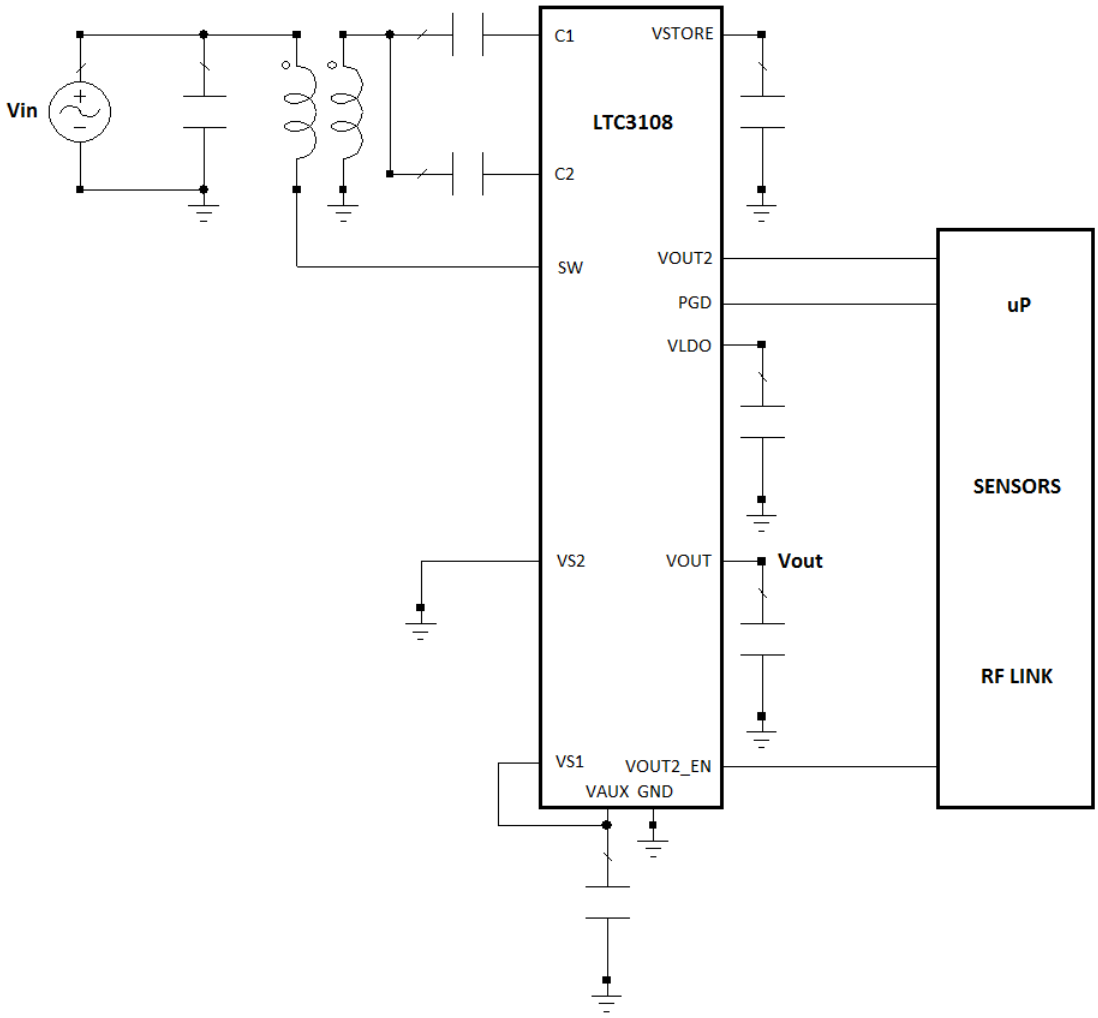

Figure 3.6. *Typical application configuration of the component LTC3108.*

3.6.3 MAX17710 – Maxim

MAX17710 is a complete system for charging and protecting micropower-storage cells [37]. It can manage poorly regulated sources (like energy harvesting) with output levels from 1µW to 100mW. It also includes a boost regulator circuit for charging from a source as low as 0.75V. An internal regulator protects the cell from overcharging, and internal voltage protection prevents it from over-discharging. I_Q takes a value of 150 nA when the regulated output is used, and down to 1nA in standby. Applications where it may be used include remote wireless sensors, semi-active radio frequency identification (RFID) tags and medical devices. The output voltage supplied to the target applications is regulated using an LDO linear regulator with selectable voltages of 3.3, 2.3 or 1.8 volts. The selection of this output voltage can be done through the connection of the SEL1 pin to ground, to the BATT pin or leaving it unconnected. An unregulated output is available as well. This IC is available in a 3x3x0.5 mm 12-pin UTDFN (Ultra Thin Dual Flat No lead) package shown in Figure 3.7.

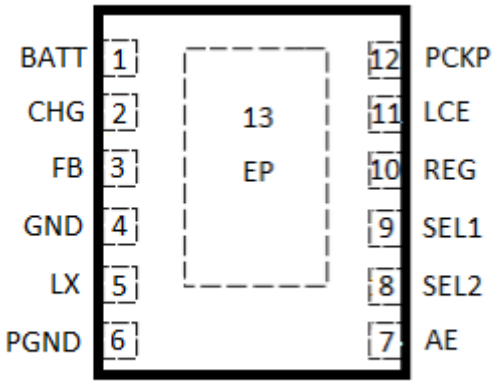

Figure 3.7. *Pin configuration of the MAX17710 component, UTDFN package*

This device has two main functions, completely independent from each other. The first one is to charge a low capacity cell with overcharge protection, and the second one to supply the LDO regulator output with overdischarge protection. When a cell is connected to the BATT pin, initial power-up of the device occurs, it only pulls 1nA from the cell and LDO is disabled.

The circuit configuration for a low power source is shown in Figure 3.8.

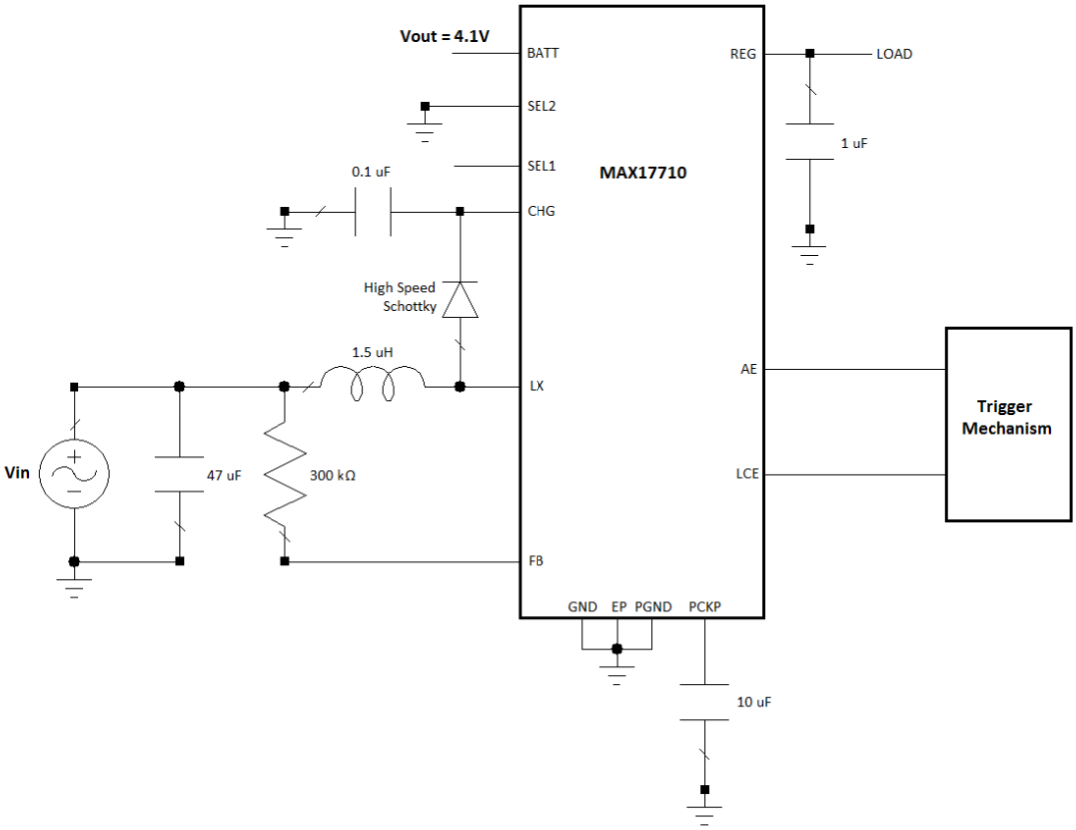

Figure 3.8. *Typical application configuration of the component MAX17710.*

The AE and LCE pins, used for controlling the regulated output, will need a mechanism that changes their voltage level from high to low or vice versa, since they are both activated by rising edge, and deactivated by a falling edge. The general scheme for the rest of the circuit should be kept as it is in the figure. This way, the device will work as a boost regulator, being able to harvest down to approximately 1µW. For example, for a 0.8V harvest source and a 4.1V cell, the device can deliver over 20mA.

In the boost regulation operation, the harvesting source charges the 47µF capacitor until the voltage on FB exceeds the FBON threshold (0.75V). At this point, LX pin is pulled low to force current through the inductor. LX begins to oscillate at 1MHz with 90% duty cycle. Each time LX is released, the inductor forces the LX voltage above CHG and charges the 0.1µF CHG pin capacitor. When CHG rises above the voltage of VBATT, charge is delivered to the cell. When the voltage of the 47µF capacitor collapses, the boost circuit is disabled. The process repeats after the capacitor is recharged.

3.6.4 Decision on chargers and protectors

Out of the three candidates discussed, the third one appears as the best choice for several reasons. First of all, it has an over discharging protection that is necessary if solid state batteries are used. As studied previously, this kind of energy storage device should not be discharged below a certain voltage level, or there would be a risk of destroying the component. This cannot be ensured in any way with the first two ICs discussed.

Another important factor is the minimum power available at the input that these devices require to work properly. For the MAX17710, it is specified that it can harvest down to 1µW. However, the devices from Linear Technology do not specify the minimum power needed, and it is likely to be higher than 1µW. As observed in the datasheet, in the best of cases, a minimum input current of 2mA is needed for the component LTC3108 to work correctly, level that will not be reached with the conditions used for the work carried out in this thesis. As it will be seen later on, the current obtained after rectification is in the order of µA when a real load is used for simulations, and is expected to decrease when the final circuitry is attached.

Taking these factors into account, the decision was made to use the component MAX17710 in the design and implementation of the prototypes.

4. DESIGN, IMPLEMENTATION AND MEASUREMENTS

The steps followed during the design and implementation of the prototypes are presented in this chapter, along with the results obtained both in simulations and measurements. A brief explanation of the frequency bands used in this research is presented as a starting point.

4.1 The frequency bands

The rectifying circuits were designed and optimized for two different frequency bands, 868MHz and 2.4GHz. These belong to the ISM radio bands, defined by the ITU, which can be used without the need of a special license in most parts of the world [38].

The election of these frequency bands was guided by possible future applications of the research that was accomplished in this work. There are nowadays many devices using these frequencies to continuously transmit power wirelessly. The 868MHz band in Europe belongs to what is known as Short Range Device (SRD) band [39], allocated between 863 and 870MHz, used by radio devices transmitting at low power levels, thus offering a low risk of interfering with each other. Different wireless equipment falls in this category, including various forms of:

- Access control (including door and gate openers)
- Alarms and movement detectors
- Closed-Circuit Television (CCTV)
- Industrial control
- Local Area Networks (LAN)
- Medical implants
- Ultra Wide Band (UWB) sensors and radars
- RFID
- Telemetry

The transmission in this band must be done using Frequency-Hopping Spread Spectrum (FHSS), Direct-Sequence Spread Spectrum (DSSS) or analog modulation with a duty cycle of 1%, and the Effective Radiated Power (ERP) is limited to 25mW. These limitations affect exclusively the transmitter end of the communication system, whereas this work was focused only on the receiver end. The final measurements, where a transmitting antenna was used, were carried out in an anechoic chamber, thus avoiding any possible interference with other equipment.

The 2.4GHz band is perhaps the most popular ISM band and the most crowded one. With 100MHz frequency range and a centre frequency of 2.45GHz, this band is used for many different applications, not only ISM, including

- Military
- Electronic news gathering and outside broadcast
- Public provision of fixed wireless access
- Wireless networking: IEEE 802.11/WiFi LANs, Bluetooth, ZigBee
- Other SRD: RFID, video applications
- ISM applications: Microwave ovens, sulphur plasma lighting

The result is that a certain power level is available at these frequencies, which will vary according to the location and the nearby equipment operating at said frequencies. The ERP in this frequency band is limited to 10mW. It must be made clear that the level in the present days is not high enough to feed the rectifying circuits designed in this thesis. Thus, the final measurements were needed to be done with an antenna transmitting at those frequencies.

4.2 868 MHz

The first step in the design of the rectifying circuits was the selection of the components to be used, in this case the diodes and the capacitors.

The diode must be able to operate at the desired frequency. As it was discussed in Chapter 2, it must have as small forward voltage drop as possible. A comparison table of different Schottky diode models from several manufacturers can be found in Appendix B. The diode chosen to be used in the circuit belongs to the HSMS-282x components from Avago [40]. These Schottky diodes are available in different package configurations, and find their typical applications in mixing, detecting, switching, sampling, clamping and wave shaping. As extracted from its datasheet, these components are suitable for input power levels higher than -20dBm, and for frequencies up to 4GHz. Thus, they were suitable also for the 2.4GHz version of the rectifier, which simplified the design. The SPICE parameters for the diode chip can be found in Table 4.1.

As two diodes connected in series were needed for the voltage doubler configuration, the specific component to be used was the HSMS-2822, which is a dual-diode device with three ports, and the package is specified as SOT-23 (Small Outline Transistor). This package can be modelled, according to the manufacturer [41], as shown in Figure 4.1.

Table 4.1. *SPICE parameters of the HSMs-282x components.*

Parameter	Description	Units	HSMS-282x
B_V	Breakdown voltage	V	15
C_{J0}	Zero-bias junction capacitance	pF	0.7
E_G	Energy gap	eV	0.69
I_{BV}	Current at breakdown voltage	A	1e-4
I_S	Reverse saturation current	A	2.2e-8
N	Bottom ideality factor	-	1.08
R_S	Series resistance	Ω	6.0
P_B	Bulk potential	V	0.65
P_T	Saturation current temperature exponent	-	2
m	Grading coefficient	-	0.5

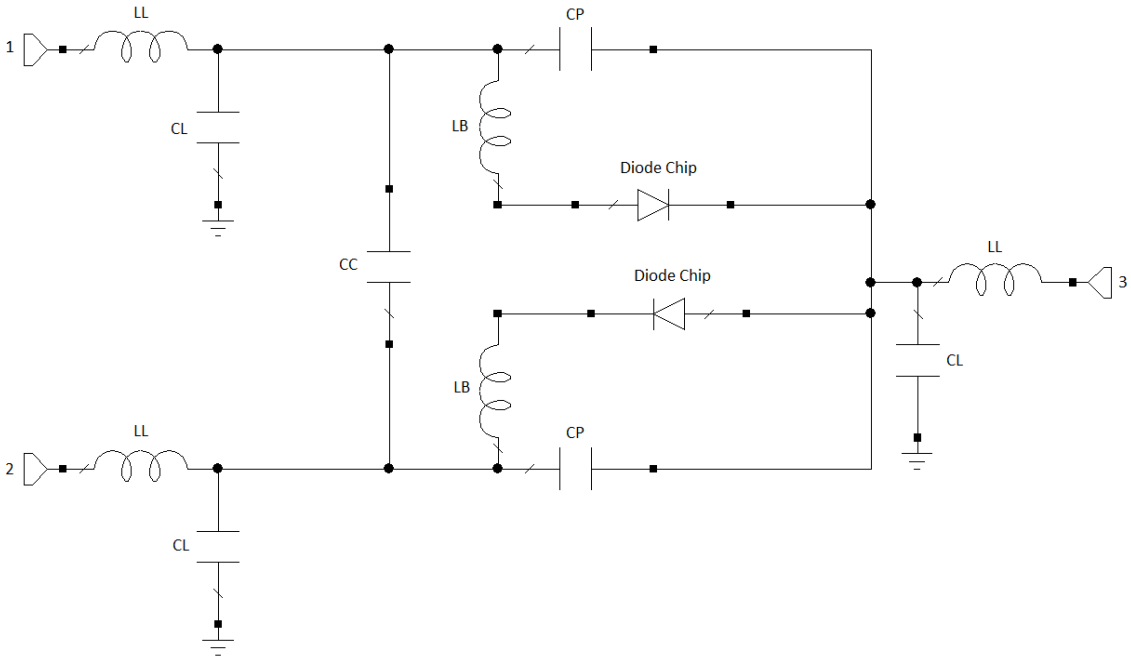

Figure 4.1. *Package model for the component HSMS-2822.*

The description and values of the elements in the package model can be seen in Table 4.2.

Table 4.2. *Description of the elements that form the package model of the component HSMS-2822.*

Element	Description	Units	Value
LL	Leadframe Inductance	nH	0.5
CL	Leadframe Capacitance	pF	0
CP	Package Capacitance	pF	0.08
CC	Coupling Capacitance	pF	0.06
LB	Bondwire Inductance	nH	1

The capacitor was chosen among the components available at the department. A selection of capacitor values from Johanson Technology was suggested by the supervisor of this thesis, and because accurate models for these components were available in the AWR simulation environment used for the design and analysis of the circuits, they were used in the final design. Although simulation results did not vary significantly when using different capacitor values, the component with a nominal capacitance of 47 pF provided the higher output voltage among the ones simulated.

4.2.1 Selection of diode configuration

After the study discussed in the previous chapter, two configurations appeared as the best options: the single series and the voltage doubler. Thus, two versions of the rectifier using the same components and with the same input power were designed and compared. The first version of the circuits can be observed in Figure 4.2, where no transmission lines were used yet, only the capacitors and the diode package model, as well as a 50kΩ load. All the components had the same values in both cases. A frequency of 868MHz was used in the simulations.

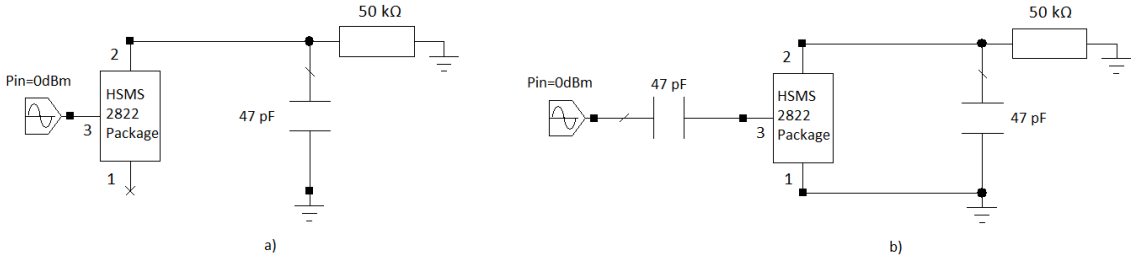

Figure 4.2. *Circuit schematics or rectifier configurations: a) single series, b) voltage doubler.*

In both cases the DC voltage at the load was measured, obtaining 0.221V for the single series configuration, and 0.3474V for the voltage doubler configuration. The load value was the same in both cases, so the output power can be obtained as

$$P_{DC\ OUT} = \frac{V_L^2}{R_L} \tag{4.1}$$

Since the output voltage obtained in the voltage doubler configuration was higher than the one in the single series configuration, the output DC power would consequently be higher as well, which results in a better efficiency, given that the input power was the same in both cases.

Even though the circuits were not matched to the input, and thus a great amount of power was lost due to reflection, this was already a good indicator that the voltage doubler configuration would be more suitable for the work being done.

The next step was to design these circuits using the transmission lines that the final prototype would have, and at the same time matching the circuit so that as little power as possible was lost. The circuits would be implemented using microstrip structure. The main properties of the used FR4 substrate are given in Table 4.3.

Table 4.3. *Parameters of the FR4 substrate.*

Parameter	Condition	Units	Value
Substrate Thickness	-	mm	1.524
Conductor Thickness	-	mm	0.035
Permittivity	@1 MHz	-	4.8
	@100 MHz	-	4.6
	@1 GHz	-	4.5
Loss tangent	@1 MHz	-	0.015
	@100 MHz	-	0.015
	@1 GHz	-	0.015

The rectifying circuit was matched to the input power source using a single stub matching configuration, because of its simplicity to implement when working with microstrip structures. In order to obtain these matching, first of all the transmission lines required to connect the elements were placed, with equal dimensions for all of them, and the input impedance was simulated. With the obtained value, the dimensions, length and width, of the two transmission lines were calculated using the Smith chart, following the method described in [7]. These two transmission lines were then placed at the input of the circuit. The resulting input impedance was however quite far from 50Ω, and it was not possible to achieve a good matching by tuning exclusively the dimensions of these two lines. Although the reason for this could not be defined with certainty, it could have been caused by the utilization of vias to establish the connections with the ground plane. Thus, the dimensions of the connecting transmission lines were also set to be tuned. Using the optimization tool of the AWR simulation environment, an optimization was carried out with the mentioned dimensions set as a starting point, making sure that they were kept between reasonable limits. The goal was set to obtain the best matching possible, i.e. to achieve a minimum value for the S_{11} (voltage reflection) parameter.

The circuit scheme including the transmission lines and the matching network of both versions can be seen in Figure 4.3.

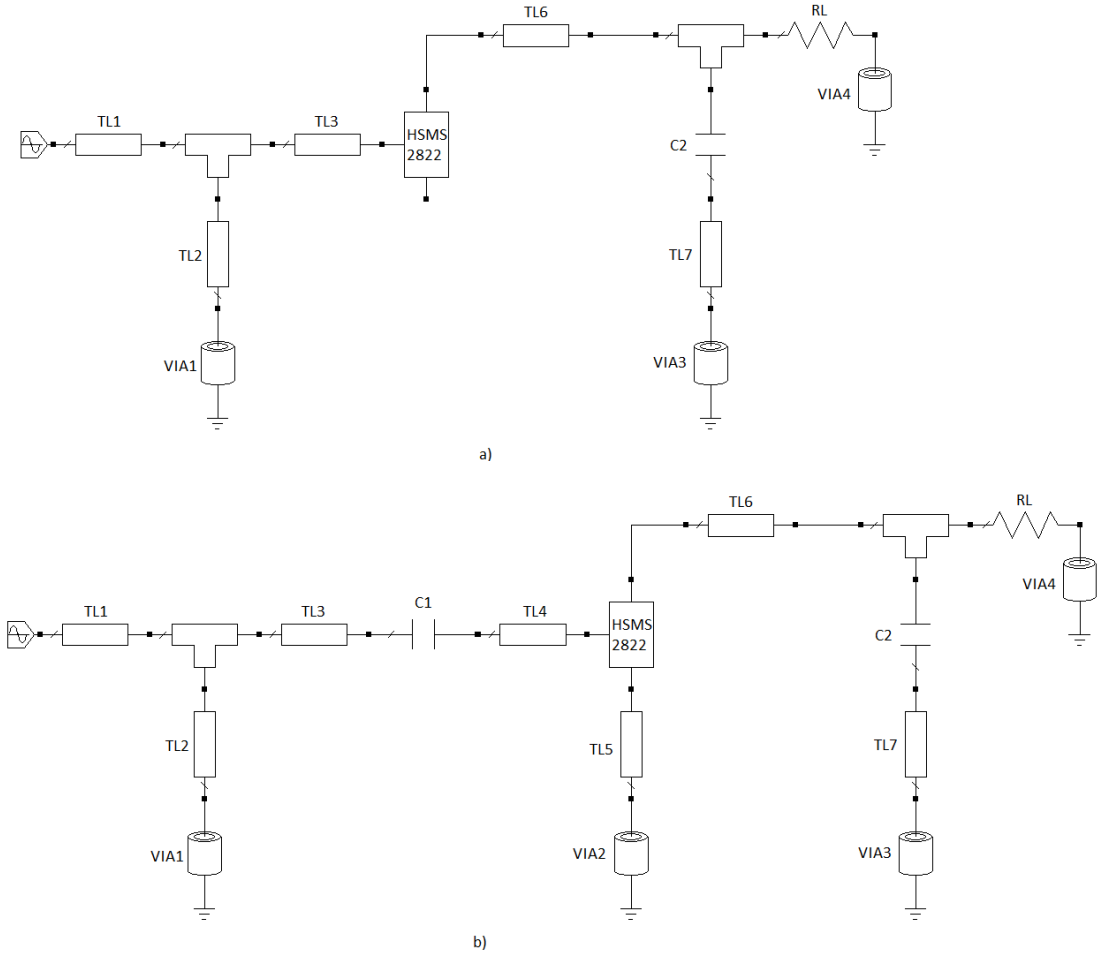

Figure 4.3. *Circuit schematics of rectifies including connections between components: a) single series, b) voltage doubler.*

The width and length of all the transmission lines in the circuits were set as variables in order to optimize the output voltage at the load. The capacitors, load and diodes kept the same values as in the previous design. The input power was set to 0 dBm. The values of the widths and lengths of all the lines for both circuits after optimization can be seen in Table 4.4.

Table 4.4. *Lengths and widths of the transmission lines shown in Figure 4.3 for both circuit configurations.*

Line	Width Single	Length Single	Width Doubler	Length Doubler
TL1	2.898	2	2.898	2
TL2	2.087	5.175	1.5	5.135
TL3	0.5	34.58	0.5	20.33
TL4	-	-	0.501	5.005
TL5	-	-	0.947	5.016
TL6	0.775	5	0.795	5.035
TL7	0.5	10.93	0.51	7.911

The vias were modelled with a square pad having side length of 2mm, and a hole with one millimetre diameter. With these settings, the output DC voltage obtained at the load was 2.563V and 3.557V for the single diode and the voltage doubler configurations, respectively. A reflection coefficient comparison and a DC output voltage comparison with a frequency sweep from 850MHz to 890MHz are shown in Figure 4.4 and 4.5 respectively.

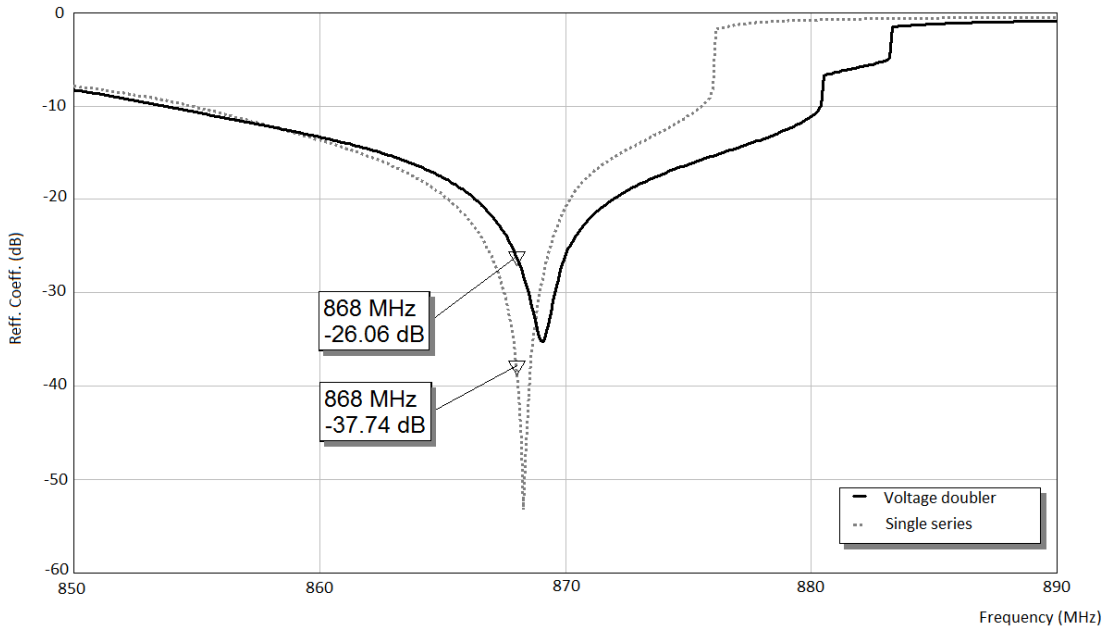

Figure 4.4. *Reflection coefficient comparison between voltage doubler and single series configurations.*

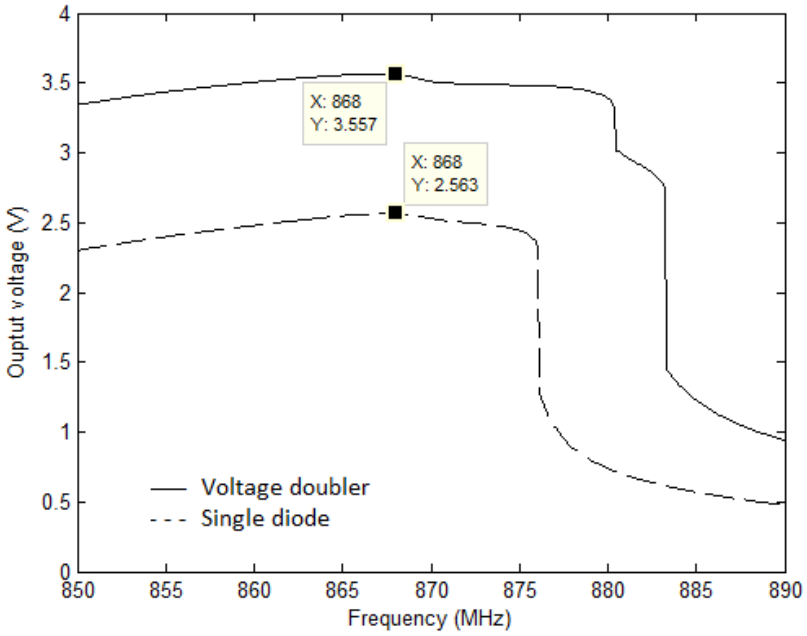

Figure 4.5. *Output voltage comparison between voltage doubler and single series configurations.*

Both configurations behaved in a similar way. However, there are some characteristics that made the voltage doubler a better option to be used in the final design. The most important factor was the output voltage, which was clearly higher than in the single series configuration. This was not so important when the output voltage level is high enough, but when working with lower input power levels, the voltage obtained after rectification would decrease. Since the charger circuit that would be used in the final design required around 0.8V at its input in order to work properly, it was sensible to select the configuration that provided the higher output voltage.

The reflection coefficient, which shows the degree of matching between the input power source and the rectifying circuit, must also be taken into consideration. Both configurations showed very good matching at the working frequency. If the usable frequency range is defined as the one where the reflection coefficient stays below -10dB (return loss is above 10dB), which is a common specification, the single diode configuration presented a usable frequency range of 20.78MHz, from 854.78MHz to 875.56MHz. On the other hand, the voltage doubler may be used between 853.69MHz and 880.38MHz, resulting in a usable frequency range of 26.69MHz.

Taking these two factors into consideration, a decision was made to proceed with the design using the voltage doubler configuration.

4.2.2 Input power optimization

Once the diode configuration was decided, the next step was to optimize the circuit for a certain input power level. The input impedance at the entrance of the rectifying circuit varied significantly when the input power changed, due to the non-linear behaviour of the diodes. Thus, the whole circuit had to be optimized at an input power level that allowed the best overall performance in terms of output voltage and bandwidth.

The rectifying circuit shown in Figure 4.3b was optimized for five different input power levels: -20, -15, -10, -5 and 0dBm. Each version was optimized separately, setting an optimization goal in the simulation environment so that the DC voltage at the load would be maximized. The chosen circuit must provide sufficiently high output voltage level not only at the input power at which it is optimized, but also at other input power levels, thus increasing the range in which it could be used.

The load impedance caused by the energy storage circuitry could not be simulated, since the IC used for this purpose did not have a simulation model and its detailed internal structure was unknown. It could not be easily measured either. However, it could be assumed to be in the range of tens of kΩ. Thus, a 50kΩ load was used for the design, and although its substitution for the final circuitry would affect the results, the changes produced would be of an acceptable magnitude. Figure 4.6 shows the variation of the output voltage and the input impedance in the circuit shown in Figure 4.3b when the load resistance takes values between 20kΩ and 100kΩ.

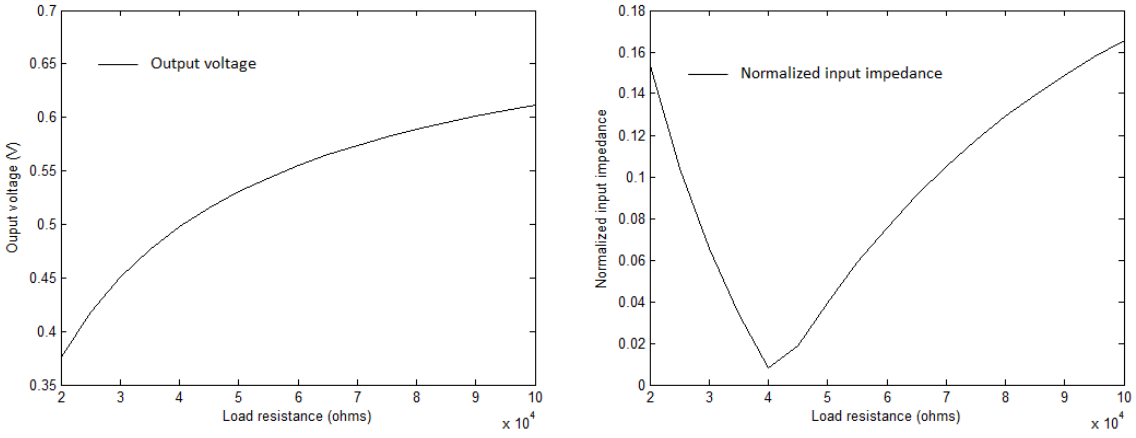

Figure 4.6. *Variation of output voltage (left) and input impedance (right) with the load resistance.*

The reflection coefficient over the frequency range from 850MHz to 890MHz can be observed in Figure 4.7. All the circuits presented similar behaviour, with a good matching at the operating frequency of 868MHz, and a usable frequency approximately between 855MHz and 880MHz.

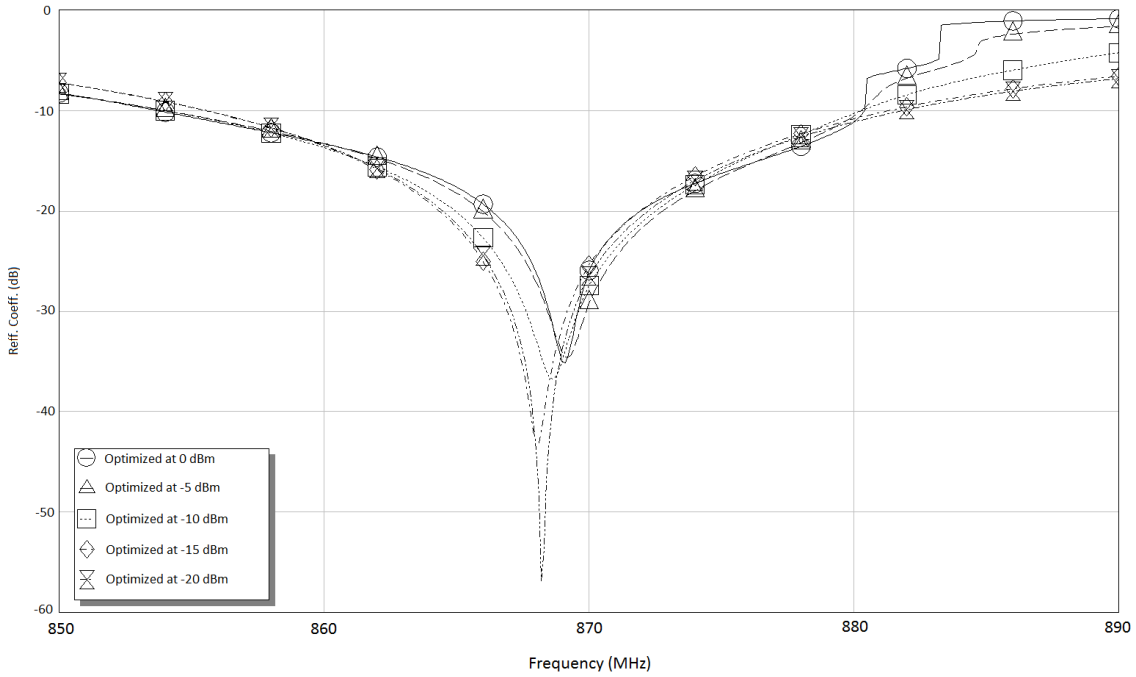

Figure 4.7. *Comparison in terms of reflection coefficient of the circuits optimized at different input power levels.*

In Figure 4.8, the output voltage at different input power levels for the five optimized circuits can be observed.

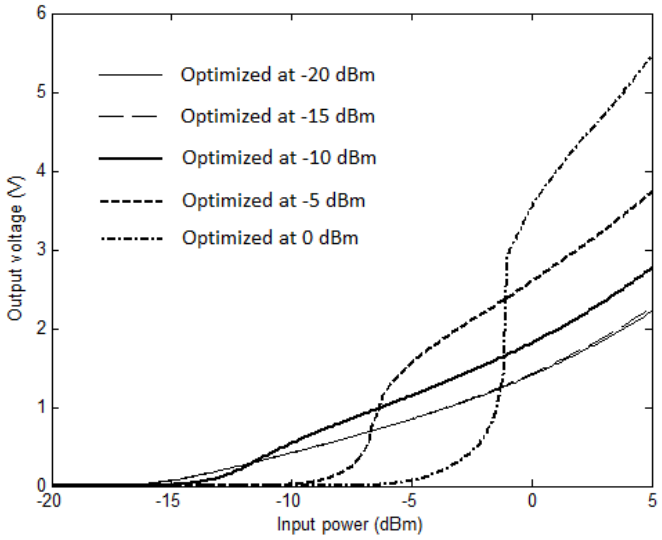

Figure 4.8. *Comparison in terms of output voltage of the circuits optimized at different input power levels.*

Every version of the circuit provided a good output voltage level when the input power is 0dBm or higher. However, the version optimized at 0dBm decreased dramatically the rectified voltage when the input power is below -5dBm. Something similar occurred when the version optimized at -5dBm was used; it produced higher voltage level than any other option when the input power was set to -5dBm, but it was not usable when it fell below that level. None of the circuits presented good performance at input power levels below -10dBm.

Thus, the decision was made to proceed with the version of the circuit that was optimized at -10dBm, since it provided the highest output voltage at that input power level and acceptable levels afterwards.

4.2.3 Layout, implementation and measurements

In order to avoid some complications that would present when designing the layout with the parameters obtained from the optimization, some widths and lengths needed to be redesigned. A bend between the line TL5 and ground was also needed to avoid overlapping between two transmission lines. The load was set to 46.3kΩ, which is the measured value of the resistor component available to be used, with a nominal value of 47kΩ. The final values of widths and lengths for all the lines present in the circuit can be seen in Table 4.5.

Table 4.5. *Final lengths and widths of the voltage doubler circuit.*

Line	Width	Length
TL1	2.9	2
TL2	2.85	8.25
TL3	0.5	8.94
TL4	0.5	9.87
TL5	0.5	8.51
TL6	0.77	5
TL7	1	5.2

If the output voltage and the value of the load are known, it is immediate to obtain the output DC power and current through the following equations:

$$P_{DC\,OUT} = \frac{V_L^2}{R_L} \;\rightarrow\; I_L = \frac{P_{DC\,OUT}}{V_L} \tag{4.2}$$

The output DC voltage, current, power and efficiency over the frequency range of this final version can be seen in Figure 4.9. An input power of -10dBm was used to obtain these results. As established in the datasheet for the charger and protector circuit that was decided to be used, MAX17710, a power as low as 1µW could be used to obtain a constant 4.1V level at its output. Thus, even if the efficiency is not very high (around 6% at 868MHz), the DC power obtained was enough for the circuit to provide charge for the battery.

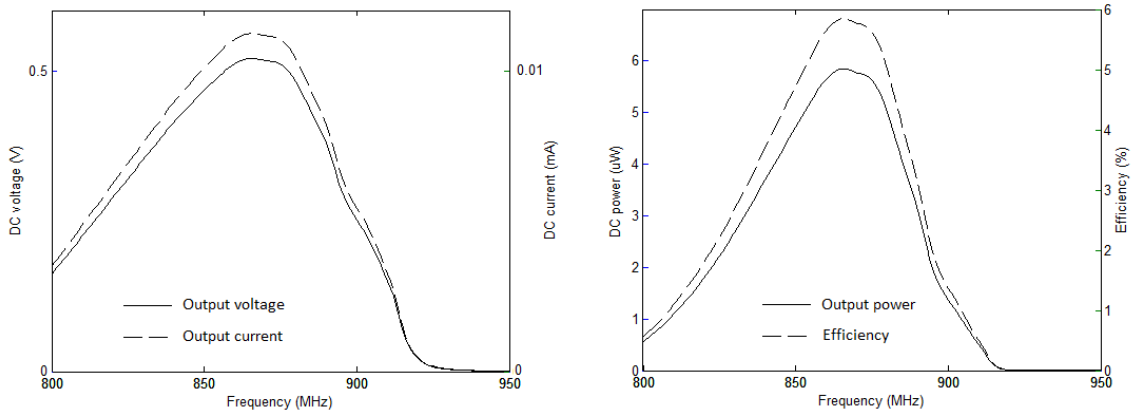

Figure 4.9. *Simulated output voltage, current power and efficiency of the circuit ready to be manufactured.*

The recommended footprint for the diodes package was obtained from its datasheet and created in the design environment. Figure 4.10 shows the final layout for the circuit with the load.

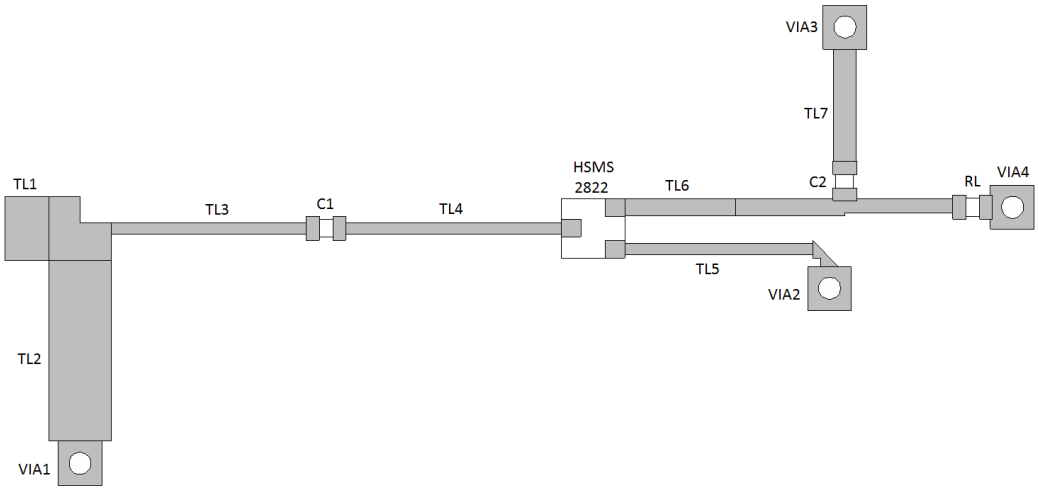

Figure 4.10. *Layout view of the rectifier circuit for 868MHz.*

The implementation was done in several steps. First, the colours of this layout needed to be changed in order to obtain the exposure mask. The packages of the components were hidden so that only the copper elements, i.e. transmission lines and pads, would be visible and in black colour. The 1:1 scale of this exposure mask can be found in Appendix C. This mask was set on top of a piece of FR4 substrate and exposed to ultra-violet light. The next step was to develop this material, in order to eliminate the photo-resistant layer from those areas where conducting material should not remain. Finally, the etching step consisted on placing the piece of FR4 in an acid mix that eliminates the copper from the areas where the photo-resistant layer had been removed.

After the layout was fabricated, the components where manually soldered between the corresponding pads. This was the most difficult step in the fabrication, due to the small size of the components, especially the capacitors and resistance, which were Surface Mount Devices (SMD).

The implementation of the circuit is shown in Figure 4.11. A SMA (SubMiniature version A) connector was connected to TL1, which has a characteristic impedance of 50Ω, for providing the input power.

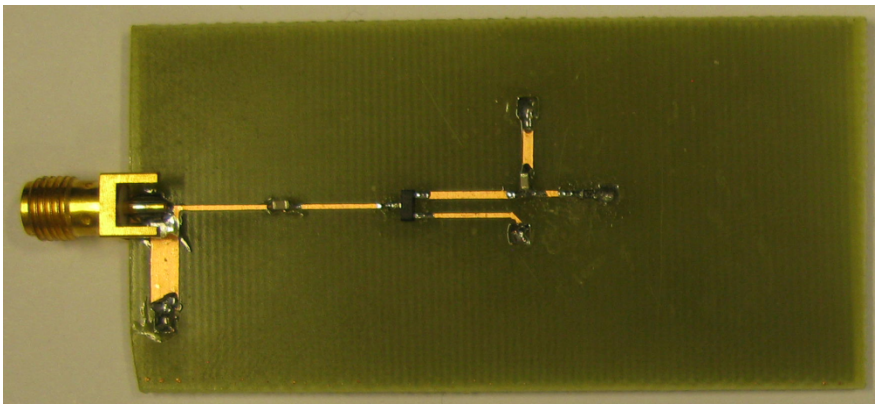

Figure 4.11. *Implementation of the rectifier circuit at 868MHz. The size of the PCB is 68 x 35 mm.*

After proper calibration, the circuit was measured with a vector network analyser (VNA), which could provide the same input power level as the one used for the simulations. Figure 4.12 shows a comparison of the simulated and measured input impedance and reflection coefficient of the circuit. There were several factors that may be responsible for the difference between the simulated circuit and the measured one, including the accuracy of the diodes package model, the non-ideal resistor used as load and the manual fabrication of the vias.

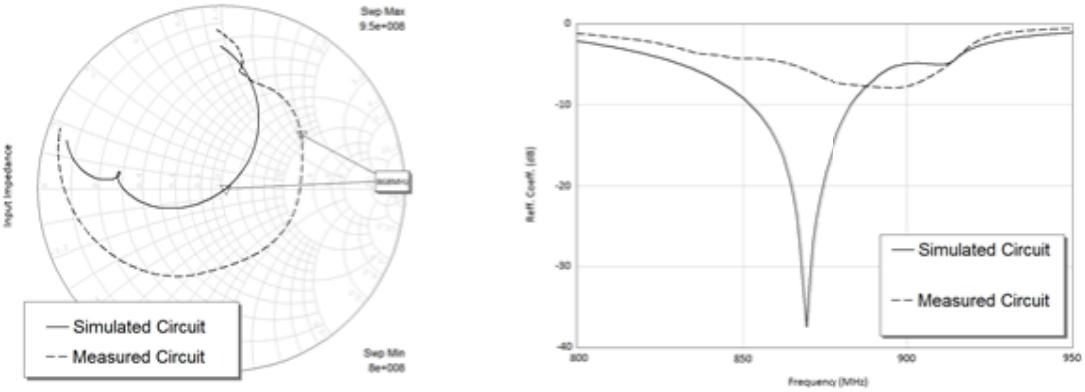

Figure 4.12. *Input impedance and reflection coefficient of the simulated and measured circuit.*

In order to measure the output voltage, probes must be placed on both terminals of the load. By doing so, certain inductance was added to the circuit, which had influence on the input impedance and reflection coefficient. To observe this influence, the circuit was measured using first long probes, and later only the tips of the probes attached to the load. The variation of the input impedance and reflection coefficient is shown in Figure 4.13.

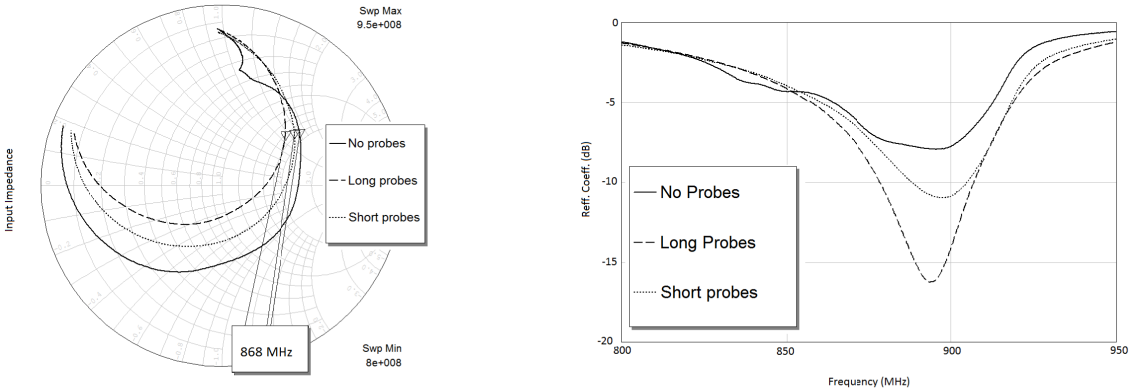

Figure 4.13. *Effect introduced by the measuring probes.*

It yielded that applying the probes to the load produced a better matching at the input. Thus, it was likely that the voltage measured this way had a slightly higher level than the real voltage available at the load. When only the tips of the probes were attached to the load, the variation introduced was lower than if longer probes were used, and thus the results were more reliable. Figure 4.14 shows the measured output voltage

and power of the circuit versus the simulated ones. As expected, the measured voltage was higher due to the effect introduced by the probes. Although the centre frequency was slightly shifted from the simulation results, the profile was very similar and acceptable voltage levels were obtained over a wider frequency range, including the design frequency of 868MHz.

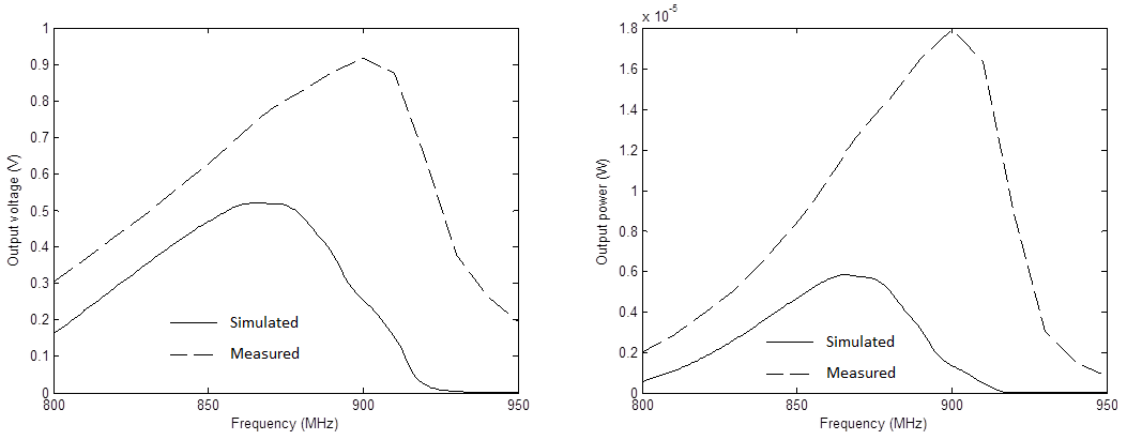

Figure 4.14. *Measured output voltage and power applying a frequency sweep.*

The same characteristics of the circuit were measured and compared with the simulated ones applying a power sweep, keeping a constant frequency of 868MHz. Results are shown in Figure 4.15.

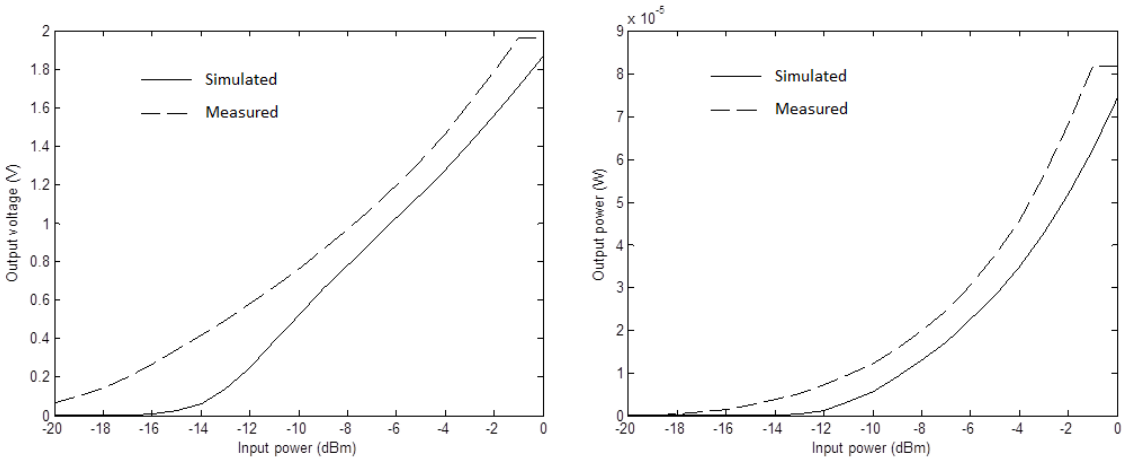

Figure 4.15. *Measured output voltage and power applying an input power sweep.*

The next step was to replace the load for the battery charger and protector circuitry. Recalling it from Chapter 3, the configuration to be implemented is shown in Figure 4.16. With this configuration, the SEL1 pin is left unconnected, and so the regulated output voltage has a value of 3.3V.

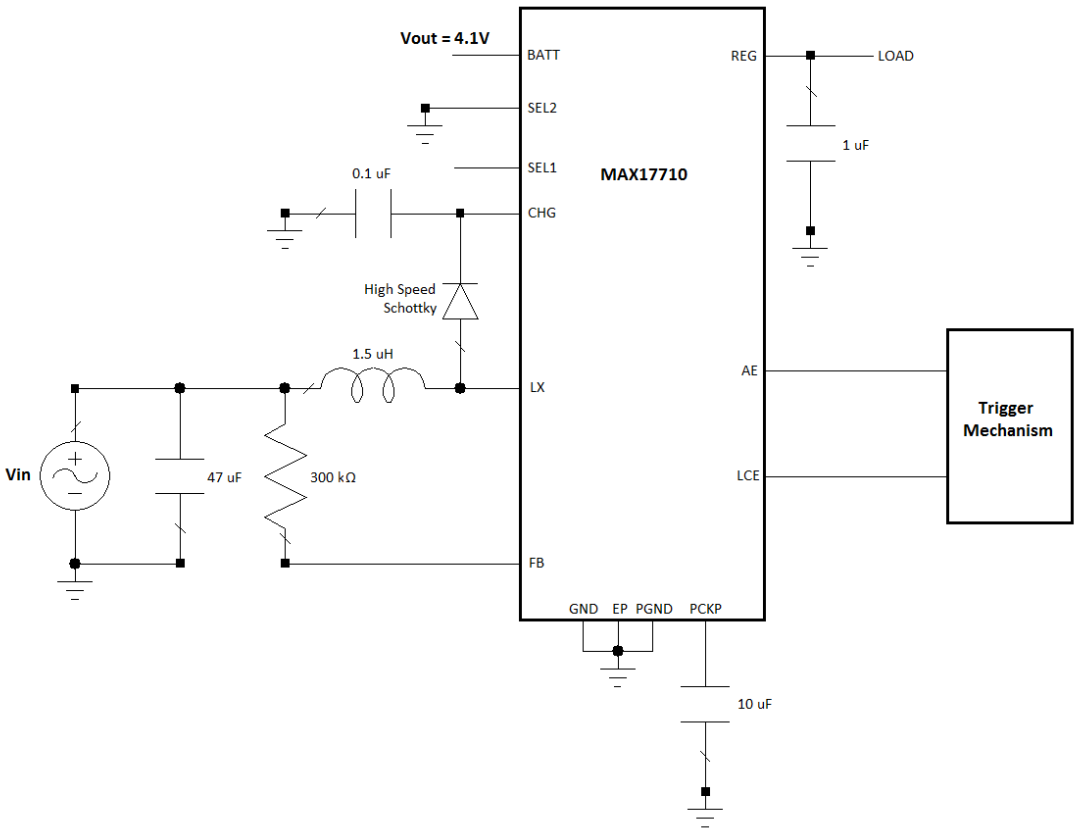

Figure 4.16. *Typical application configuration of the component MAX17710.*

In order to be able to retrieve the power from the battery, a way to activate the regulated output had to be implemented. According to the datasheet, this output is activated by first forcing the AE pin in the MAX17710 IC from low to high level, then doing the same for the LCE pin, and finally placing a low level in AE. This could be achieved by connecting said pins to switches that alternate their output between a low level, such as that provided by the ground plane, and a high level, provided by the battery itself.

The land pattern for each component was obtained from the corresponding datasheets, and the layout for the whole circuitry was designed. Figure 4.17 shows this layout. The 1:1 scale exposure mask obtained from this layout is found in Appendix C.

The resistor connected to the regulated output in parallel with the 1µF capacitor could be used to discharge the battery. Pads 1 and 2 were originally designed and implemented to attach the battery to the printed circuit board (PCB). However, when a newer version of the battery came into use, these pads were no longer necessary. Nevertheless, they did not have any effect on the rest of the circuit, so the circuit implemented containing these pads could still be used.

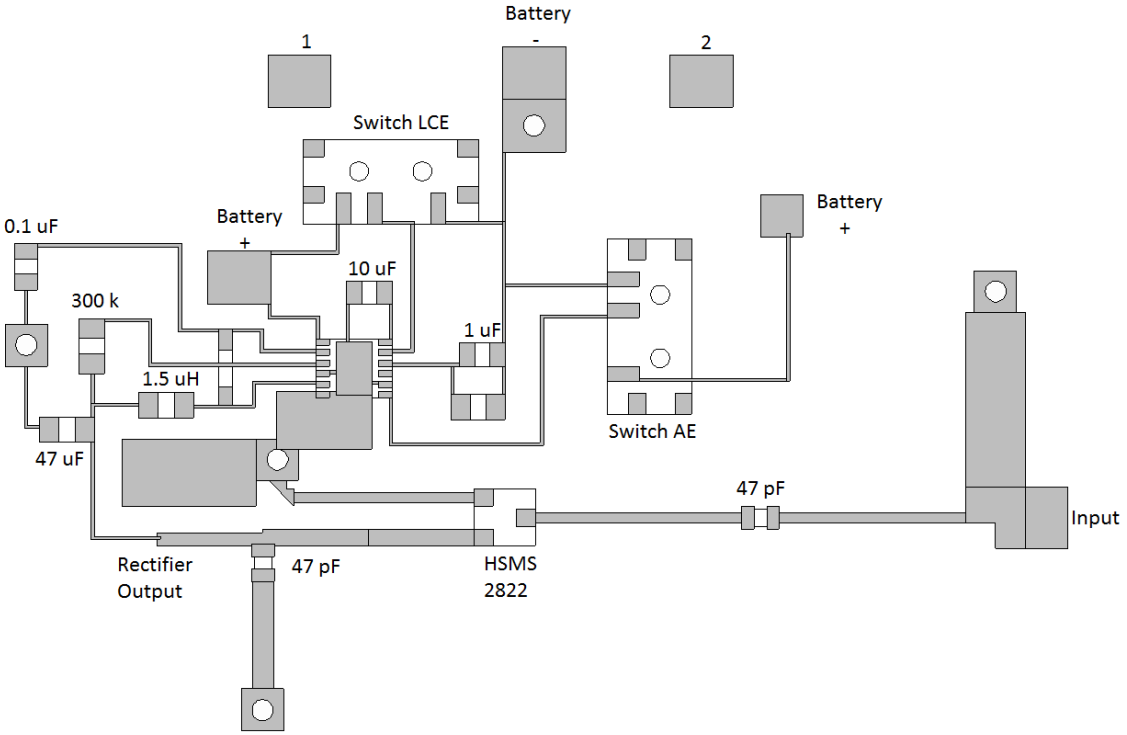

Figure 4.17. *Layout view of the rectifier and energy storage circuitry for 868 MHz.*

The implementation of this circuit presented some challenges. The etching step described previously could no longer be used, because the pads of the IC and the paths connecting them were of such a small size that the copper was removed when the acid mix was applied. A less aggressive etching solution of sodiumpersulfate was applied after the developing step, obtaining satisfactory results.

The attachment of the IC could not be place manually due to its package configuration. Thus, it was needed to first place solder paste in the pads and then place the component with precision equipment. The result was then put into a reflow oven that established the connections.

This manufactured circuit with the battery connected to the corresponding pads can be seen in Figure 4.18.

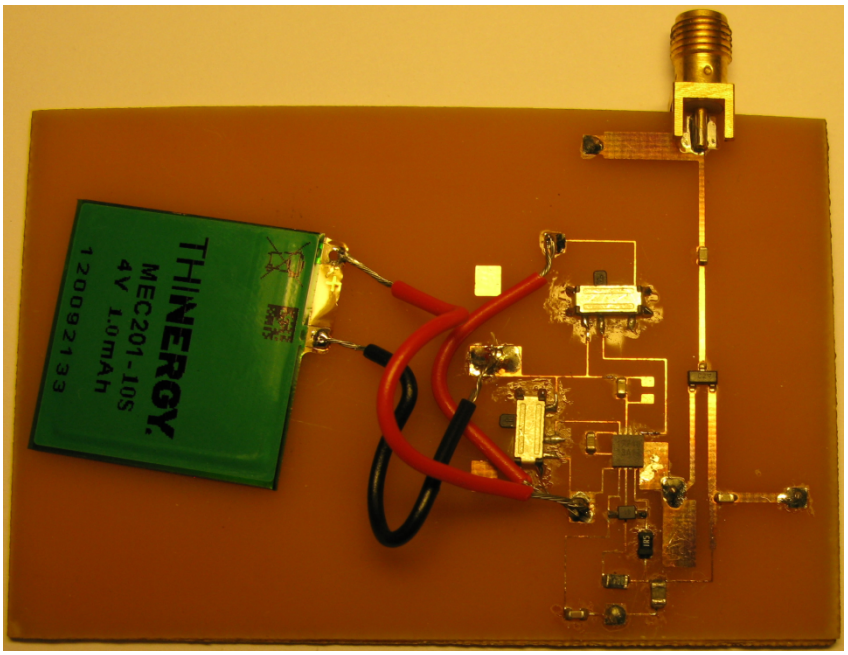

Figure 4.18. *Implementation of the rectifier and energy storage circuitry for 868MHz.The size of the PCB is 80 x 52 mm.*

The input impedance and reflection coefficient of this circuit is shown in Figure 4.19. There was a slight variation with respect to the designed circuit with a resistance as a load, but the matching at the design frequency remained acceptable.

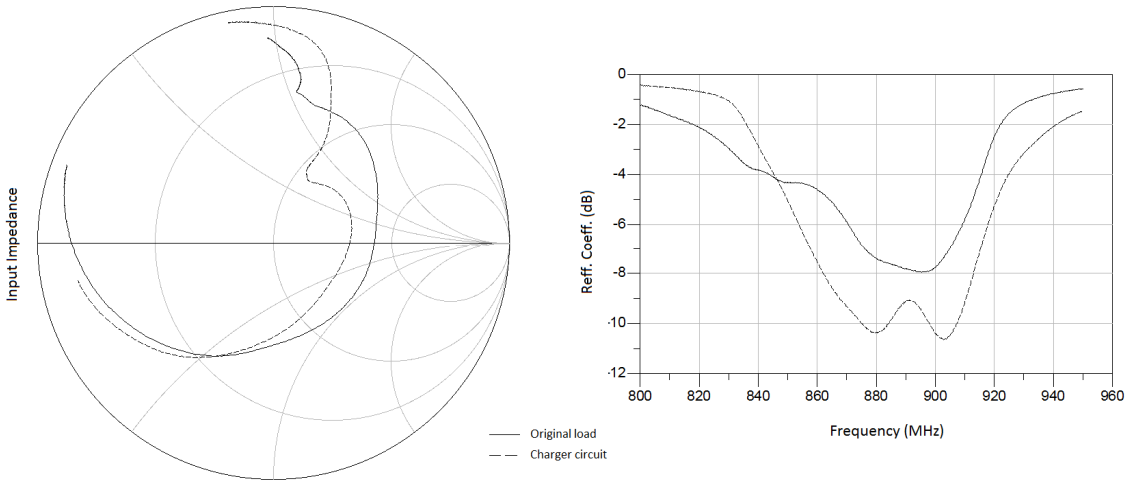

Figure 4.19. *Measured input impedance and reflection coefficient of the circuits designed for 868MHz.*

In order to function properly, the charger circuit needs a start-up voltage that is provided by the battery itself once it is connected. Once the circuit is functioning properly, the voltage at different nodes varies continuously through time, making it necessary to carry out the measurements with an oscilloscope instead of a multimeter, in order to observe the temporal behaviour of these signals.

Once the battery is connected to the circuit, the IC gets the necessary start-up voltage and enters boost mode operation. As described in Chapter 3, in this mode the 47µF capacitor is charged until the voltage in the FB pin exceeds its threshold, which has a nominal value of 0.75V. Once this occurs, the LX pin is internally pulled low to force current through its inductor, which begins to oscillate at 1MHz. Every time LX is released, its voltage is forced above CHG and charges the 0.1µF capacitor. If the voltage in this capacitor rises over the voltage of the battery, charge is delivered to the battery. When the voltage in the source capacitor collapses, the boost circuit is disabled and the process repeats.

In order to observe correctly the behaviour of the circuit, an oscilloscope was used to measure the temporal evolution at different points of interest. In the first place, the input was set to 868MHz and -10dBm. As shown in Figure 4.20, the voltage on the battery remained approximately constant and around 4V, while the 47µF got charged until its voltage collapses.

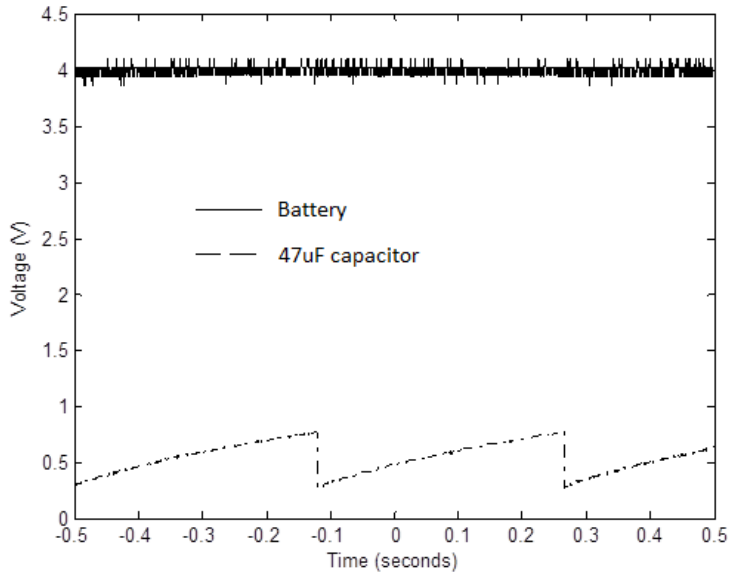

Figure 4.20. *Temporal behaviour of the voltage at different components of the circuit.*

The voltage in the FB and CHG pins was of great interest, since it showed if the circuit is working properly and delivering charge to the battery. The voltage in those pins, measured at the same time, is shown in Figure 4.21a, and a detail of the time when charge was delivered can be seen in Figure 4.21b.

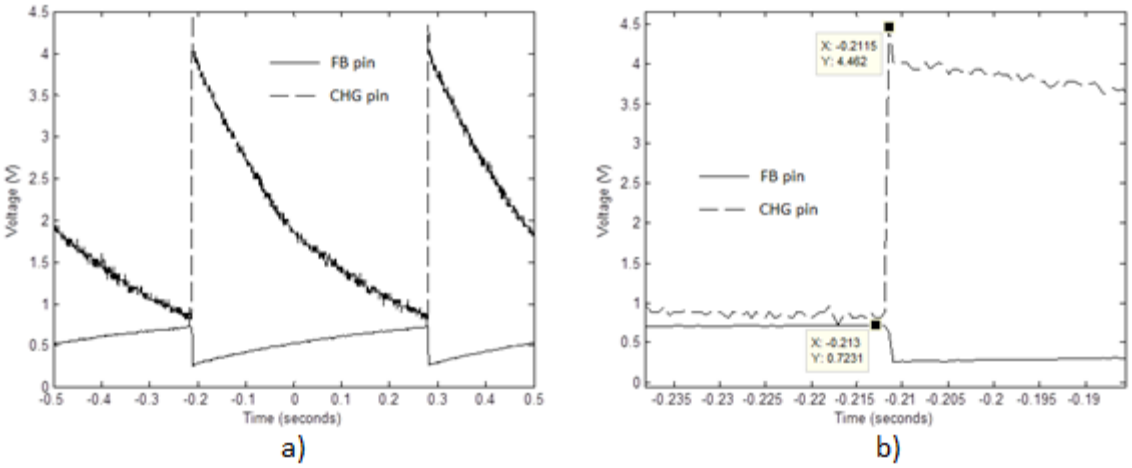

Figure 4.21. *Temporal behaviour at FB and CHG pins of the component MAX17710: a) when charge is being delivered to the load, b) detail of the measurement.*

The voltage in the FB pin increased until it reaches its threshold value, in this case approximately 0.72V. At this point, the boost mechanism was activated, which resulted in a voltage at the CHG pin higher than the battery voltage, and thus, during that fraction of time, charge is delivered to it. This process is repeated continuously, delivering charge to the battery every time the FB threshold level is exceeded.

The behaviour of the circuit should stay the same regardless the power level available at the input of the rectifier. The only variation is expected to be the time it takes to exceed the FB threshold level. As the power increases, the charging of the 47µF capacitor is expected to be faster, thus increasing the frequency with which charge is delivered to the battery. This effect can be observed in Figure 4.22. The profile and voltage levels of the signals under observation remain the same, whereas the frequency at which charge is delivered increases as the input power is increased, being 2.03Hz, 6.743Hz, 17.921Hz and 48.6Hz for an input power level of -10dBm, -5dBm, 0dBm and 5dBm respectively. As the frequency increases, the CHG capacitor discharges less before it is charged again.

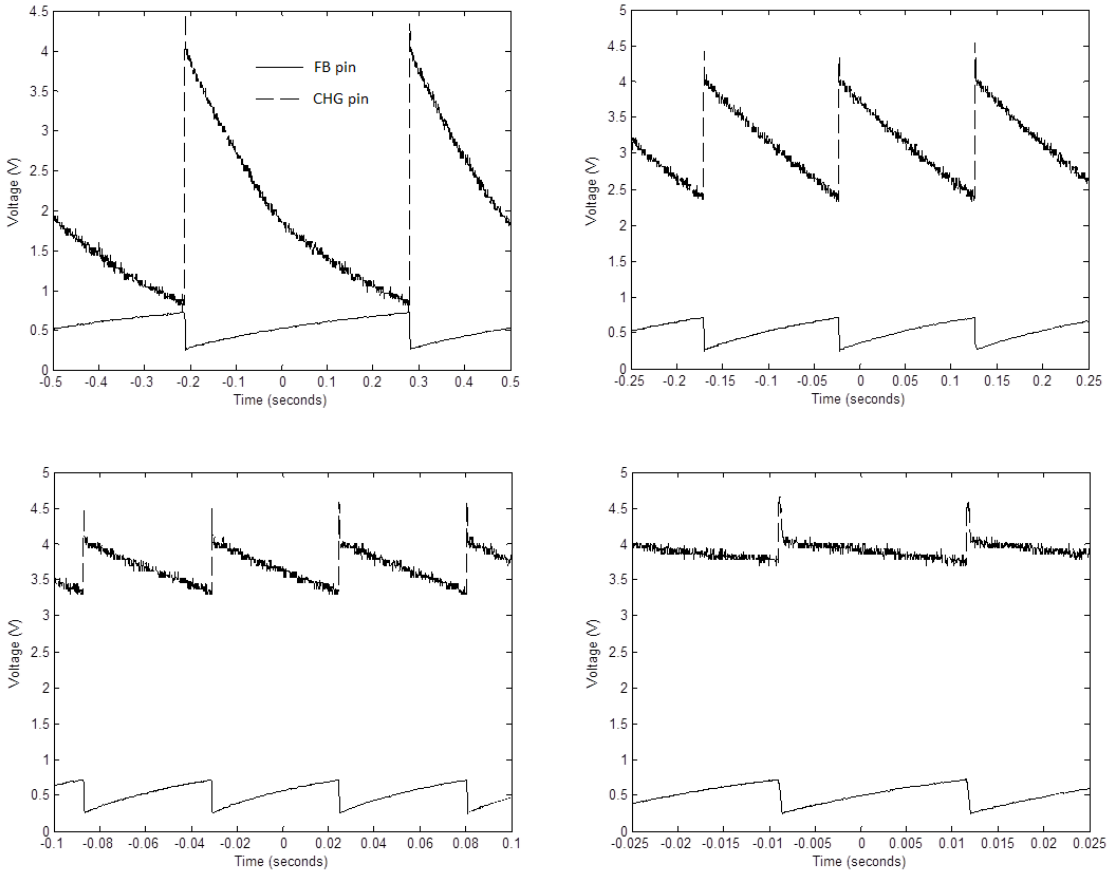

Figure 4.22. *Temporal evolution of the voltage at FB and CHG pins when different input power levels are applied.*

Once it is proved that the circuit behaves correctly, providing charge to the battery from a rectified signal, the last step is to include an antenna that intercepts radiated energy and converts it to an AC signal that is provided to the input of the rectifier. The design of the antenna is not included in this thesis, and so the layouts were provided for a patch antenna with a centre frequency of 868MHz with coaxial feed. The input impedance and reflection coefficient of the manufactured antenna is shown in Figure 4.23.

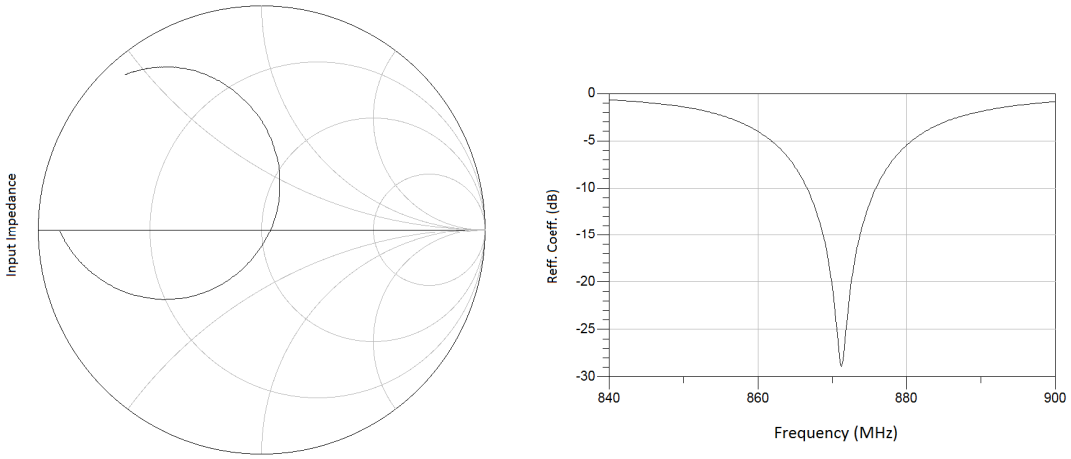

Figure 4.23. *Input impedance and reflection coefficient of the manufactured patch antenna.*

The final measurements, with the rectifier and charging circuitry attached to the antenna and obtaining the power transmitted by another antenna, were carried out in an anechoic chamber. The power amplifier ZHL-2-8 [42], which provides a power gain typically between 31 and 35dB, was placed between the signal generator and the transmitting antenna, in order to obtain a significant power at the receiver. The measurement setup is represented in Figure 4.24. Measurements were done to obtain an input power range for the transmitter that produces similar power levels at the output of the receiver as the ones used in the previous setups. The results could be expected to agree quite precisely with the measurements done previously, because the power fed into the circuit was almost the same. The only cause of disagreement between these two measurements was the impedance mismatching between the sources, which in the previous measurement was exactly 50Ω and in the final measurement, carried out with the fabricated antenna, it varied slightly. Figure 4.25 shows the comparison of these measurements.

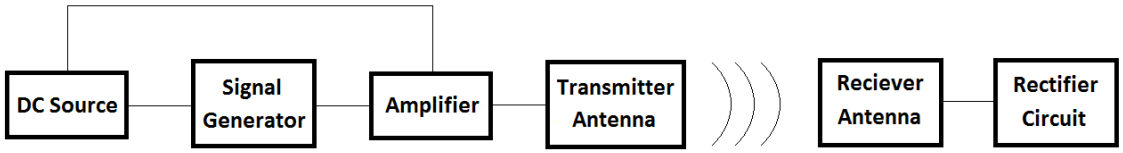

Figure 4.24. *Measurement setup.*

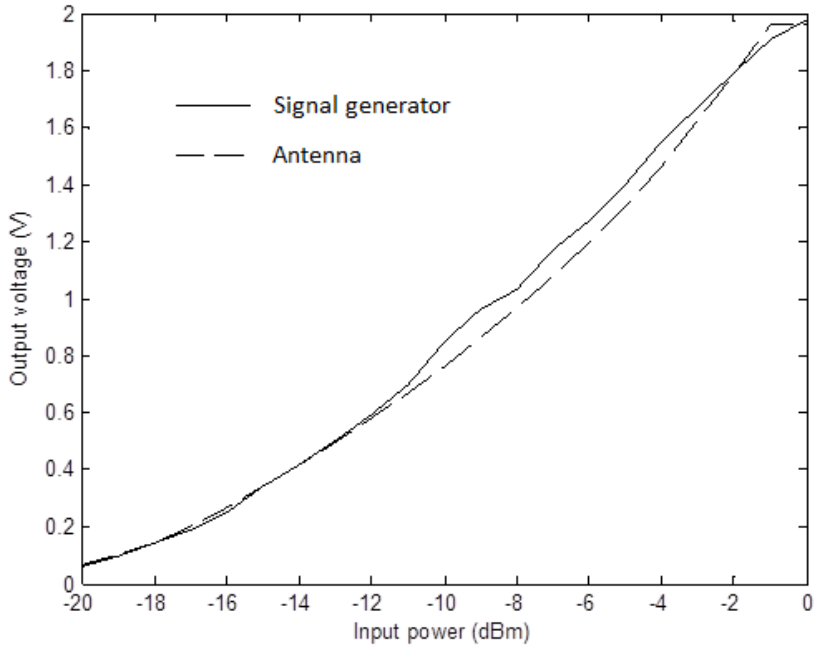

Figure 4.25. *Output voltage as a function of the input power level when the input power is provided by the signal generator or a receiver antenna.*

As for the measurements of the whole circuit, with the battery attached to the output of the charging and protecting circuitry, no representable values could be obtained, due to the lack of time and difficulty of measuring with the oscilloscope inside the anechoic chamber. However, it was checked that the voltages at the pins of interest, FB and CHG, varied continuously through time between the expectable ranges, indicating that charge was being delivered to the battery.

4.3 2.4 GHz

The design and implementation of the 2.4GHz circuit follows the same line as the 868MHz one. Thus, several steps need not be explained further. The diode component to be used is still the same one, HSMS-2822, since its frequency range includes the 2.4GHz band as well.

The diode configuration remains also as the voltage doubler. Since all the components in the circuit and the substrate are the same as the ones used in the 868MHz version, and the only change is the frequency, the performance of this configuration will still be better than that of the single diode configuration. It also has the advantage of allowing a configuration with several stages [14] in order to increase the output voltage, in case the one obtained is not high enough due to the higher losses that will appear as a result of increasing the frequency.

4.3.1 Input power optimization

The circuit is optimized for different input power levels following the same steps described for the 868MHz version, in order to decide which version is optimal for the purposes of this work. The reflection coefficients of the different versions can be observed in Figure 4.26. All the versions present good matching at the design frequency, with more than 30dB return loss in all cases. The circuit that was optimized at -10dBm input power has larger bandwidth than the other circuits, with the one optimized at 0dBm being the most narrowband circuit.

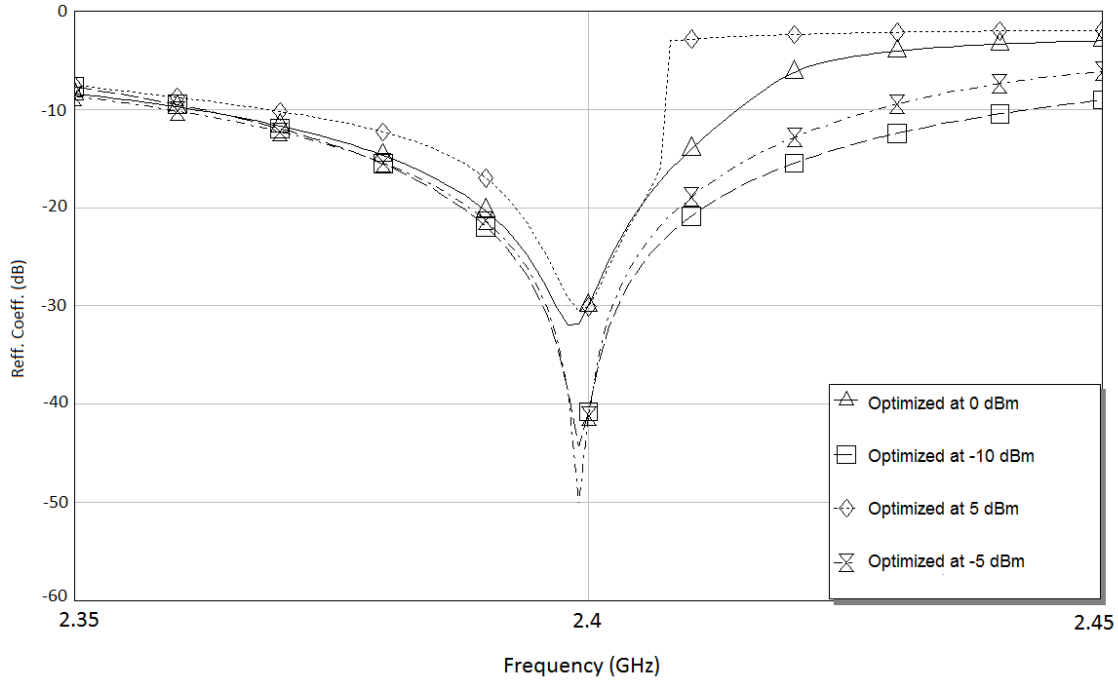

Figure 4.26. *Comparison of the reflection coefficient of the circuits optimized at different input power levels.*

However, since the design frequency does not vary but has a constant value of 2.4GHz, a more important result that must be taken into account is the output DC voltage obtained from rectification at the design frequency, when the input power level varies. This comparison can be observed in Figure 4.27, where an input power sweep from -10dBm to 5dBm is used.

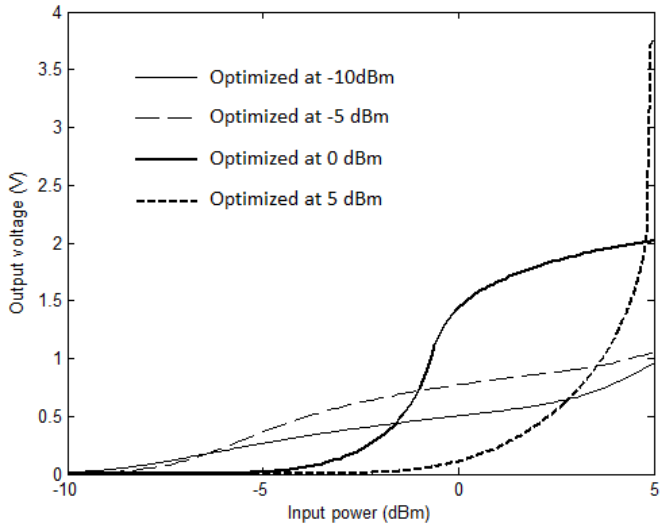

Figure 4.27. *Output DC voltage as a function of input power for the circuits optimized at different input power levels.*

The circuit optimized at -10dBm presented a rectified voltage at its output that was generally lower than the one presented by the circuit optimized at -5dBm, making it a bad option to choose. On the other hand, the circuit optimized at 0dBm obtained a significant output DC voltage only when the input power reached around 2 or 3dBm, level which may be too high to be reached in the operating environment. A final decision was made to implement the circuit optimized at 0dBm, due to the fact that, although the voltage at its output was lower than the -5dBm version until the input power level reached -1dBm, it grew significantly after that point.

4.3.2 Layout, implementation and measurements

As mentioned before, the schematic of this circuit had the same elements and distribution as the one used for the 868MHz version. However, the widths and lengths of the lines obviously had changed in order to obtain a centre frequency of 2.4GHz. These new values are shown in Table 4.6.

Table 4.6. *Transmission line dimensions of the rectifier circuit optimized at 2.4GHz.*

Line	Width	Length
TL1	2.9	3
TL2	0.77	12.52
TL3	2.35	6.04
TL4	2.59	5.18
TL5	0.57	6.81
TL6	1	7.17
TL7	0.51	17.68

The input impedance variation at 0dBm input power level over the frequency range of 2.3 to 2.5GHz is shown in Figure 4.28.

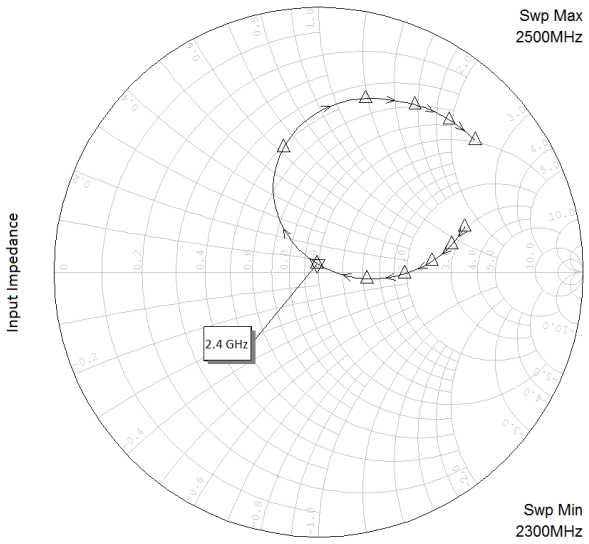

Figure 4.28. *Simulated input impedance of the rectifier circuit optimized at 2.4GHz.*

The simulated output DC voltage, current, power and efficiency for an input power level of 0dBm can be seen in Figure 4.29.

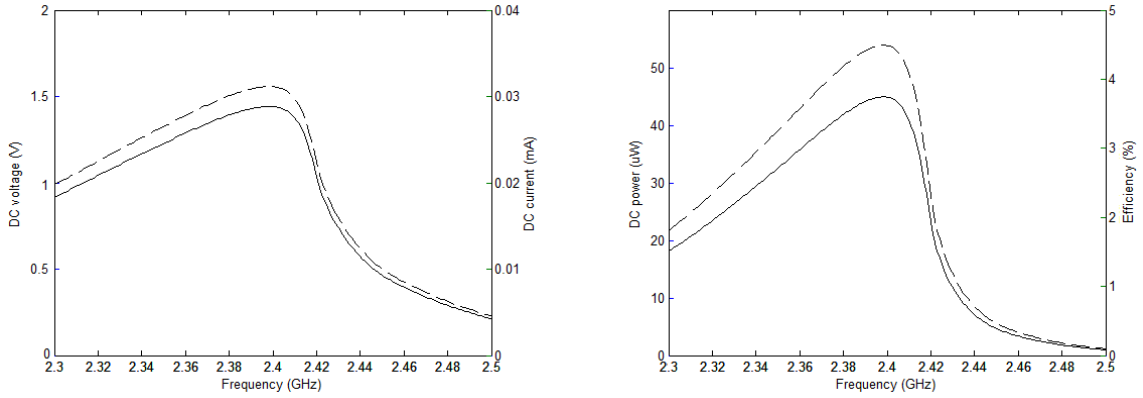

Figure 4.29. *Simulated output DC voltage, current, power and efficiency of the circuit optimized at 2.4GHz.*

Following the same procedure as for the 868MHz version, the layout to be used for the fabrication of the circuit was obtained, including the components footprints and vias to the ground. Figure 4.30 shows this layout before the final exposure mask was generated.

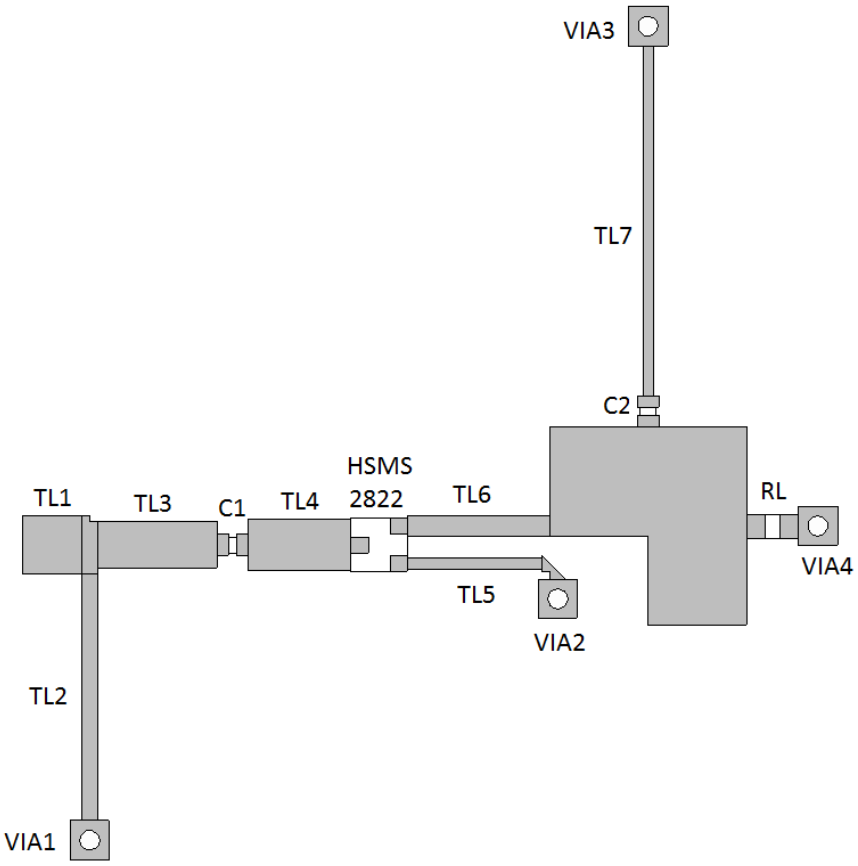

Figure 4.30. *Layout view of the rectifier circuit for 2.4GHz.*

This layout was fabricated and the necessary components attached, including the SMA port for providing the input power to the circuit, following the same steps described for its corresponding version at 868MHz. A 1:1 scale of the exposure mask obtained can be found in Appendix C. The implementation can be seen in Figure 4.31.

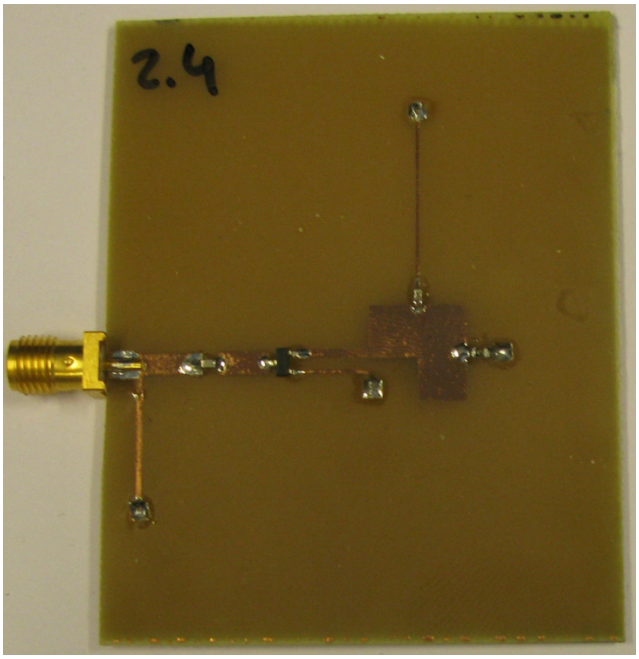

Figure 4.31. *Implementation of the rectifier circuit optimized at 2.4GHz.The size of the PCB is 53 x 65 mm.*

The VNA was properly calibrated again for the desired frequency range, and the input impedance and reflection coefficient were measured. However, the results varied significantly from the simulations, as it can be observed in Figure 4.32. The centre frequency of the implemented version was shifted up almost 300MHz, to 2.684GHz.

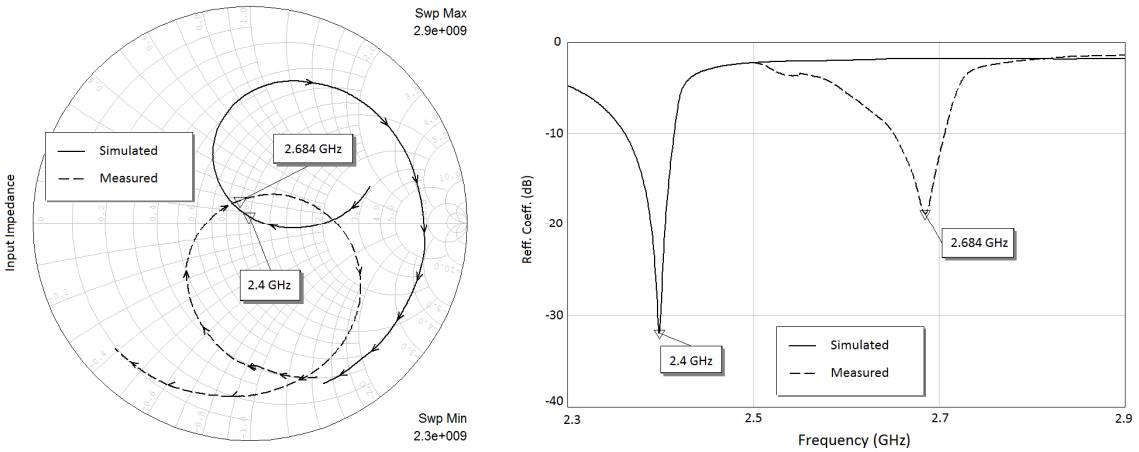

Figure 4.32. *Measured input impedance and reflection coefficient of the rectifier circuit optimized at 2.4GHz.*

A faulty component could be the cause of this variation. The first attempt to find the solution was to replace the diodes by another component, and later the capacitors and the load. None of them changed the results, so it was concluded that the problem was not caused by a mistakenly selected component.

The next step was to run an electromagnetic simulation that would account for the layout itself. Thus, an extraction of the layout was done and the structure was then simulated with the same components. The result of this simulation can be seen in Figure 4.33.

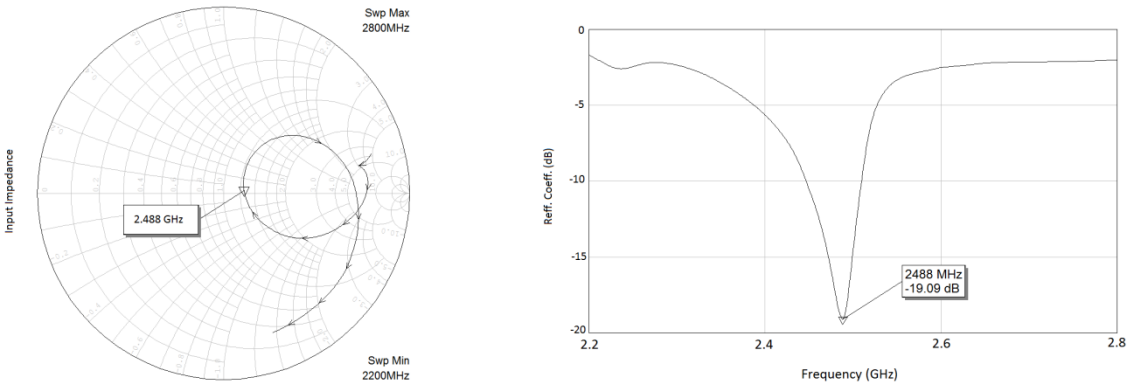

Figure 4.33. *Simulated input impedance and reflection coefficient of the 2.4GHz rectifier circuit using electromagnetic simulation.*

Taking into account the interaction between the transmission lines with the electromagnetic simulation, the centre frequency of the circuit was shifted up to 2.488GHz. This variation was in the same direction as the one observed in the implemented circuit, although its magnitude was not as large.

Having ruled out all these possible causes for the difference between the simulated and the implemented circuits, it was concluded that the reason for it was the model used for the diode component, which, even if it was designed as specified by the manufacturer, it appeared to be inaccurate at these high frequencies. Since this was something that could not be predicted in the simulations due to the lack of time, the solution adopted was to design the circuit for a lower centre frequency, expecting an upshift in the implemented circuit that would result in a centre frequency around 2.4GHz.

The upshift observed in the first implemented circuit was of around 300MHz. Thus, the first attempt was to design the circuit to be centred at 2.1GHz. After the re-optimization and implementation, the circuit was measured. However, the upshift that occurred in this version was of a smaller magnitude than before. It yielded that the frequency shift was not constant, but proportional to the design frequency. Taking into account the shifts occurred in this two versions, it was deduced that a circuit designed to be centred at 2.2GHz, when implemented it would be centred at 2.4GHz. A re-optimization was carried out and the new circuit was implemented. Figure 4.34 shows the measured input impedance and reflection coefficient of the two versions measured.

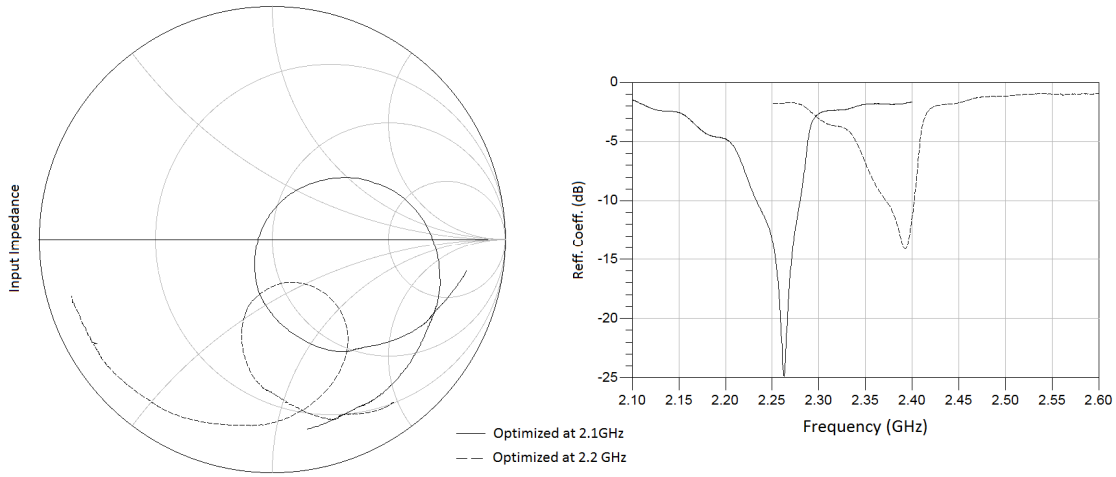

Figure 4.34. *Measured input impedance and reflection coefficient of the rectifier circuit optimized at 2.1GHz and 2.2GHz.*

Table 4.7 shows the final lengths and widths of the transmission lines corresponding to the last version of the circuit.

Table 4.7. *Transmission line dimensions of the rectifier circuit optimized at 2.2GHz.*

Line	Width	Length
TL1	2.9	3
TL2	0.5	19.03
TL3	2.1	5.05
TL4	1.6	6.15
TL5	0.5	8.08
TL6	1	10.44
TL7	0.5	15.52

In Figure 4.35 an input power range from -10dBm to 5dBm at the frequency of 2.4GHz was applied to the circuit and the output voltage was measured in order to compare it with the simulated output voltage over the same input power range for the circuit optimized at 2.4GHz. Although these circuits had different widths and lengths for their transmission lines, they showed a similar behaviour.

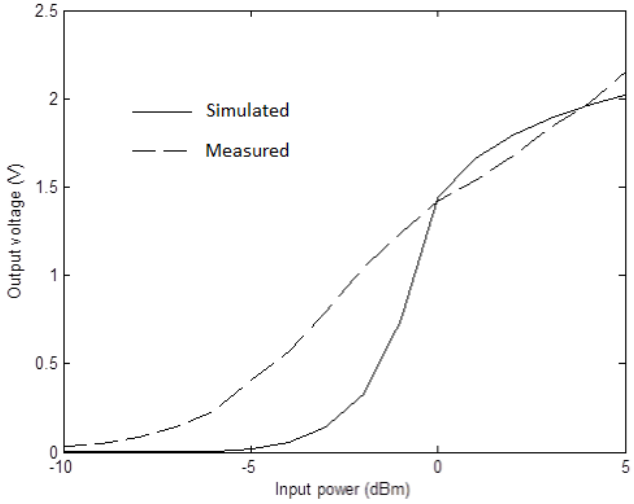

Figure 4.35. *Simulated and measured output DC voltage of the rectifier circuit.*

Once the final version of the circuit with the load had been implemented and measured, the layout where the charging circuitry replaces the load was designed. The same layout for said circuitry used for the 868MHz version of the circuit could be used here, attaching it to the output of the circuit optimized at 2.2 GHz, which, as it had been proved, presented a centre frequency close to 2.4GHz. Figure 4.36 shows the final layout.

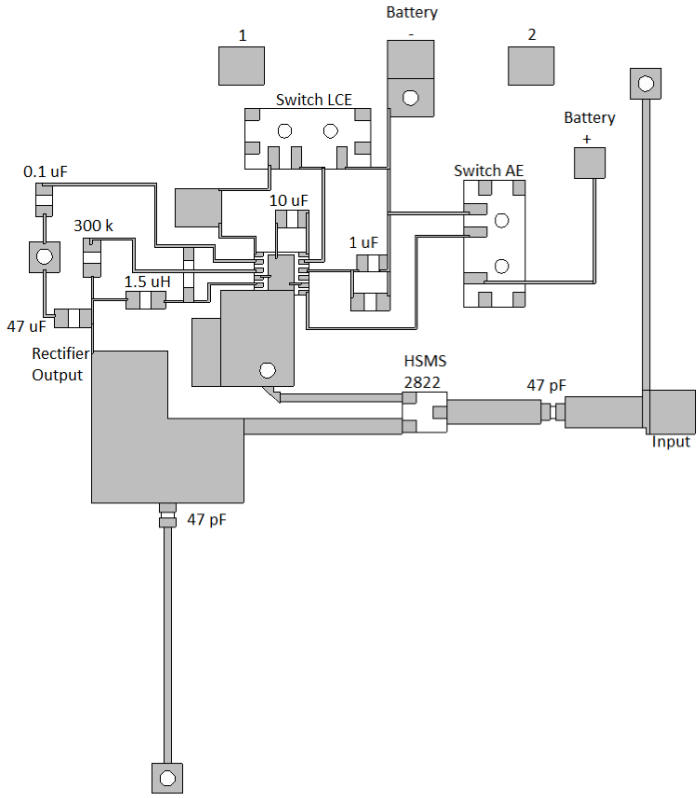

Figure 4.36. *Layout view of the rectifier and energy storage circuitry.*

The circuit was manufactured following the same steps as in its corresponding version for 868MHz. The obtained exposure mask can be seen in Appendix C. The physical implementation, once the battery was attached, can be seen in Figure 4.37. Except for the changes in the widths and lengths of the transmission lines that form the rectifier and define the centre frequency, the circuit was completely equivalent to the one used for the 868MHz frequency band, so its behaviour and different components do not need to be explained again as they should be clear at this point.

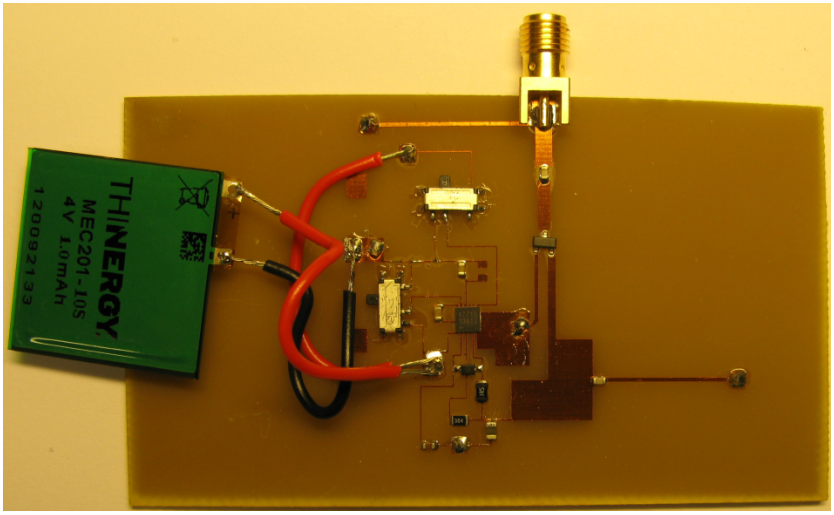

Figure 4.37. *Implementation of the rectifier and energy storage circuitry for 2.4GHz. The size of the PCB is 89 x 49 mm.*

The S-parameters of this circuit were measured using the VNA before attaching the battery since, as it was discussed previously, once this attachment is done there was continuous variation of the signals through the circuit and, with them, a variation of the results. Figure 4.38 shows the measured input impedance and reflection coefficient corresponding to an input power level of 0dbm.

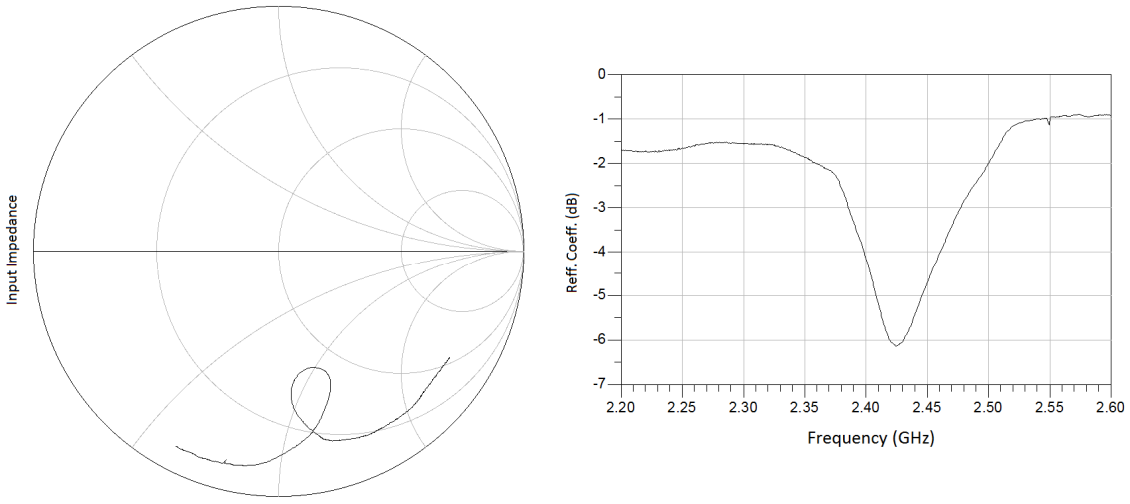

Figure 4.38. *Measured input impedance and reflection coefficient of the implemented rectifier and energy storage circuitry for 2.4GHz.*

As it can be seen, the circuit was centred in the proximities of the desired frequency band, although the return loss was not very high. However, as long as a sufficiently high DC voltage was obtained from rectification, the charger circuitry would work correctly and the battery could be charged, which was the final goal of this work.

The battery was attached to the circuit following the same procedure used previously, in order to provide the start-up voltage that the component MAX17710 needs. The rectified voltage obtained, and thus the power, was not sufficiently high for input power levels below -5dBm. Thus, it was only for input powers over that level that charge was delivered to the battery. In a similar way as it was done for the 868MHz version, the temporal variation of the voltage at the FB and the CHG pins of the IC was obtained with an oscilloscope for three different input power levels: -5, 0 and 5dBm. Figure 4.39 shows the results.

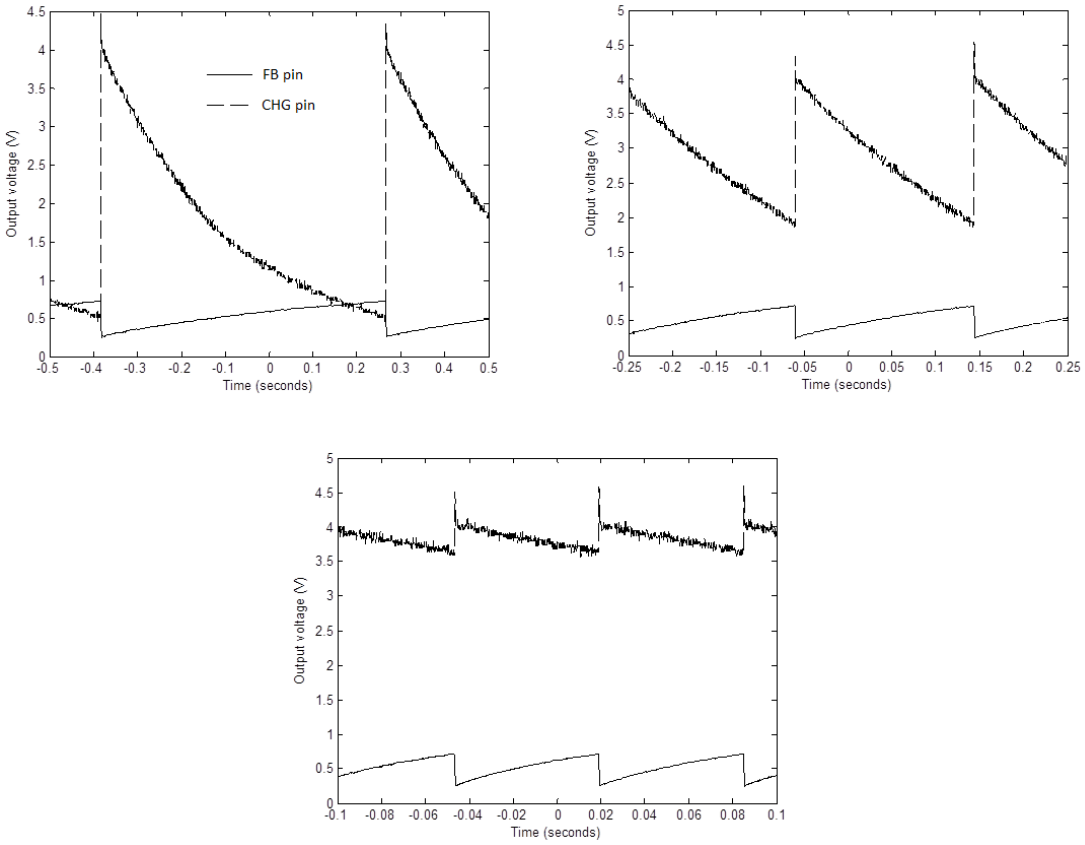

Figure 4.39. *Temporal evolution of the voltage at FB and CHG pins when different input power levels are applied.*

Analogously to the procedure followed in the 868MHz version of the circuit, the final step included the fabrication of the antenna and measurements in the anechoic chamber. The layout for this antenna was given again, and it was fabricated using the same ground plane as the antenna used for 868MHz, but a different patch, obviously of smaller dimensions since the frequency had increased. The input impedance and reflection coefficient of the antenna are shown in Figure 4.40.

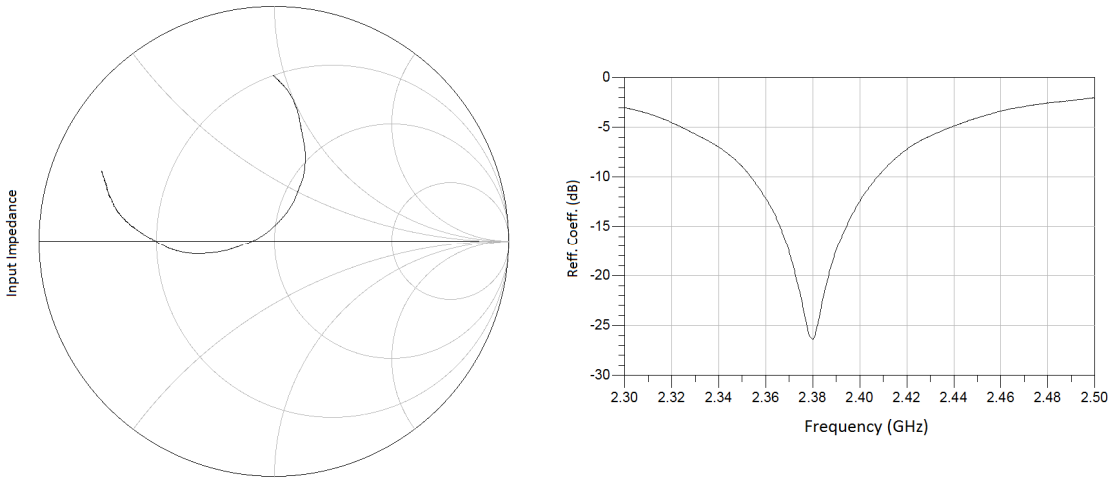

Figure 4.40. *Measured input impedance and reflection coefficient of the patch antenna for 2.4GHz.*

Placing the ZVE-8G amplifier [43] between the signal generator and the transmitter in the anechoic chamber, the receiver antenna could supply up to -5dBm output power, which was delivered to the rectifying circuit. However, this power level range was not enough to obtain measurements that could be directly compared with previous results. Nevertheless, it was high enough to check that when the whole circuit, including the battery attached to it, was connected to the antenna, the voltage levels at the FB and CHG pins varied continuously between its expectable ranges, thus proving that charge was being delivered to the battery.

5. CONCLUSIONS

Four different energy storage devices were reviewed and discussed before any further research could be carried out, since these components imposed some limitations to the final designs. Once the advantages and disadvantages of each of them were studied, it became clear that solid state batteries fitted best in this work due to their unique characteristics, especially their size and charging method. Although supercapacitors possess interesting properties as well, they were ruled out when future applications were considered, where long periods of inactivity and absence of charge delivered to the device might appear, making it a necessity not to lose significant amounts of the stored energy.

Solid state batteries presented an extra challenge, as a constant voltage of 4.1V needed to be present between its terminals in order to be correctly charged. The voltage obtained after rectification would be highly variable as it depends on the power available at the input of the rectifier, and due to the low input power levels that were handled the voltage level obtained would be significantly lower than that required by the battery. Thus, extra circuitry needed to be included to boost and stabilize the rectified signal at the required voltage level. This imposed new restrictions to the design of the rectifying circuits, since the main IC responsible of these operations required a minimum voltage level of around 0.5V.

Two different rectifying circuits were designed to operate optimally at the ISM frequency bands of 868MHz and 2.4GHz. The input impedance of the energy storage circuitry could not be measured beforehand due to its complexity, but it was assumed to present high impedance. Simulations showed that the output DC voltage obtained after rectification did not change dramatically with strong variations of the load impedance. Keeping this in mind, the circuitry was replaced by a real load of 47kΩ for the designs of the rectifying circuitry. The output DC voltage measured at the input of the energy storage circuitry once the prototypes were implemented was in fact higher than the one obtained in simulations.

Due to the nonlinearity of the diodes responsible of the rectification, the input power level needed to be taken into account for the design of the rectifier circuits. The circuits were designed in such a way that the obtained output DC voltage met the goal for an input power level range as wide as possible. Due to the higher losses that appear when the frequency is increased, the 2.4GHz version of the circuit allowed a narrower range than the 868MHz version. Once implemented, it also presented high discrepancies with the simulation results. After ruling out some possible causes, it was concluded that the package model of the diodes component was inaccurate at high frequencies. The

solution adopted was to design the circuit for a lower frequency that would account for this variation once implemented.

Minimizing the size of the prototypes was a design objective of this work. This was achieved, first of all, by selecting the smaller components available when different possibilities were present. The rectifier circuit was designed to achieve an optimal performance while keeping the dimensions as small as possible. Finally, the layout was designed so that a minimum area resulted when placing both the rectifier circuit and the energy storage circuitry components.

The main goal of this project, that was to store the energy obtained after rectification, was achieved at the two frequency bands studied. An immediate conclusion was that higher power levels are needed when the 2.4GHz band. For the same conditions of input power level, the 868MHz would charge the battery in a shorter time. The 2.4GHz band is more popularly used by many electronic devices. However, the maximum power that can be transmitted by devices operating at 2.4GHz is lower than for those operating at 868GHz, whereas the free-space attenuation is directly proportional to the frequency. Thus, the power available at both frequencies is completely dependent on the amount of devices operating nearby.

Further research can be carried out to find out what those levels are at certain locations. More efficient antennas can be designed and attached to the prototypes constructed for this work in order to increase the power available for rectification. In addition, the effect of including low-pass or band-pass filters to eliminate the contribution of higher harmonics can also be studied.

Possible applications of the prototypes obtained in this work include sensors that need to carry out measurements at fixed points in time, and are hibernating otherwise. While they are in this state, the battery would store energy harvested from its environment, eliminating the need of an external power supply, creating this way self-sustainable, environmentally-friendly devices.

REFERENCES

[1] Pozar, D. M., *Microwave Engineering*, Addison-Wesley Publishing Company, Inc., New York, USA, 1990, Chapter 12.

[2] Stutzman, W. L., Thiele, G. A., *Antenna Theory and Design*, Second edition, John Wiley & Sons, Inc., New York, USA, 1998, Chapter 1.

[3] Balanis, C. A., *Antenna Theory, Analysis and Design*, Third edition, John Wiley & Sons, Inc., Hoboksen, New Jersey, USA, 2005, Chapter 2.

[4] Balanis, C. A., *Antenna Theory, Analysis and Design*, Third edition, John Wiley & Sons, Inc., Hoboksen, New Jersey, USA, 2005, Chapter 1.

[5] Carver, K. R., Mink, J. W., "Microstrip Antenna Technology", *IEEE Transactions on Antennas and Propagation*, Vol. AP-29, pp. 2-24, January 1981.

[6] Munson, R. E., "Conformal Microstrip Antennas and Microstrip Phased Arrays", *IEEE Transactions on Antennas and Propagation*, Vol. AP-22, pp. 74-78, January 1974.

[7] Pozar, D. M., *Microwave Engineering*, Addison-Wesley Publishing Company, Inc., New York, USA, 1990, Chapter 6.

[8] Banzhaf, W., *Computer Aided Analysis Using PSPICE*, Second edition, Prentice-Hall, Inc., Upper Saddle River, New Jersey, USA, 1992.

[9] McSpadden, J. O., Fan, L., Chang, K., "Design and experiments of a high-conversion-efficiency 5.8-GHz rectenna", *IEEE Transactions on Microwave Theory and Techniques*, Vol. 46, Iss. 12, pp. 2053-2060, December 1998.

[10] Ren, Y. J., Farooqui, M.F., Chang, K., "A Compact Dual-Frequency Rectifying Antenna With High-Orders Harmonic-Rejection", *IEEE Transactions on Antennas Propagation*, Vol. 55, Iss. 7, pp. 2110-2113, July 2007.

[11] Bouthinon, M., Razban, T., Coumes, A., "Microstrip Circuit for Converting Microwave Low Power to DC Energy", *IEE Proceedings - Microwaves, Antennas and Propagation*, Vol. 132, Iss. 2, pp. 107-109, April 1985.

[12] Takhedmit, H., Merabet, B., Cirio, L., Allard, B., Costa, F., Vollaire, C., Picon, O., "Design of a 2.45 GHz Rectenna Using a Global Analysis Technique", *Third European Conference on Antennas and Propagation*, pp. 2321-2325, June 2009.

[13] Harouni, Z., Cirio, L., Osman, L., Gharsallah, A., Picon, O., "A Dual Circularly Polarized 2.45-GHz Rectenna for Wireless Power Transmission", *IEEE Antennas and Wireless Propagation Letters*, Vol. 10, pp. 306-309, April 2011.

[14] Marian, V., Menudier, C., Thevenot, M., Vollaire, C., Verdier, J., Allard, B., "Efficient Design of Rectifying Antennas for Low Power Detection", *2011 IEEE MTT-S International Microwave Symposium Digest (MTT)*, pp. 1-5, August 2011.

[15] Takhedmit, H., Merabet, B., Cirio, L., Allard, B., Costa, F., Vollaire, C., Picon, O., "A 2.45-GHz Dual-diode RF-to-dc Rectifier for Rectenna Applications", *2010 European Microwave Conference*, pp. 37-40, September 2010.

[16] Takhedmit, H., Merabet, B., Cirio, L., Allard, B., Costa, F., Vollaire, C., Picon, O., "A 2.45-GHz Low Cost and Efficient Rectenna", *2010 Proceedings of the Fourth European Conference on Antennas and Propagation (EuCAP)*, pp. 1-5, April 2010.

[17] Zhang, J., Jia, Z., "Design of Voltage Doubling Rectifier Circuit in Wireless Sensor Networks", *2010 IEEE International Conference on Progress in Informatics and Computing (PIC)*, Vol. 1, pp. 456-459, December 2010.

[18] Vera, G. A., Georgiadis, A., Collado, A., Via, S., "Design of a 2.45 GHz Rectenna for Electromagnetic (EM) Energy Scavenging", *2010 IEEE Radio and Wireless Symposium (RWS)*, pp. 61-64, March 2010.

[19] Heikkinen, J., Kivikoski, M., "A Novel Dual-frequency Circularly Polarized Rectenna", *IEEE Antennas and Wireless Propagation Letters*, Vol. 2, Iss. 1, pp. 330-333, Feb. 2005.

[20] Garthwaite, J., *How ultracapacitors work (and why they fall short)*, July 2011. Available: http://gigaom.com/cleantech/how-ultracapacitors-work-and-why-they-fall-short/.

[21] Becker, H. I., *Low voltage electrolytic capacitor*, July 1957.

[22] Schindall, J., "The Charge of the Ultra-Capacitors", *IEEE Spectrum*, November 2007.

[23] Whittingham, M. S., "Electrical Energy Storage and Intercalation Chemistry", *Science*, Vol. 192, No. 4244, pp. 1126-1127, June 1976.

[24] Goodenough, J. B., "Electrochemical Cell with New Fast Ion Conductors", U.S. Patent 4302518, April 5, 1979.

[25] Yazami, K., in *International Meeting on Lithium Batteries*, Rome, April 1982.

[26] Yoshino, A., Sanechika, K., Nakayima, T., "Secondary Battery", U.S. Patent 4668595, May 10, 1985.

[27] Manthiram, A., Goodenough, J.B., "Lithium Insertion into $Fe_2(SO_4)_3$ Frameworks", *Journal of Power Sources*, Vol. 26, Iss. 3-4, pp. 403-408, May 1989.

[28] Thackeray, M. M., David, W. I. F., Bruce, P.G., Goodenough, J. B., "Lithium Insertion into Manganese Spinels", *Materials Research Bulletin*, Vol. 18, Iss. 4, pp. 461-472, April 1983.

[29] *Material Safety Data Sheets: Lithium-Ion Batteries (Li-Ion)*, National Power Corporation, May 2004. Available: http://www.tek.com/msds-material-safety-data-sheets/liion-battery.

[30] Spotnitz, R., “Abuse Behaviour of High-power, Lithium-ion Cells”, *Journal of Power Sources*, Vol. 113, Iss. 1, pp. 81-100, January 2003.

[31] Timmer, J., “New Solid-state Compount Beats Old School Lithium-Ion Batteries”, *ARS Technica*, August 2011. Available: http://arstechnica.com/science/2011/08/new-solid-state-compound-beats-old-school-lithium-ion-batteries/.

[32] *Toshiba to Launch Innovative Rechargeable Battery Business*, Thoshiba, December 2007. Available: http://www.toshiba.co.jp/about/press/2007_12/pr1101.htm.

[33] *Lithium-ion Battery Charging Basics*, PowerStream Technology, March 2010. Available: http://www.powerstream.com/li.htm.

[34] Shi, Z., Lü, L., Ceder, G., “Solid State Thin Film Lithium Micro Batteries”, in *Advanced Materials for Micro- and Nano-Systems (AMMNS)*, January 2003.

[35] *LTC3105 - 400mA Step-Up DC/DC Converter with Maximum Power Point Control and 250mV Start-Up*, Datasheet, Linear Technology

[36] *LTC3108 - Ultralow Voltage Step-Up Converter and Power Manager*, Datasheet, Linear Technology.

[37] *MAX17710 Energy-Harvesting Charger and Protector*, Datasheet, MAXIM.

[38] Bao, N., Shen, L. F., “Access Policies for Frequency Hopping System Based on Frequency Relativity in ISM Band”, in *2011 IEEE Global Telecommunications Conference (GLOBECOM 2011)*, pp 1-5, December 2011.

[39] *ISM-Band and Short Range Device Regulatory Compliance Overview*, Application Report SWRA048, Texas Instruments, May 2005.

[40] *HSMS-282x Surface Mount RF Schottky Barrier Diodes*, Datasheet, Avago Technologies.

[41] *Linear Models for Diode Surface Mount Packages*, Application Note 1124, Avago Technologies.

[42] *ZHL-2-8 Coaxial Amplifier*, Datasheet, Mini-Circuits.

[43] *ZVE-8G Coaxial Amplifier*, Datasheet, Mini-Circuits.

A. APPENDIX: AVAILABLE ENERGY STORAGE DEVICES

Table A.1. *Characteristics of available supercapacitors.*

Manufacturer	Series	Capacitance (F)	Voltage (V)	Minimum Size (mm)
Illinois Capacitors	DCN	0.25-400	2.7 / 5.4	17x16x9
	DFC	0.007-0.7	1.4-12	12.5x12.3x4
	DC	0.1-8	2.7-5.5	9.7x5.5
AVX Corp	A	0.01-1	3.5-16	28x17x2.3
	B	0.0068-0.1	3.6-15	28x17x2.3
Cooper Bussman	A	0.47-4.7	2.5	20x8
	B	0.22-2.2	2.5	5x11
	HB	3-110	2.5	8x20.5
	HV	1-100	2.7	8x13
	M	1-9	2.5	8x13
	PA	0.22-0.47	5	9x17x22
	PB	0.1-1	5	5.5x10.8x12.5
	PM	0.47-3	5	8.5x16.8x14
	KR	0.1-1.5	5.5	11.5x10x5
Cornell Dubilier	EDLHW	3.3-70	2.3 / 2.1	12.5x23
	EDLF	0.047-1	5.5	13.5x9.5
	EDLNF	0.1-1.5	5.5	13.5x7.5
	EDLSG	0.47-1.5	5.5	19x5
	EDLSD	0.022-0.33	5.5	10.5x5
	EDLEN	0.2	3.3	6.8x1.8
Maxwell Technologies	PC10	10	2.5	29.6x23.6x4.8
	HC	1-150	2.7	12x8
	BC	310-350	2.7	61.5x33.3
Panasonic Industrial	SD	0.022-0.33	5.5	10.5x5.5
	SG	0.47-1.5	5.5	19x5.5
	SE	0.022-0.22	5.5	10.5x5.4
	RG	0.22-1	3.6	10.5x5
	RF	0.1-0.68	5.5	13.5x9.5
	NF	0.1-1.5	5.5	13.5x7.5
	F	0.033-1	5.5	13.5x9.5
	EN	0.2	3.3	6.8x1.8
	EP	0.033	3.3	3.8x1.5
	HZ	3.3-10	2.5	22x8
	HW	1-70	2.1-2.3	22x8
	ER	0.015	2.6	3.2x2.5x1

Table A.2. *Characteristics of available lithium-ion batteries.*

Manufacturer	Series	Capacitance (Ah)	Voltage (V)	Minimum Size (mm)
BYD	LP	0.56-2.02	3.7	30x39x6.4
	LC	2-2.2	3.7	18.1x65
LG Chem	ICR	1.3-2.8	3.6-3.75	18.29x65.05
	ICP	0.83-1.18	3.7	3.85x33.85x49.6
Eemb	Cylindrical	0.3-2.2	3.7	10x44-18x64.5
Battery Co.	Button	0.008-0.17	3.6	12.5x2-30x4.8
Panasonic	Cylindrical	2-3.1	3.6-3.7	18.6x65.2
Industrial	Prismatic	1.95	3.7	34x50x10.6

Table A.3. *Characteristics of available lithium-polymer batteries.*

Manufacturer	Series	Capacitance (Ah)	Voltage (V)	Minimum Size (mm)
BYD	SL	0.085-3	3.7	2.7x20x29
LG Chem	ICP	0.255-3.35	3.7	1.65x28.1x59.9
Hyper Battery	HYLPM	0.11-12.8	3.7	2.5x17x48
Minamoto	LP	0.03-5	3.7	3x17x30
YOK Energy	YE	0.12-1.9	3.7	3.2x16x45

Table A.4. *Characteristics of available solid state batteries.*

Manufacturer	Component	Capacitance (mAh)	Voltage (V)	Recharging Conditions	Size (mm)
Infinite Power Solutions	MEC225	0.13	3.9V	>1 µA, 4.1 V	12.7x12.7x0.17
	MEC220	0.3-0.4	3.9V	>1 µA, 4.1 V	25.4x12.7x0.17
	MEC201	0.7-1	3.9V	>1 µA, 4.1 V	25.4x25.4x0.17
	MEC202	1.7-2.5	3.9V	>1 µA, 4.1 V	25.4x50.8x0.17
	MEC120	0.3-0.4	3.9V	>1 µA, 4.1 V	25.4x12.7x0.17
	MEC101	0.7-1	3.9V	>1 µA, 4.1 V	25.4x25.4x0.17
	MEC102	1.2-1.7	3.9V	>1 µA, 4.1 V	25.4x50.8x0.17
Cymbet	CBC3105	0.005	3.3V	>4 µA, 4.1 V	5x5x0.9
	CBC012	0.012	3.8V	>4 µA, 4.1 V	5x5x0.9
	CBC3112	0.012	3.3V	>4 µA, 4.1 V	7x7x0.9
	CBC050	0.05	3.8V	>4 µA, 4.1 V	8x8x0.9

B. APPENDIX: AVAILABLE RECTIFIER DIODES

Table B.1. *Characteristics of available rectifier diodes.*

Company	Component	Voltage Drop (V)	Frequency (GHz)	Package
Avago	HSMS-285x	0.15 @ 0.1 mA 0.25 @ 1 mA	<1.5	1-4 diodes in different configurations
	HSMS-282x	0.34 @ 1 mA 0.5 @ 10 mA	<4	1-4 diodes in different configurations
	HMPS-282x	0.34 @ 1 mA 0.5 @ 10 mA	<6	1-2 diodes in different configurations
ON Semiconductors	NSR0320	0.24 @ 10 mA 0.3 @ 100 mA 0.45 @ 900 mA	-	1 diode, SOD-323
	BAT series	0.22 @ 0.1 mA 0.41 @ 30 mA 0.52 @ 100 mA	-	Different configurations
Vishay	BAS385	0.24 @ 0.1 mA 0.32 @ 1 mA 0.4 @ 10 mA	-	Single diode, MicroMELF

C. APPENDIX: EXPOSURE MASKS

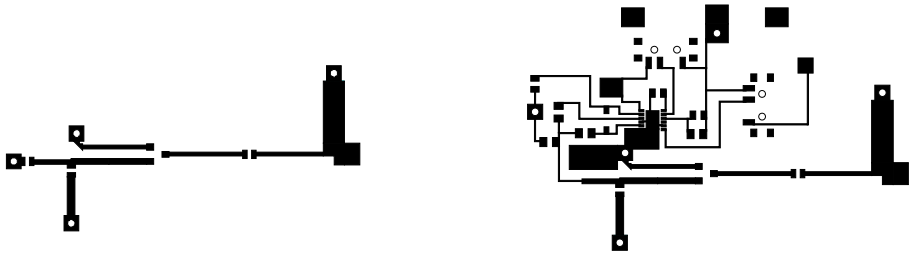

Figure B.1. *Exposure masks of the 868MHz versions of the designed circuits. Left: with a resistor as a load. Right: with the energy storage circuitry layout included.*

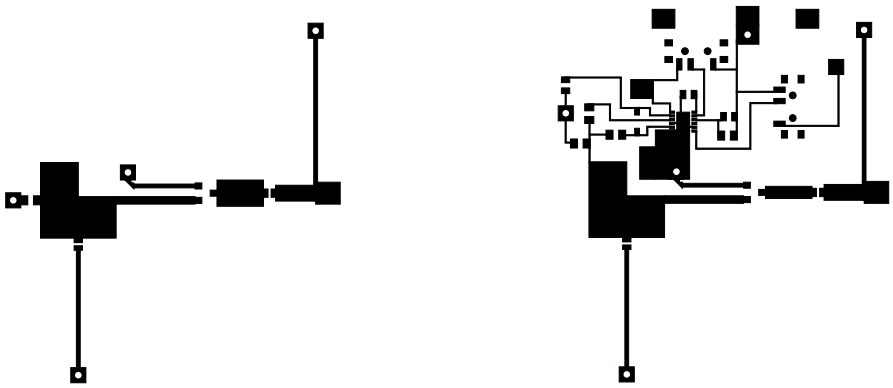

Figure B.2. *Exposure masks of the 2.4GHz versions of the designed circuits. Left: with a resistor as a load. Right: with the energy storage circuitry layout included.*